BIOGEOCHEMICAL INTERACTIONS AND CYCLING OF SULFUR, IRON, AND CARBON IN SULFATE-IMPACTED RIPARIAN WETLANDS AND WILD RICE WATERS

A THESIS
SUBMITTED TO THE FACULTY OF THE
UNIVERSITY OF MINNESOTA
BY

JOSHUA MICHAEL TORGESON

IN PARTIAL FULFILLMENT OF THE REQUIREMENTS
FOR THE DEGREE OF
MASTER OF SCIENCE

CARA SANTELLI

AUGUST 2019

Acknowledgements

I would like to acknowledge my advisor, Cara Santelli, for her unwavering support and insight throughout this project and my graduate studies. I would like to thank Crystal Ng for her invaluable perspective and assistance with this project. Phenomenal fieldwork preparation, organization, and support was provided by Kelly Duhn. Carla Rosenfeld provided invaluable assistance with XAS data collection, troubleshooting, and processing. Field sampling, data collection, and lab support was provided by Patrick O'hara, Amanda Yourd, Kelly Duhn, Carla Rosenfeld, Riley Schmitter, Aubrey Dunshee, Christopher Schuler, Alexander Waheed, McKaylee Duquain, Elizabeth Roepke, Mary Sabuda, Jacqueline Mejia, Tingying Xu, Harsh Anurag, Eleanor Fadely, Susannah Howard, Lilah White, Leila Saberi, Luke Cousins, Jordan Loy, Kerry Callaghan, Elizabeth Lundstrom, Peter Scheuermann, Andrew Wickert, Daniel Larkin, and Megan Kelly. I would like to thank William Seyfried, Brandy Toner, and Josh Feinberg for their valuable insight, suggestions, and perspectives. I would also like to acknowledge Amy Myrbo, Edward Swain, Daniel Larkin, Cara Santelli, Alexander Waheed, Diana Dalbotten, Mae Davenport, Laura Matson, Lilah White, Mark Bellcourt, Michael Dockry, Darren Vogt, Kiara Caruso, and the rest of the *Kawe Gidaa-Naanaagadawendaamin Manoomin* team. Fe-EXAFS and S-XANES work was carried out at the Advanced Photon Source at Argonne National Laboratory; I would like to specifically thank Ken Kemner, John Katsoudas, Shankar Amal, and Tianpin Wu. I would also like to thank my family and friends for their constant support.

Dedication

This thesis is dedicated to my wife, Monica Torgeson, for her endless support and patience throughout my studies. I also dedicate this thesis to Nicholas Rodgers because I said I would.

Abstract

Elevated sulfate (SO_4^{2-}) concentrations in surface waters are a growing global problem that are exacerbated by input from anthropogenic activities (e.g. mining of metalliferous sulfide deposits, road salting, agricultural runoff, etc.). Microbial and microbially-mediated chemical reduction of SO_4^{2-} to sulfide in the porewater of freshwater aquatic systems has been shown experimentally and through field observations to inhibit the growth of many aquatic macrophytes, including wild rice (Ojibwe: manoomin; *Zizania palustris*), a culturally significant grain for the Ojibwe people. While interactions between sulfur (S), carbon (C), and iron (Fe) cycles are recognized, secondary "cryptic" S cycles are much less understood; these cycles favor the reduction of sulfate over iron, contrary to traditional thermodynamic expectations. These cycles have been demonstrated experimentally through research by Hansel et al. (2015) and have been suggested to occur at Second Creek in models by Ng et al. (2017). Using field observations, hydrologic monitoring, and geochemical analyses, we found that dramatic changes in hyporheic flux result in changes in porewater SO_4^{2-} concentrations. Additionally, using X-ray absorption spectroscopy, we have found that intermediate valence S species, not Fe monosulfide, may act as primary sinks for excess dissolved sulfide. Our comparison study between a SO_4^{2-}-impacted stream and a comparably less-impacted river demonstrates that the accumulation of porewater sulfide may be suppressed through limited TOC, excess sediment Fe, or through generation of S-intermediates. These results provide insight into S cycling in freshwater environments and demonstrate the ability to characterize S intermediates in natural sediments using novel spectroscopic techniques, providing further insight into the role of "cryptic" S cycling.

Table of Contents

List of Tables

List of Figures

1. INTRODUCTION

1.1 CULTURAL HISTORY AND ECOLOGY OF WILD RICE

Northern wild rice (manoomin; *Zizania palustris*) carries cultural significance, economic importance, and is a valuable food resource for sovereign American Indian Nations (Jenks, 1899). In the mid-1500s, the Anishinaabe people migrated from the Atlantic coastline to the *Anishinaabe Aki* ("The land of the people"; the Great Lakes region) following a prophecy that would lead them to a place where food grows on the water (Katanski, 2017). The wild rice found growing on lake and river systems in the Great Lakes region was recognized as a gift from the Creator due to its abundance, ease of storage, and nutritional value. Wild rice became a sacred grain for the Ojibwe, and it is intertwined with spiritual practices, economy, history, and many other facets of Ojibwe culture. Today, wild rice is still harvested by many native people in the Great Lakes region using traditional techniques passed down from previous generations and the process of harvesting wild rice is central to the relationship between Ojibwe and the Creator (Walker and Doerfler, 2008). In 1837, The Treaty of St. Peters guaranteed the protection of the Ojibwe people to harvest and manage wild rice stands on ceded land.

Wild rice grows in shallow lakes and streams 1 to 3 feet deep throughout the eastern half of the United States and adjoining parts of Canada (Moyle, 1944). The growth cycle starts with the deposition of wild rice grains in muddy lake or river bottoms in autumn. These seeds germinate in late spring, producing leaves which rise through the water column and, by late June to July, float on the water surface. The wild rice plant blossoms in mid-July, growing up to 8 feet above the surface and producing mature rice grains. In autumn, the seeds ripen, disarticulate, and drop into the water, restarting the growth cycle. Due to the dependence of wild rice on the surrounding water and sediment, wild rice has been shown to be highly sensitive to water level fluctuations and porewater chemistry (Moyle, 1945; Myrbo *et al.*, 2017; Pastor *et al.*, 2017).

1.2 PAST RESEARCH

Surveys of wild rice in the 1930s and 1940s by Dr. John Moyle, a researcher for the Department of Conservation, led to the conclusion that wild rice crops were intolerant to elevated concentrations of sulfate (SO_4^{2-}) in the surface water, with no large rice stands occurring in waters with SO_4^{2-} concentrations greater than 10mg/L and generally no rice growing in water bodies exceeding 40mg/L SO_4^{2-} (Moyle, 1944). In 1973, after the formation of the Environmental Protection Agency (EPA) and the passage of the Clean Water Act, the 10mg/L sulfate surface water standard was adopted by Minnesota for wild rice waters. The Fond du Lac Band of Lake Superior Chippewa also adopted a 10mg/L sulfate standard for wild rice waters on the Reservation when its water quality standards were federally approved in 2001.

In 2010, controversy regarding the scientific basis of Moyle's 10mg/L standard arose due to the relative nontoxicity of SO_4^{2-} and a lack of biochemical explanation for wild rice growth inhibition (Myrbo *et al.*, 2017). Additionally, studies published after Moyle's research have shown that macrophytes are more sensitive to sulfide, the reduced form of SO_4^{2-}, in porewater rather than SO_4^{2-} in the surface water (Koch *et al.*, 1990; Gao *et al.*, 2003). In 2011, in response to the controversy surrounding the 10mg/L surface water SO_4^{2-} limit, a 5-year mesocosm and hydroponics experiment was conducted by the Minnesota Pollution Control Agency supported by the Fond du Lac and Grand Portage Bands of Lake Superior Chippewa (Pastor *et al.*, 2017). This experiment was conducted to understand the influence of elevated concentrations of SO_4^{2-} and sulfide through all stages of wild rice growth and to understand the response of wild rice populations to accumulations of porewater sulfide and elevated concentrations of surface water SO_4^{2-}. These studies revealed that increased concentrations of surface water SO_4^{2-} resulted in increased concentrations of porewater sulfide, and elevated concentrations of porewater sulfide

inhibited both the growth of wild rice seedlings and the viability of the seeds produced by mature plants.

In addition to mesocosm and hydroponics experiments, the MPCA conducted a large-scale field study to investigate the relationship between wild rice growth and the chemical and physical conditions within shallow aquatic systems (Myrbo *et al.*, 2017). This study was conducted from 2011 to 2013 and included 131 different sites, with water, sediment, and porewater samples collected and analyzed. The results of these analyses were used to construct and evaluate structural equation models to understand the sediment and water chemistry variables that contribute to the generation of elevated porewater sulfide. This study found that three key variables contribute to porewater sulfide production: sediment iron, sediment organic carbon, and surface water SO_4^{2-} concentrations (Pollman *et al.*, 2017).

1.3 ANTHROPOGENIC SULFATE LOADING IN NORTHERN MINNESOTA

Minnesota's iron mining industry began in the late 1860's with the discovery of high-grade iron ore on the Vermilion Range (Braden & Lapakko, 2012). This ore had been exposed to extensive weathering and oxidation at the surface, requiring little processing before shipment to iron and steel manufacturing facilities in the eastern United States (Berndt, 2003). Mining of taconite, a lower-grade ore from hard, sedimentary rock, began in 1949, resulting in an extensive accumulation of metal-sulfide containing waste rock (Kohn & Specht, 1958; Braden & Lapakko, 2012). Approximately 160 million tons of sulfide-bearing waste rock have been generated from taconite mining and this waste rock has accumulated in pits across northern Minnesota (Braden & Lapakko, 2012). These sulfide-bearing waste rocks undergo extensive oxidation, leaching SO_4^{2-} to the environment through the following reaction (Equation 1: Belzile *et al.*, 2004):

(1) $$Fe_{1-x}S_{(s)} + (2 - (1/2)x)O_{2(aq)} + xH_2O \rightarrow$$

$$(1\text{-}x)Fe^{2+}_{(aq)} + SO^{2-}_{4(aq)} + 2xH^{+}_{(aq)}$$

Where *x* varies from 0 to 0.125 and represents the starting iron (Fe) to S ratio present in the original mineral. This reaction would typically result in a decrease in pH and lead to acid-mine drainage; however, pH is effectively buffered in these tailing basins due to the dissolution of carbonate minerals present in the host rock (Figure 1) (Lapakko, 1988). The minerals primarily responsible for buffering include siderite $(Mn,Fe)CO_3$ and ankerite $(CaFe(CO_3)_2)$, as shown in the following reactions (Equation 2; Ptacek and Blowes, 1994; Equation 3; Perkins, 2011):

(2) $$(Mn,Fe)CO_{3(s)} + H^{+}_{(aq)} \rightarrow HCO_3^{-}{}_{(aq)} + (Mn,Fe)^{2+}_{(aq)}$$

(3) $$CaFe(CO_3)_{2(s)} + H^{+}_{(aq)} \rightarrow Ca^{2+}_{(aq)} + Fe^{2+}_{(aq)} + HCO_3^{-}{}_{(aq)}$$

The average mass percent of carbonates (~12.24%) in the tailings is much higher than the average mass percent of metal-sulfides (0.13%), resulting in a circumneutral pit outflow from the waste-rock pits which is high in dissolved metals and SO_4^{2-} (Lapakko, 1988; Zanko *et al.*, 2008).

1.4 GEOCHEMICAL INTERACTIONS OF Fe, S, AND C

As SO_4^{2-} from the oxic surface water diffuses into the hyporheic zone of aquatic systems and encounters anoxic, reducing conditions, SO_4^{2-} can act as a terminal electron acceptor for microbial SO_4^{2-} reduction (MSR) through the following reactions (Equation 4; Lovely & Klug, 1986; Equations 5 & 6; Boetius *et al.*, 2000):

(4) $$CH_3COO^{-}_{(aq)} + SO_4^{2-}{}_{(aq)} \rightarrow HS^{-}_{(aq)} + 2HCO_3^{-}{}_{(aq)}$$

(5) $$4H_{2(aq)} + SO_4^{2-}{}_{(aq)} + H^{+}_{(aq)} \rightarrow HS^{-}_{(aq)} + 4H_2O_{(l)}$$

(6) $$CH_{4(aq)} + SO_4^{2-}{}_{(aq)} \rightarrow HCO_3^{-}{}_{(aq)} + HS^{-}_{(aq)} + H_2O_{(l)}$$

The bisulfide (HS^-) produced in these reactions fractionates into sulfide (S^{2-}) and HS^-, with the fraction of each contingent upon system pH; for simplicity, this paper will refer to the sum of these species as 'sulfide'. Experimental research and field observations have linked increased concentrations of porewater sulfide to growth inhibition of several macrophytes, including wild rice (Koch *et al.,* 1990; Gao *et al.,* 2003; Myrbo *et al.,* 2017; Pastor *et al.,* 2017).

While increased concentrations of porewater sulfide has been linked to the inhibition of aquatic plant growth, transformations of sulfide and SO_4^{2-} to other intermediate valence S-species and complexation of sulfide with dissolved metals may act as a mechanism for decreasing the biochemical availability and accumulation of harmful dissolved sulfide. The intermediate S-species generated in aquatic systems are highly dependent on local physical, geochemical, hydrologic, and microbial conditions (Findlay *et al.,* 2017). Sulfide generated in the porewater of aquatic systems can undergo several transformations with oxygen or Fe as electron acceptors, as shown below (Equation 7: Boudreau, 1991; Equation 8: Thamdrup *et al.,* 1993; Equation 9: Langmuir, 1997):

(7) $$HS^-_{(aq)} + 2O_{2(aq)} \rightarrow H^+_{(aq)} + SO_4^{2-}{}_{(aq)}$$

(8) $$2HS^-_{(aq)} + FeOOH_{(s)} + H^+_{(aq)} \rightarrow S^0_{(aq)} + FeS_{(s)} + H_2O_{(l)}$$

(9) $$Fe^{2+}_{(aq)} + HS^-_{(aq)} \leftrightarrows FeS_{(s)} + H^+_{(aq)}$$

Under O_2-poor conditions, microorganisms may also use nitrate as an electron acceptor, as shown in the following reactions (Equation 10, 11, and 12: Jing *et al.*, 2008):

(10) $$5HS^-_{(aq)} + 8NO_3^-{}_{(aq)} + 3H^+_{(aq)} \rightarrow 5SO_4^{2-}{}_{(aq)} + 4N_{2(g)} + 4H_2O_{(l)}$$

(11) $$2HS^-_{(aq)} + 2NO_3^-{}_{(aq)} + 2H^+_{(aq)} \rightarrow SO_4^{2-}{}_{(aq)} + S^0_{(aq)} + N_{2(g)} + 2H_2O_{(l)}$$

(12) $$5HS^-_{(aq)} + 2NO_2^-{}_{(aq)} + 7H^+_{(aq)} \rightarrow 5S^0_{(aq)} + N_{2(g)} + 6H_2O_{(l)}$$

Additionally, under O_2-poor conditions, chemical sulfide oxidation may be coupled to reduction of ferrihydrite (FeOOH) and manganese oxide (MnO_2), yielding zero valent sulfur (S^0; ZVS), as shown in the following reactions (dos Santos Afonso & Stumm, 1992; Yao & Miller, 1996; Equation 13: Böttcher & Thamdrup, 2001; Equation 14: Findlay *et al.*, 2014):

(13) $$2HS^-_{(aq)} + MnO_{2(s)} \rightarrow Mn^{2+}_{(aq)} + 2S^0_{(aq)} + 2OH^-_{(aq)}$$

(14) $$2FeOOH_{(s)} + HS^-_{(aq)} + 5H^+_{(aq)} \rightarrow 2Fe^{2+}_{(aq)} + S^0_{(aq)} + 4H_2O_{(l)}$$

ZVS produced in equations 8, 12, 13, and 14 is most stable as solid orthorhombic sulfur (S_8), but ZVS produced through microbial metabolism is often more soluble than ZVS produced through abiotic reactions and the exact speciation of ZVS can vary among different metabolic pathways (Kleinjan *et al.*, 2003; Findlay *et al.*, 2017). Under high sulfide to oxidant ratios, ZVS has been experimentally shown to be the primary oxidation product of sulfide oxidation, due to kinetic and thermodynamic constraints (Findlay *et al.*, 2017). Dissolved ZVS can react with sulfide through abiotic processes or through microbial reactions to form polysulfides (S_x^{2-}) and can undergo microbial disproportionation, producing SO_4^{2-} and sulfide (Equation 15: Chen & Morris, 1972; Findlay *et al.*, 2017; Equation 16: Thamdrup *et al.*, 1993):

(15) $$(x\text{-}1)S^0_{(aq)} + HS^-_{(aq)} \leftrightarrows S_x^{2-}{}_{(aq)} + H^+_{(aq)}$$

(16) $$2S^0_{(aq)} + 4H_2O_{(l)} \rightarrow HS^-_{(aq)} + SO_4^{2-}{}_{(aq)} + 7H^+_{(aq)}$$

Where X typically varies from 2 to 9 in dynamic environmental systems. Polysulfides can react with ferrous Fe and undergo a similar reaction to equation 9, producing amorphous Fe monosulfide (mackinawite; FeS), as shown in the following equations (Equation 17: Findlay *et al.*, 2014):

(17) $$Fe^{2+}_{(aq)} + S_9^{2-}{}_{(aq)} \rightarrow FeS_{(s)} + S_{8(s)}$$

Fe monosulfides may transition to Fe disulfides (pyrite; FeS_2) via several thermodynamically favorable pathways (Morgan *et al.*, 2012). This transition can be inhibited or reduced when environmental conditions favor dissolution of Fe monosulfide constituents, under conditions with limited sulfide and excess Fe, or in environments with elevated concentrations of reactive organic carbon (ROC) (Burton *et al.*, 2006; Burton *et al.*, 2011; Morgan *et al.*, 2012).

Under conditions favoring lower sulfide to oxidant ratios, oxidation of ZVS to sulfite (SO_3^{2-}) or microbial disproportionation to SO_4^{2-} and sulfide has been shown to be a thermodynamically and kinetically favorable reaction (Findlay *et al.*, 2017; Equation 18: Langmuir, 1997; Equation 19: Janssen *et al.*, 1996):

(18) $$S^0_{(aq)} + O_{2(aq)} + H_2O_{(l)} \rightarrow SO_3^{2-}{}_{(aq)} + 2H^+_{(aq)}$$

(19) $$SO_3^{2-}{}_{(aq)} + S^0_{(aq)} \rightarrow S_2O_3^{2-}{}_{(aq)}$$

Sulfite produced in equation 18 generally has low stability and will either fully oxidize to SO_4^{2-}, react with ZVS to form $S_2O_3^{2-}$, or undergo microbial disproportionation to SO_4^{2-} and sulfide (Equation 20 & 21: Langmuir, 1997; Equation 22: Janssen *et al.*, 1996):

(20) $$SO_3^{2-}{}_{(aq)} + \frac{1}{2}O_{2(aq)} \rightarrow SO_4^{2-}{}_{(aq)}$$

(21) $$SO_3^{2-}{}_{(aq)} + S^0_{(aq)} \rightarrow S_2O_3^{2-}{}_{(aq)}$$

(22) $$4SO_3^{2-}{}_{(aq)} + H^+_{(aq)} \rightarrow 3SO_4^{2-}{}_{(aq)} + HS^-_{(aq)}$$

In addition to oxidation of ZVS to SO_3^{2-} by oxygen, as shown in equation 18, experimental work has shown that both pyrite oxidation and MnO_2 reduction can result in the production of thiosulfate ($S_2O_3^{2-}$) (Luther, 1987; Burdige & Nealson, 1986); thiosulfate may also be produced during incomplete MSR (Findlay *et al.*, 2017). Under circumneutral pH conditions, thiosulfate can become oxidized to SO_4^{2-} in the presence of an oxidizer, or it can be microbially

disproportionated to SO_4^{2-} and sulfide (Equation 23: Frederiksen & Finster, 2003; Equation 24: Fahd, 2014), effectively recycling the S-species back to their most oxidized state.

(23) $$S_2O_3^{2-}{}_{(aq)} + 8FeOOH_{(s)} + 14H^+{}_{(aq)} \rightarrow 2SO_4^{2-}{}_{(aq)} + 8Fe^{2+}{}_{(aq)} + 11H_2O_{(l)}$$

(24) $$S_2O_3^{2-}{}_{(aq)} + H_2O_{(l)} \rightarrow SO_4^{2-}{}_{(aq)} + HS^-{}_{(aq)} + H^+{}_{(aq)}$$

1.5 ORGANIC S BIOSYNTHESIS

In addition to biochemical cycling of S-species for energy, organisms thriving in the sediments of aqueous systems require S to produce S-containing protein amino acids (Moran *et al.*, 1999). Previous studies have found that organic S compounds can become concentrated in some sediments, accounting for up to 90% of total S in some environments (Jokic *et al.*, 2003). In freshwater aquatic sediments, these organic compounds have been found to be generally split between 4 major organic S pools: sulfonates (e.g., homocysteic acid; $R\text{-}SO_3^-$) , thiols (e.g., cysteine; R-S-H), disulfides (e.g., cystine; R-S-S-R'), and monosulfides (e.g., methionine; R-S-R'); (Bostick *et al.*, 2005; Zeng *et al.*, 2013).

Sulfonates can be formed by organisms in the sediment through a variety of biosynthesis pathways (Leadbetter & Godchaux, 1988; Zeng *et al.*, 2013). While structural analogs of sulfonate serve important biochemical functions in organisms, field research has found that sulfonates are generally less abundant than other organic S compounds, likely due to lower production rates or rapid organosulfur reduction of sulfonate to sulfide by SO_4^{2-} reducing bacteria (SRB) or other sulfidogenic bacteria (Lie, 1999; Zeng *et al.*, 2013).

Thiols, monosulfides, and disulfides have been shown to accumulate in some environmental systems, contributing up to 70% of the total sediment S (Zeng *et al.*, 2013). These

S-compounds often form through reactions involving functional organic matter and sulfides; formation of these organic S phases has been suggested to effectively remove large quantities of dissolved sulfide from sediment porewater (Pollman *et al.*, 2017). While inorganic intermediate S compounds are generally considered to be labile in the presence of oxidizers, organic S compounds are comparably stable (Prietzel *et al.*, 2009).

1.6 "CRYPTIC" SULFUR CYCLING

In addition to the biogeochemical reactions outlined in sections 1.4 and 1.5, many other S intermediates are expected to be synthesized chemically and microbially (e.g. tetrathionate; $S_4O_6^{2-}$, pentasulfur hexoxide; $S_5O_6^{2-}$, hexsulfur hexoxide; $S_6O_6^{2-}$, etc.) (Zhang & Jeffrey, 2010). These compounds are generally highly reactive and undergo hydrolysis or degradation to other S compounds (Equations 25 & 26: Grabarczyk *et al.*, 2015; Equations 27 to 32: Zhang & Jeffrey, 2010):

(25) $\text{TsdA-Cys-S}^-_{(aq)} + S_2O_3^{2-}{}_{(aq)} \rightarrow \text{TsdA-Cys-S}_3O_3^-{}_{(aq)} + 2e^-$

(26) $\text{TsdA-Cys-S}_3O_3^-{}_{(aq)} + S_2O_3^{2-}{}_{(aq)} \rightarrow \text{TsdA-Cys}^-_{(aq)} + S_4O_6^{2-}{}_{(aq)}$

(27) $S_4O_6^{2-}{}_{(aq)} + S_2O_3^{2-}{}_{(aq)} \rightarrow S_5O_6^{2-}{}_{(aq)} + SO_3^{2-}{}_{(aq)}$

(28) $S_4O_6^{2-}{}_{(aq)} + SO_3^{2-}{}_{(aq)} \rightarrow S_3O_6^{2-}{}_{(aq)} + S_2O_3^{2-}{}_{(aq)}$

(29) $2S_4O_6^{2-}{}_{(aq)} \rightarrow S_3O_6^{2-}{}_{(aq)} + S_5O_6^{2-}{}_{(aq)}$

(30) $S_3O_6^{2-}{}_{(aq)} + H_2O_{(l)} \rightarrow S_2O_3^{2-}{}_{(aq)} + SO_4^{2-}{}_{(aq)} + 2H^+_{(aq)}$

(31) $2S_5O_6^{2-}{}_{(aq)} \rightarrow S_4O_6^{2-}{}_{(aq)} + S_6O_6^{2-}{}_{(aq)}$

(32) $S_6O_6^{2-}{}_{(aq)} \rightarrow S_5O_6^{2-}{}_{(aq)} + S^0{}_{(aq)}$

Because these (and other intermediate S) reactions occur rapidly, concentrations of the less-stable S compounds are generally difficult to measure in aquatic systems; however, they can result in the replenishment, depletion, or transformation of more stable S-phases (i.e. $S_2O_3^{2-}$, SO_4^{2-}, S^0, and sulfides) and can significantly contribute to the overall cycling of Fe, S, and C (Reese *et al.*, 2002; Hansel *et al.*, 2015).

The thermodynamic ladder is used throughout geobiochemistry to predict favorable redox reactions between electron donors and terminal electron acceptors. Based on this energy-based hierarchy, microbial reduction of ferric Fe compounds is expected to dominate over MSR in low-SO_4^{2-} terrestrial and freshwater environments; therefore, SO_4^{2-} reduction is assumed to minimally impact Fe cycling in these systems (Hansel et al., 2015). Column experiments by Hansel *et al.*, 2015 suggest that SO_4^{2-} reduction may precede or occur concurrently with Fe reduction, implying that observations of end-product concentrations (e.g. dissolved porewater Fe & S-compounds) is insufficient for gaining insight into the cycling of Fe and S. In these column experiments, nearly 40% of the observed reduction of ferrihydrite was coupled to oxidation of sulfide to ZVS. This was followed by re-reduction of ZVS to sulfide and further coupled Fe-sulfide redox, accounting for an additional 30% of observed ferrihydrite reduction. These results demonstrate that low concentrations of SO_4^{2-} can drive large-scale cycles of Fe, suggesting that the role of S in the cycling of Fe in freshwater and terrestrial environments has been largely overlooked.

1.7 X-RAY ABSORPTION SPECTROSCOPY

X-ray absorption spectroscopy (XAS) has emerged as an effective technique for element-sensitive studies of environmental systems due to its ability to nondestructively analyze samples under anoxic conditions (Zeng *et al.*, 2013). X-ray absorption near edge structure (XANES) is a XAS technique capable of describing the oxidation state and distribution of key elements, including Fe and S (Al-Sid-Cheikh *et al.*, 2015; Zeng *et al.*, 2013). Another form of XAS,

Extended X-ray absorption fine structure (EXAFS), allows for characterization of the local chemical environment, including interatomic distances between bonded atoms and identification of nearest neighboring atoms (Bhattacharyya *et al.,* 2017). Utilization of XAS for the characterization of Fe and S minerals and compounds in sediments collected from SO_4^{2-} impacted aquatic systems may elucidate the transport, fate, and overall influence of elevated surface water SO_4^{2-} on the porewater and sediment biogeochemistry and mineralogy (Mitchell *et al.,* 2009; Prietzel *et al.*, 2009). XANES provides oxidation state information by exciting and ejecting inner-shell electrons using high-energy, monochromatic X-rays (Teo, 1986). As the energy of the incident X-rays increases, it reaches an energy capable of causing the excitation and subsequent ejection of inner-shell electrons; the incident X-ray energy required to eject inner-shell electrons is called the "K-edge" and this is unique to each element and varies slightly based on oxidation state (Teo, 1986; Martinez, 2007; Wu, 2014).

During a normal XAS scan, the energy of the incident X-rays starts a few hundred eVs below the K-edge and the wavelength of incident radiation is gradually decreased (Teo, 1986). When the incident X-ray energy reaches the K-edge (~2.4720keV for S, ~7.1120 for Fe) the intensity of fluoresced photons increases by several orders of magnitude, resulting in the characteristic "white line" edge jump (Teo, 1986). An analyte that is more positively charged (oxidized) requires greater energy to eject a core electron and, conversely, an analyte that is more negatively charged (reduced), requires less energy to eject core electrons (Teo, 1986; Liu *et al.*, 2014; Wu, 2014). The spectra resulting from XANES are compared with mineral standards of known composition (Teo, 1986; Couture *et al.*, 2013). Peak shifts in the sample due to differences in oxidation state can be compared to mineral standards to determine the distribution of analyte charge in the original sample.

As the energy of incident X-rays continues to increase past the K-edge, information related to bond distances between the analyte and neighboring atoms is generated; this is the EXAFS region (Teo, 1986; Wu, 2014). Fluctuations in the spectra produced in the EXAFS region can be attributed to constructive and destructive interference caused by scattering interactions between the outgoing photoelectron and neighboring atoms (Teo, 1986, Bhattacharyya *et al.*, 2017). EXAFS can be used to determine bond lengths between the analyte and neighboring atoms by first normalizing the absorption coefficient (μ) to the background absorptions (μ_o) (Equation 33: Teo, 1986):

(33) $$x(E) = \frac{\mu(E) - \mu o(E)}{\mu o(E)}$$

The absorption rate [x(E)] must then be related to structural parameters by converting the energy into the photoelectron wavevector (k) using the EXAFS equation (Equation 34: Teo, 1986):

(34) $$X(k) = \sum_j \quad N_j S_i(k) F_j(k) e^{-2\sigma_j^2 k^2} e^{-2r_j/\lambda_j(k)} \frac{\sin(2kr_j + \phi_{ij}(k))}{kr_j^2}$$

Where $F_j(k)$ is the backscattering amplitude from each N_j neighboring atoms of the j^{th} type with a Debye-Waller factor of σ_j at a distance of r_j away, $\Phi_{ij}(k)$ is the total phase shift experienced by the photoelectron, e^{-2r_j/λ_j} is due to the inelastic losses in the scattering process, λ_j is the electron mean free path, and $S_i(k)$ is the amplitude reduction factor (Teo, 1986; Wu, 2014). To obtain bond distance data from the photoelectron wavevector, the reciprocal lattice space calculated from equation (25) is Fourier-transformed, resulting in bond distances plotted on the x-axis (Teo, 1986; Ravel and Newville, 2005; Wu, 2014). Several data fitting programs have been created to perform these calculations, allowing for rapid analysis of XAS results (Ravel and Newville, 2005). EXAFS analysis is useful for determining mineral structures; by comparing the

distances of neighboring atoms with known atomic radii and spectra from mineral standards, the atoms neighboring the analyte can be identified, allowing for bulk mineral composition estimates (Teo, 1986; Gong *et al.*, 2012; Zeng *et al.*, 2013).

2. XAS Analysis of Iron and Sulfur Biogeochemical Cycling Under Spatiotemporally Dynamic Redox Conditions in a Sulfate-Impacted, Riparian Wetland.

2.1 BACKGROUND

Second Creek (SC) is a stream located on the 'Iron Range' in Northern Minnesota (Figures 2, 3, & 4). This stream is flanked by a riparian wetland system which is part of an ongoing biogeochemical and hydrologic monitoring study performed by the University of Minnesota, with 3 years of past physical hydrology and biogeochemical data available (Ng *et al.*, 2017; Yourd, 2017). The waters that feed this stream are pumped from Fe-mining waste-rock pits which contain minerals associated with taconite mining in northern Minnesota (including hematite, Fe_2O_3; $(Fe,Mn)CO_3$; goethite, FeO(OH); and Fe sulfides) (Lapakko, 1988; Zanko *et al.*, 2008). Weathering of this waste-rock releases elevated concentrations of SO_4^{2-}, resulting in downstream SO_4^{2-} concentrations in excess of 300mg/L.

The bulk surface water, pore-water, and sediment geochemistry of Second Creek has been previously characterized during the summers of 2015 and 2016 by Ng *et al.*, 2017 and Ng *et al.* (in review); selected results are shown in Figure 5. In general, field observations and reactive transport modeling by Ng *et al.*, 2017 and Ng *et al.* (in review) corroborated the results of the MPCA's field, mesocosm, and hydroponic experiments, supporting a relationship between porewater sulfide accumulation, Fe, and organic C content. Additionally, results from Yourd 2017 indicate hydrologic flux magnitude and direction significantly influence porewater geochemistry; during periods of upwelling, surface water SO_4^{2-} transport into the sediment was found to be relatively limited. Conversely, during periods of downwelling, SO_4^{2-} diffusion into the sediment and subsequent reduction was found to be much more significant. Despite the

abundance of dissolved Fe in the porewater and Fe-containing minerals in the sediment, simulated e^- redox rates from Ng *et al.*, 2017 suggest that the reduction of SO_4^{2-} dominates over Fe reduction in all sampled locations and time periods (Figure 6). This suggests that "cryptic" cycling of S may be the dominant driver of Fe cycling in this freshwater environment.

2.2 MATERIALS, METHODS, AND SAMPLE CHARACTERIZATION

2.2.1 SAMPLING DESCRIPTION

Sediment cores were collected from Second Creek, a SO_4^{2-}-impacted riparian wetland system near Hoyt Lakes, Minnesota. Sediment cores were collected in a transect across the stream channel, the east and west banks of the channel, and from two ponds that flank the stream. The sediment cores were retrieved using an HTH gravity corer in May, June, July, August, and October 2017. Separate sediment cores were collected from each location for porewater collection and sediment sample collection.

For sediment collection, each core was flash-frozen with dry ice, transferred to a portable glove bag purged with nitrogen gas, and subsampled in the field. Each core was subsampled at three depth intervals of approximately 4cm, 10cm, and 20cm from the water-sediment interface. Sediment subsamples were collected at each depth for measurement of acid-volatile sulfide (AVS) content, solid Fe, X-ray absorption spectroscopy analysis, and DNA extractions. 5mL of 1% (w/w) zinc chloride was added to AVS samples for preservation. Approximately five to ten grams of sediment were collected in 40mL I-Chem™ clear VOA glass vials with 0.125in septa for all samples except the DNA samples which were collected in 2.5mL centrifuge tubes. All samples were sealed in mylar bags with an AnaeroPack® satchet, stored on dry ice, and moved to a -80°C freezer until analysis.

Porewater was collected using two distinct methods; multichambered equilibrium dialyzers ("peepers") with wells spaced at 1.56cm vertical intervals were deployed two weeks prior to sampling to allow for high vertical spatial sampling resolution of porewater. Peepers require approximately two weeks to equilibrate, allowing for high spatial resolution, but low temporal precision (U.S. EPA, 2001). To allow for temporally precise measurements, 10-cm Rhizon™ filters (pore size 0.12-0.18μm) were inserted vertically into sediment cores collected specifically for porewater collection. The outlet of the Rhizon samplers were attached with a needle to an evacuated 10mL crimped amber serum vial to draw porewater from the core. Plastic wrap was used to cover the top of the core to prevent oxygen diffusion. The rhizon sampler extracts porewater from 10cm intervals, sacrificing spatial resolution for temporal precision. From both peeper and rhizon samplers, samples were collected for measurement of dissolved sulfide (preserved with 1mL of 1% (w/w) zinc chloride), dissolved bulk cations and anions, and alkalinity. Additionally, methane samples (preserved with 0.05g trisodium phosphate) were collected from the peepers, and porewater pH was measured in the field within an hour of sample collection. All porewater samples were stored on wet ice during transport then transferred to refrigeration in the lab until analysis.

Surface water samples were collected using 1-L Nalgene bottles; these samples were collected for measurement of bulk cations, bulk anions, and alkalinity. Surface water samples were collected in open water prior to sediment sampling to avoid suspended sediment loosened by the gravity corers. The Nalgene bottles were filled and capped below the surface of the water to eliminate head space. These samples were stored on wet ice during transit and stored under refrigeration until analysis.

Piezometers and stream gauges were deployed at Second Creek to record hydrologic conditions throughout the field season. Seven piezometers were installed: three in the channel,

one in the east wetland, one in the west wetland, and one in each pond flanking the creek (Figure 1). Seepage meters were used to measure flux direction in the channel sediment during each sampling interval.

2.2.2 SEDIMENT ANALYSIS

Acid Volatile Sulfides

Acid-volatile sulfides were measured using a method modified from *Allen et al., 1993*. This method measures the fraction of sediment sulfide available for (bio)geochemical reactions. To perform this measurement, 1 to 5 grams of homogenized sediment were transferred from the sampling vial to an Erlenmeyer flask inside a glove bag purged with nitrogen gas. 50mL of deoxygenated nanopure water was added to the flask along with a magnetic stir bar. The flask was then securely stoppered using a S-free rubber stopper with a 10mL glass pipette inserted through the center. Tubing (ATP Vinyl-Flex PVC plastic tubing; 1/8" ID x ¼" OD) was also inserted alongside the glass pipette to serve as an outlet for gas flow. The flask was secured into the AVS apparatus (Figure 7) using Female and Male Cole-Parmer luers with lock rings. A three-way stopcock was inserted at the inlet to allow for simultaneous measurement of multiple sediment samples. The outlet of the Erlenmeyer flask led to an impinger containing ~75mL of nanopure water to retain chloride. The outlet of this impinger led to a second impinger containing ~75mL of 0.05M silver nitrate and 0.517M nitric acid. The entire system was flushed with nitrogen gas at a rate of 1L/minute for 15 minutes with constant stirring followed by an addition of 15mL of 6M hydrochloric acid. After the addition of acid, the flow rate was decreased to 0.2L/minute. After 45 minutes, the second impinger was filtered through a pre-weighed 0.45µm mixed cellulose ester membrane that had been dried at 105°C for 45 minutes. The membrane was then dried again and weighed to determine the mass of silver sulfide that had precipitated. This

mass was used to back-calculate the original amount of sulfide that had been volatilized from the addition of acid.

Extractable Fe

Solid Fe in Second Creek sediment samples was measured using a dithionite extraction modified from *Bhattacharyya et al., 2018*. This method allows for the extraction of nearly all Fe from the sediments (poorly crystalline and "crystalline", non-silicate). For this measurement, 0.5 to 1.0g of sediment was added to a pre-weighed 15mL falcon tube. 10.00 mL of a solution containing 0.3M sodium dithionite, 0.35M sodium acetate, and 0.2M sodium citrate was added to the tube. The tube was inverted several times to thoroughly mix the sediment into the solution. The tube was then placed into a 60^{o} water bath for 4 hours, followed by centrifugation at 4,700 rpm for 5 minutes. The supernatant was then extracted using a 15mL syringe and pressed through a 45µm syringe filter. 20µL of filtered supernatant was then added to a UV-vis cuvette along with 1.44mL of nanopure water, 40µL of 0.2M hydroxylamine hydrochloride, 0.1M hydrochloric acid solution and 1.00mL of 0.005M ferrozine, 2.5M ammonium acetate solution. The sample reacted for 25 minutes before measurement on a Cary 60 UV-vis spectrophotometer at 562nm wavelength.

2.2.3 AQUEOUS GEOCHEMICAL ANALYSES

Bulk Anions and Cations

Anion and cation samples were measured by ion chromatography (IC) using a Metrohm Professional IC Vario 1 AnCat. Anions were measured using the Metrohm protocol 'AN-S-199' with the anion eluent concentration reduced from 8.5mmol/L sodium carbonate to 4.25mmol/L; measured anions included chloride (Cl^-), bromide (Br^-), nitrite (NO_2^-), nitrate (NO_3^-), and SO_4^{2-} (Metrohm, 2019a). Porewater samples collected using peepers and rhizon samplers were prepared

by adding 3.00mL of porewater to an IC sample tube and diluting with 4.00mL of nanopure water.

Cations measured included calcium (Ca^{2+}), sodium (Na^{+}), magnesium (Mg^{2+}), and potassium (K^{+}); these were measured using Metrohm protocol AN-C-103 (Metrohm, 2019b). Porewater samples collected using peepers and rhizon samplers were prepared by adding 2mL of porewater to an IC sample tube, 200µL of 0.1M nitric acid, and 8mL of nanopure water.

Dissolved Phosphate

Due to the high concentration of dissolved Fe previously measured in the porewater of Second Creek (up to 85mg/L), precipitation of Fe in under oxic conditions was of concern (Yourd, 2017). Fe precipitation could lead to sorption of phosphate in the anion samples, so phosphate was measured colorimetrically using acidified samples to avoid precipitation of Fe. Porewater samples were prepared by adding 1mL of porewater to a UV-vis cuvette followed by 100µL of a 0.57mM ascorbic acid, 2.25M sulfuric acid solution and 100µL of a 20.4mM ammonium heptamolybdate tetrahydrate, 1.51mM potassium antimonyl tartrate, 3.18M sulfuric acid solution. The samples reacted for 30 minutes, followed by analysis on a Cary 60 UV-vis spectrophotometer at 880nm.

Dissolved Sulfide

Dissolved sulfide concentrations were measured colorimetrically using a method modified from Cline (1969). 1mL of porewater fixed with 1% (wt/wt) zinc chloride was added to cuvettes followed by 500µL of a N,N-dimethyl-*p*-phenylenediamine sulfate, sulfuric acid, hydrochloric acid, and ferric chloride solution. After a 5- to 10-minute reaction period, the samples were analyzed on a Cary 60 UV-vis spectrophotometer at 670nm.

Dissolved Iron

Concentrations of dissolved ferrous and ferric Fe were measured using a method modified from Stookey, 1970. 40µL of each porewater sample was diluted in 1mL of nanopure water and 1mL of ferrozine acetate reagent; each sample was then thoroughly mixed. After a 25-minute reaction period, the samples were analyzed on a Cary 60 UV-vis spectrophotometer at 562 nm to measure dissolved ferrous Fe. After measurement of dissolved ferrous Fe, 40µL of hydroxylamine HCl was added to each sample and reference standard to reduce all dissolved ferric Fe. The samples and standards were mixed, and after a 20-minute reaction period, total Fe was measured using the Cary 60 UV-vis spectrophotometer at 562 nm. Ferric Fe concentrations were calculated by subtracting the concentration of dissolved ferrous Fe from the concentration of total dissolved Fe.

Alkalinity Measurements

Alkalinity measurements were performed using a colorimetric titration technique. A Bromocresol green solution buffered to pH 4.5 to 4.8 was used to indicate the end point of the titration. Titration measurements were performed in triplicate to ensure reproducible results.

Dissolved Methane

Dissolved methane concentrations were measured using gas chromatography. To perform this measurement, the headspace from each methane sample vial was injected into a gas chromatograph. The concentration of dissolved methane was then calculated using the following equations:

(35) $$C_{samp} = (A_{samp} * C_{std})/A_{std}$$

(36) $$C_{diss} = C_{samp} * \left(\frac{V_{TH}}{V_{Wat}}\right) * \left(\frac{10^{-3}}{R*K}\right) * P$$

Where C_{samp} is the concentration of methane in the sample (partial pressure), A_{samp} is the peak area of the sample, C_{std} is the concentration of methane in the reference standard, A_{std} is the peak area of the reference standard, C_{diss} is the concentration of dissolved methane in the sample, and V_{TH} is the total volume of the headspace.

2.2.4 Fe-EXAFS SPECTROSOPY SAMPLE PREPARATION AND DATA COLLECTION

Sediment samples were shipped to the synchrotron facility inside sealed mylar bags stored on dry ice. Sample preparation was performed inside a glove box purged with oxygen-free nitrogen gas immediately after thawing samples to prevent oxidation or alteration. Fe K-edge EXAFS spectra were collected at the Materials Research Collaborative Access Team (MRCAT) bending magnet station, sector 10-BM at The Advanced Photon Source (APS) at Argonne National Laboratory (ANL) in Lemont, IL equip with a Si(111) crystal monochromator; the storage ring was operated at 7.0 GeV. Powdered Fe(II/III) minerals and organic compounds with well characterized composition were used as reference standards in the analysis. Samples were prepared by pressing the wet sediment paste into a 1x4cm slit bored into a 1/8" polycarbonate sample holder. The sediment was capped on both sides with Kapton film (25µm thick) and the film edges were sealed with Kapton tape. The samples were transported from the glove bag to the beamline inside mason jars purged with oxygen-free nitrogen gas. Fe-EXAFS analysis was performed inside a Lytle detector purged with nitrogen gas to avoid oxidation and to reduce scatter signal. XAS spectra were recorded in fluorescence and transmission modes for reference standards and in fluorescence mode for sediment samples. Principal component analysis (PCA) and linear combination fitting (LCF) was performed using the program Athena (Newville, 2005).

2.2.5 S-XANES SAMPLE PREPARATION AND DATA COLLECTION

Sediment samples were shipped and prepared like the Fe-EXAFS methods listed in 2.2.4. Instead of pressing the samples into a polycarbonate holder, samples were pressed into a 3.5mm hole bored into a polyether ether keton sample holder. The back of the hole was sealed with Kapton tape (25μm thick) and the front was left open to avoid trapped nitrogen gas. S-XANES spectra were collected at The XSD Spectroscopy Group bending magnet beamline, sector 9-BM at APS at ANL using a Si(111) monochromator. Powdered S minerals and organic compounds with oxidation states ranging from -2 to +6 were used as reference standards in the analysis.

S-XANES analysis was performed inside a sealed chamber purged with helium. S-XANES spectra were recorded in fluorescence mode for sediment samples using a 4-element Vortex® SSD and in Total Electron Yield mode for reference standards. PCA and LCF was performed using the program Athena (Newville, 2005).

2.3 RESULTS

2.3.1 PHYSICAL HYDROLOGY

The vertical hydraulic gradient (VHG) data collected from the piezometer in the west wetland at Second Creek (PZI2) are plotted in figure 8; corresponding regional precipitation data is shown in figure 11. PZI2 data indicate that the west wetland hydraulic gradient was mostly positive (upwelling conditions) from June 10th to July 25th, with seven brief reversals; during this time the range of VHG magnitude ranged from -0.009 to 0.008. From July 25th to August 1st, VHG magnitude rapidly increased from -0.001 to 0.043. Except for two brief reversals in early August, VHG magnitude remained positive for the remainder of the field season, ranging from -0.013 to 0.12.

Vertical hydraulic gradient data from the east channel and center channel piezometers (PZCE and PZCC, respectively) of Second Creek are plotted in figures 9 and 10. Data from PZCE indicates that the channel hydraulic gradient was negative from June 10th to July 28th with a VGH magnitude ranging from -0.05 to 0. VGH magnitude became positive on July 28th but reversed shortly afterwards on August 8th. After August 8th, VGH magnitude reversed again, remaining positive with an average magnitude between 0 and 0.16 for the remainder of the field season.

The east wetland piezometer (PZE2) had similar variations in flow direction to piezometer PZCC (Figure 11). From June 10th to July 29th, VHG magnitude was negative with a range of 0 to -0.02. From July 29th to August 10th, VHG reversed several times, then remained positive for the remainder of the field season with magnitudes ranging from -0.009 to 0.24. Two large peaks in VHG magnitude occurred in late September and early October with magnitudes nearly twice the maximum measured by any other piezometer.

2.3.1 GEOCHEMISTRY OF SURFACE WATER, SEDIMENT POREWATER, AND SEDIMENTS

pH remained circumneutral in all locations with a minimum of 6.5 and a maximum of 8.3 (figure 13). Generally, pH decreased with depth from the sediment-water interface leveling off at ~20cm in the west wetland, ~5cm in the channel, and within the first few centimeters of the east wetland. Porewater pH seems to be slightly lower in the wetlands than in the channel, with average porewater pH measurements of 7.1 and 7.2 respectively. Averaging all pH measurements with depth for all locations shows pH is slightly elevated above the sediment-water interface (pH~7.6) and sharply decreases below the sediment-water interface (pH~7.25). pH continues to decrease throughout the sampled length, reaching an average pH of approximately 7.0 between 40-50cm depth.

2.3.2 SPECIATION AND CONCENTRATION OF POREWATER Fe AND S

Porewater Fe

Pore-water dissolved Fe concentrations are generally highest in the west wetland (121-1128µM range; 400±200µM average) and lowest in the channel (32-427µM range; 150±90µM average) with intermediate concentrations in the east wetland (74-870µM range; 400±200µM average) (Figure 14; Table 1). Ferrous Fe predominates as the primary species of dissolved Fe in all three locations, comprising 80±10% of the dissolved Fe in the channel porewater and 91±6% and 90±5% the east and west wetland porewater, respectively. Dissolved Fe concentrations are low in the surface water (<10µM) but dramatically increase below the sediment-water interface.

Porewater Sulfate

Concentrations of porewater SO_4^{2-} in the sediments of Second Creek steadily decrease with depth in the Channel and west wetland, leveling off to concentrations of 30±20 and 20±10mg/L, respectively, at a depth of ~5cm (Figures 15, 16, and 17). East wetland porewater measurements show similar trends to the channel and west wetland in August (leveling off to a concentration of 14±1mg/L) and July, although July SO_4^{2-} concentrations remain elevated throughout the sampled depths with an average concentration of 50±3mg/L. Concentrations of SO_4^{2-} at Second Creek are similar with depth and time below ~5cm during the months of June, August, and October in the channel and west wetland with average concentrations of 20±10 and 14±5mg/L, respectively; but, like in the east wetland, average concentrations are comparably elevated in July (50±10 and 40±3mg/L, respectively). In the east wetland, SO_4^{2-} concentrations decrease from 49±3mg/L in July to 14±1mg/L in August. In October, the duplicate peepers in the east wetland indicate differing trends of porewater SO_4^{2-}; one reaching concentrations in excess of 120mg/L before decreasing to 14±1mg/L at a depth of ~30cm, the other remains at low

concentrations (7±2mg/L) throughout the sampled depth. Rhizon samples generally measured elevated concentrations of SO_4^{2-} relative to the peeper samples, suggesting dynamic SO_4^{2-} concentrations over 2-week timescales.

Porewater Sulfide

Concentrations of porewater sulfide were low in all three locations, with an overall average porewater concentration of 0.17mg/L (0.006 to 1.08mg/L range) (Figure 18). Dissolved sulfide concentrations were generally higher in the east and west wetlands than in the channel, with average concentrations of 0.19, 0.18, and 0.12mg/L, respectively. Concentrations of dissolved sulfide are generally constant during June and August for all locations, but more variability occurs during the July and October sampling periods. In July in the west wetland, sulfide concentrations appear to rise from ~30cm depth to ~40cm depth, increasing to an average concentration of 0.6mg/L. In the channel, the July peepers indicate dissolved sulfide concentrations are elevated to ~0.8mg/L near the surface, then steadily decrease to normal values below ~10cm. In the east wetland, dissolved sulfide concentrations increase to ~10cm, then decrease steadily over the sampled depths.

2.3.3 EXTRACTABLE Fe AND AVS FRACTION

The channel and west wetland have comparable concentrations of extractable Fe (139.8 and 136.2 µmol Fe/g sediment average, respectively) while the east wetland has a greater amount of extractable Fe (160.0 µmol Fe/g sediment average) (figure 19). In the east and west wetlands, extractable Fe content is generally elevated in the upper sampling interval (~4cm depth) and decreases with increasing depth. There are two exceptions to this trend: the first is during the October sampling period in which the east wetland increases in concentration from the upper interval to the middle interval (~10cm), then decreases to the bottom interval (~20cm). The

second exception is during the August sampling period in which the west wetland increases in extractable Fe content with depth. In the channel, extractable Fe is comparably less variable with depth, except during the July sampling period, during which an increased amount of extractable Fe is present in the upper sampling interval.

Measurements of acid-volatile sulfides represent the fraction of sulfide in the sediments available for biogeochemical interactions. The AVS sediment fraction is comparable in the channel and the east wetland (51.1 and 53.8 µmol S/g sediment average, respectively); the west wetland has a higher AVS fraction (94.9µmol S/g sediment average). The AVS fraction is nearly always less than the fraction of sediment Fe, except for in the west wetland in June in which the Fe:AVS ratio at the top, middle, and bottom sampling intervals are 0.82, 0.90, and 2.85, respectively. The average Fe:AVS ratio in the west wetland is the lowest of the three sites (Fe:AVS = 2.89), followed by the east wetland (Fe:AVS = 3.92) and the channel has the highest sediment Fe:AVS ratio (Fe:AVS = 6.73).

2.3.5 MOLECULAR-SCALE CHARACTERIZATION OF SEDIMENT IRON

The normalized Fe K-edge EXAFS spectra and results of corresponding LCFs for the west wetland, channel, and east wetland are shown in figures 20, 21, and 22, respectively. Principle component analysis indicates that 93.4% of the variance of the 42 sample EXAFS spectra can be fit using four principal components. Adding a fifth component increases the fit to 94.8%. Target transform analysis found that all reference standards appeared to be suitable components for data analysis; therefore, all reference standards were incorporated into all LCF fits (Table 2; Figure 23). Optimal fits were selected using the minimum number of components, with additional components added only if the additional components improved the r-factor by at least 15%.

Ferrous sulfate and ferrous chloride were found to be a major component in many sediment samples. The high solubility of these compounds decreases the likelihood of these compounds remaining stable as solids in the sediments; instead, these components likely represent ferrous Fe adsorbed to mineral surfaces. The ferrous salts analyzed during Fe K-edge EXAFS were hydrated, so interactions between the ferrous Fe atoms and the surrounding waters of hydration are likely to dominate over interactions between the ferrous Fe and the accompanying anion. Furthermore, replacing ferrous sulfate with ferrous chloride when performing linear combination fits resulted in in the same net percent composition of ferrous salts. For these reasons, the total net fractions of ferrous sulfate and ferrous chloride have been combined and will be referred to as "adsorbed Fe(II)". As with the ferrous salts, the ferric chloride reference standard likely represents ferric Fe adsorbed to mineral surfaces due to its high solubility and the hydrated nature of the salt used for analysis. For these reasons, fits of ferric citrate will be referred to as "adsorbed Fe(III)".

A small number of samples had chalcopyrite indicated as a possible fit component. Due to the similarity between the line form of the reference spectra of pyrite and chalcopyrite, these components have been combined and referred to as "iron disulfide" in figures 20 through 22. Table 2 lists the fractional composition of these two reference standards separately. This high level of similarity is likely due to Fe being bound to S in the mineral structure, resulting in little interactions between Fe and copper at the molecular scale.

West Wetland

Linear combination fits of sediments collected in the west wetland of Second Creek show highly dynamic spatial and temporal Fe mineralogy. In June, Fe monosulfide (FeS; mackinawite) is present at all depths ranging from ~25 weight percent Fe in the middle and lower sampling intervals to 42% in the upper interval. The only other Fe-species measured in the upper sediment

interval was adsorbed Fe(II). Biotite comprises ~43 wt% of the Fe-bearing minerals in the middle sampling interval and adsorbed Fe(III) comprises the remaining 32%. Fitting of the lower sediment interval detects several additional Fe-compounds including adsorbed Fe(II), vivianite, Fe disulfides, and pyrrhotite.

In July, the west wetland sediments are much less variable than other months. Both the upper and lower sampling intervals contain similar weight percent biotite, adsorbed Fe(II), adsorbed Fe(III), and Fe disulfide. The lower sampling interval contains a small fraction of mackinawite.

In August, the three sampling intervals from the west wetland display differing mineralogies. The upper interval is primarily comprised of adsorbed Fe(II) with a small amount of Fe disulfide. The middle sampling interval contains biotite and vivianite with smaller amounts of adsorbed Fe(II) and Fe disulfide. The lower sampling interval is primarily comprised of biotite and adsorbed Fe(III), with a small fraction of Fe disulfide.

In October, the upper and middle sampling intervals from the west wetland are nearly identical. Both intervals contain ~13% biotite, ~30% adsorbed Fe(II), ~22.5% vivianite, ~7% Fe disulfide, and ~27.5% mackinawite. The lower sampling interval is comprised of over 40% biotite, ~40% adsorbed Fe(III), ~10% adsorbed Fe(II), and <10% Fe disulfide.

Channel

The fits for sediments collected in the Channel of Second Creek show comparably less variable mineralogy compared to the west wetland. In June, adsorbed Fe(II) and mackinawite are the dominant Fe-bearing species in the upper sampling interval, with biotite and adsorbed Fe(III) comprising less than 25% of the remaining Fe-bearing species. In the middle sampling interval,

biotite and adsorbed Fe(II) are the only two Fe species present. The lower sampling interval is primarily composed of biotite and ferrihydrite with about 10 wt% Fe disulfides.

In July, all three sampling intervals are nearly identical with all intervals containing similar amounts of biotite (31 wt% Fe average), adsorbed Fe(II) (25 wt% Fe average), adsorbed Fe(III) (21 wt% Fe average), and Fe monosulfide (23 wt% Fe average).

In August, LCF indicate the channel sediments primarily contain biotite and adsorbed Fe(III) in the upper sampling interval. In the middle interval, the biotite and Fe(III) fractions decrease to less than 35 wt%, with adsorbed Fe(II) and Fe monosulfide comprising the remaining fraction. At the lower sampling interval, biotite and adsorbed Fe(III) are below detection (<5 wt%), with only adsorbed Fe(II) and Fe monosulfide fit to the sample spectra.

October sediment samples contain similar Fe-bearing compounds at all depths, with biotite, adsorbed Fe(III), adsorbed Fe(II), and Fe monosulfide comprising the upper sediment interval in approximately equivalent fractions. The middle sediment interval contains slightly less adsorbed Fe(III) and Fe(II) and also contains ~8 wt% Fe disulfide. The bottom sediment interval is similar to the upper interval, with less Fe monosulfide and a larger fraction of adsorbed Fe(III) and Fe(II).

East Wetland

Sediments collected from the east wetland is similar in Fe composition to the channel during most sampling times and sediment intervals. In June, the upper sampling interval contains adsorbed Fe(II), pyrrhotite, and Fe monosulfide, with a small fraction of adsorbed Fe(III). The middle and bottom sampling intervals are nearly identical, with both intervals containing only biotite and adsorbed Fe(II).

In July, the upper and middle sampling intervals both contain biotite, adsorbed Fe(II) and Fe(III), and Fe monosulfide; the lower sediment interval was not analyzed using Fe K-edge EXAFS. The middle sampling interval contains slightly less Fe monosulfide than the upper interval, with biotite and adsorbed Fe(II) comprising a slightly larger fraction.

In August, the upper interval of the east wetland sediments contain nearly equal fractions of adsorbed Fe(II) and Fe monosulfide. The lower sampling interval also contains nearly equal fractions of these components, but it also contains a smaller fraction of biotite and adsorbed Fe(III). The middle sampling interval was not analyzed using Fe K-edge EXAFS.

The east wetland samples collected in October have a high degree of spatial variability; the upper sediment interval contains nearly equal parts of adsorbed Fe(II), vivianite, and Fe monosulfide. In the middle sampling interval contains biotite, adsorbed Fe(II), goethite, Fe disulfide, and Fe monosulfide. The lower sampling interval contains biotite, adsorbed Fe(III), Fe disulfide, and pyrrhotite.

2.3.6 MOLECULAR-SCALE ANALYSIS OF SEDIMENT SULFUR

The normalized S-XANES spectra and the results of corresponding LCFs for the west wetland, channel, and east wetland are shown in figures 24, 25, and 26, respectively. Principle component analysis indicates that 99.4% of the variance of the 22 S-XANES sample spectra can be fit using the top 4 components; adding the fifth component increases the cumulative variance to 99.8%. Target transform analysis indicates that all reference standards are acceptable components for the 22 S-XANES samples; therefore, all reference standards are used in all LCF fits. Optimal fits were selected using the minimum number of components with additional components included only if they improved the r-factor by at least 15%.

The two peaks visible in most spectra are the result of two major pools of S: reduced organic (e.g. methionine, cystine, etc.) and/or inorganic (e.g. mackinawite, chalcopyrite, etc.) S components and ZVS comprise the first peak visible around 2470-2475eV; highly oxidized S compounds (e.g. SO_4^{2-}, thiosulfate) comprise the second peak visible around 2480-2485eV (Zeng *et al.*, 2013).

S-XANES spectra were fit using reference standards selected to represent a range of S oxidation states ranging from -2 to +6, including a mix of inorganic and organic compounds (Table 3; Figure 27). The results of the LCF fits indicated that 26.8% of the S-species in the bulk sediment in all locations contains oxidized forms of S, while the remaining S fraction contains reduced forms of S (73.2%) including organic/inorganic sulfides (37.8%) and ZVS (35.4%). Of the oxidized S fraction, 60.9% is present as thiosulfate and the remaining 39.1% is inorganic SO_4^{2-} (16.3% and 10.5% bulk composition, respectively).

Channel

In the channel, LCFs suggest inorganic SO_4^{2-} is a minor constituent at all depths and time points (<8% average) while reduced S species are generally most prevalent in the sediment column (83.2% average), with ZVS comprising the largest average fraction (40.7%). Oxidized S species appear to increase with depth in the channel, increasing from an average fractional percent of 12.9% at the shallowest sampling interval (~4cm) to 28.1% in the middle sampling interval (~10cm) and finally increasing to 29.6% at the lowest sampled interval (~20cm).

West Wetland

The S speciation of the west wetland is comparable to that of the channel with inorganic SO_4^{2-} comprising a very small fraction of the overall sediments (<6% average) and reduced S species comprising the largest pool of S components (~82.2%). The average fraction of ZVS in

the west wetland (39.7%) is also comparable to that of the channel (40.7% average). During the month of June, the west wetland shows very little variability in sediment composition with increasing depth. In August, LCF results suggest that the pool of oxidized S components increases slightly from the upper sampling interval (~4cm; ~28.3%) to the lower sampling interval (~10cm; ~42.3%). In October, a similar trend is observed with oxidized S compounds increasing from the upper sampling interval (~10cm; ~9.1%) to the lower sampling interval (~20cm; ~19.5%); there is also a shift in the S-components comprising the reduced S fraction, with ZVS comprising a smaller fraction than in previous months and Fe monosulfides, disulfides, and chalcopyrite comprising a larger fraction.

East Wetland

In the east wetland, S components seem to generally mirror those identified in the channel for the upper sampling intervals; however, with increasing depth a greater portion of the S pool is comprised of oxidized S components. In June, no oxidized S components were identified by the LCF results for the upper sampling interval (~4cm), but the oxidized S pool increases to ~48.7% at the middle sampling interval (~10cm) and to ~81.8% in the bottom sampling interval (~20cm).

2.4 DISCUSSION

2.4.1 RELATIONSHIP BETWEEN HYDROLOGY, SULFATE LOADING, AND SUBSURFACE GEOCHEMISTRY

Concentrations of dissolved SO_4^{2-} in the porewater of all three sampled locations are substantially higher during the month of July than most other sampling times (Figures 16-18). This increase in dissolved SO_4^{2-} concentrations occurs after a sharp increase in downward groundwater flux which occurred in late July (Figures 8-11). These results confirm simulations by

Yourd, 2017, supporting the relationship between hydrologic flux and porewater geochemistry. Despite increased concentrations of dissolved SO_4^{2-} in porewater samples collected using peepers, concentrations in porewaters collected using Rhizon samplers during the July sampling trip remain comparable to other sampled months. Due to the extended equilibration period required for the peeper samplers (~2 weeks), these trends suggest rates of SO_4^{2-} reduction are rapid enough to decrease porewater SO_4^{2-} to previous values on short times scales (<2 weeks).

Following the intense increase in surface water flux into the sediment in late July, porewater sulfide concentrations become more varied at each sampled site, with a peak at a depth of ~30cm in the west wetland, an increase in dissolved sulfide in the upper 10cm of porewater of the channel, and a peak around 10cm in the east wetland. Samples collected using rhizon samplers show values closer to previous months, suggesting rapid cycling of these increased sulfide concentrations. No major changes in AVS content is observed from June to July, suggesting very little of the excess SO_4^{2-} has been reduced and precipitated as inorganic sulfide minerals. While sediment samples collected in July were not analyzed using S-XANES, sediment samples collected in August show elevated concentrations of ZVS in sediments collected in the channel and the east wetland.

S-XANES from sediments collected in the west wetland shows an increase in organic monosulfides, inorganic SO_4^{2-}, and thiosulfate from June to August. These results suggest that oxic, SO_4^{2-}-enriched water enters the sediment during the intense period of downwelling and are reduced to sulfide or thiosulfate; thiosulfate may also be produced during partial oxidation of ZVS, as shown in equation 18, or through oxidation of pyrite in the subsurface. The sulfide produced through MSR or disproportionation of thiosulfate may be subsequently re-oxidized forming ZVS during chemotrophic sulfide oxidation by nitrate or O_2. Organic disulfides generally accumulate in sediments through reactions between dissolved sulfide and organic matter, or

through the decay of organic matter (Zeng et al., 2013); simulations and field measurements by Yourd, 2017 suggest the west wetland has a larger pool of organic C than the channel, which may explain the increased concentrations of organic monosulfide generated in the sediments of the west wetland.

Fe K-edge EXAFS results show little variability with sediment depth during the month of July in all locations, suggesting similar cycling and mineralogy of Fe at all depths following an influx of excess SO_4^{2-}. In the channel and east wetland, biotite and Fe monosulfide are the only two minerals identified from LCF, suggesting a small amount of the sulfide generated through MSR is precipitated as sulfide minerals. The remaining fraction of Fe is present as adsorbed Fe(II) and Fe(III). In the west wetland, Fe disulfides are present in elevated concentrations (>25wt% Fe) in the upper sediment interval, and lower concentrations in the lower sediment interval (<10%). This may be caused by the stronger reducing conditions at this location, resulting in the production of more crystalline Fe sulfide minerals rather than re-oxidation to ZVS, SO_4^{2-}, or other S-containing intermediates.

In early October in the east wetland, an intense peak of downward groundwater flux occurs that is >2x the magnitude of most other observed changes in flux. During the October sampling trip one of the duplicate peepers collected from this location show extremely high concentrations of dissolved SO_4^{2-} in the upper ~25cm of the sediment porewater. As in the July sampling period, sulfide measurements indicated elevated concentrations of dissolved SO_4^{2-} in the porewater of the east channel in October at depths of ~25cm and ~45cm. Samples collected using Rhizon samplers show lower concentrations of dissolved sulfide and only slightly elevated concentrations of dissolved SO_4^{2-}, suggesting rapid (<2 week) cycling of S during the downward flux of SO_4^{2-}-enriched surface water into the subsurface. AVS content changes minimally from August to October, suggesting little of the excess sulfide produced from MSR precipitates as

poorly crystalline FeS minerals. Results from Fe K-edge EXAFS show a slight accumulation of Fe disulfide and pyrrhotite in late October, suggesting a small fraction of the S entering the subsurface forms stable, crystalline Fe-bearing minerals that are not measured by AVS. Fit results from S-XANES analysis show an accumulation of ZVS in the upper sediment interval, suggesting a similar response to increased SO_4^{2-} concentrations to previous months. The middle sampling interval shows near equal parts of organic monosulfide, thiosulfate, and inorganic SO_4^{2-}; this could be explained by an accumulation of thiosulfate in the sediment porewater, followed by microbial disproportionation to SO_4^{2-} and sulfide, with subsequent formation of organic monosulfide from the produced sulfide species.

2.4.2 CYCLING OF Fe AND S AND THE ACCUMULATION OF ZVS

ZVS was found to be a primary S-species in most sediment samples collected from Second Creek with its fractional composition varying greatly between months, particularly following periods of increased flux of SO_4^{2-}-enriched surface water into the subsurface. This supports water column and sediment experiments performed by Findlay et al., 2017 which found that, while ZVS can form as a stable end-product under favorable conditions, under unfavorable conditions (i.e. high oxidant to S ratios) ZVS consumption can occur very rapidly, favoring the accumulation of thiosulfate and SO_4^{2-} instead.

Results from S-XANES suggest that FeS comprises a small fraction (<25wt% S) of the total S pool in most sediments, with FeS concentrations below detection (<5wt% S) in over half of the sediment samples. Instead, an accumulation of ZVS, inorganic disulfide, organic monosulfide, and thiosulfate were found to be major sinks of S in the sediments. Results from AVS measurements suggest FeS content is elevated with respect to previously studied systems (Pollman *et al.*, 2017), yet it comprises a small fraction of the overall S pool. Two geochemical mechanisms may be responsible for this:

1. Sulfide formed through MSR may rapidly undergo chemical sulfide oxidation by ferrihydrite or O_2 in the subsurface. Ferrihydrite was only identified by Fe-EXAFS analysis in one of the samples, however the abundance of adsorbed ferrous and ferric Fe, and the high concentrations of porewater Fe could indicate that ferrihydrite forms during periods of downwelling when oxygenated surface water flows into the subsurface. Reduction of ferrihydrite (or O_2) may be coupled to rapid oxidation of porewater sulfide, producing ZVS and ferrous Fe, as shown in equation 14.
2. Fe monosulfide produced under favorable conditions (i.e. anoxic, reducing environment) may become oxidized during periods of downwelling, producing ZVS and ferrihydrite (equation 35: Burton *et al.*, 2009):

(35) $$FeS_{(s)} + \frac{3}{4}O_{2(aq)} + \frac{1}{2}H_2O_{(l)} \rightarrow \frac{1}{8}S^0{}_{8(s)} + FeOOH_{(s)}$$

Additionally, experiments by Wilkin & Barnes, 1996 found that under weakly oxidizing conditions, Fe monosulfides can lose Fe through oxidation to ferrihydrite, forming pyrite (equation 36-37: Wilkin & Barnes, 1996):

(36) $$2FeS_{(s)} + \frac{1}{2}H_2O_{(l)} + \frac{3}{4}O_{2(aq)} \rightarrow FeS_{2(s)} + FeOOH_{(s)}$$

The ferrihydrite produced in equations 35 and 36 may then react with dissolved sulfide, producing more ZVS, as shown in equation 14. Together, equations 35 and 36 may explain the low amount of Fe monosulfide measured in the sediment and the comparably higher fraction of inorganic disulfide minerals and ZVS.

2.5 CONCLUSIONS

2.5.1 IMPLICATIONS FOR "CRYPTIC" S CYCLING IN FRESHWATER ENVIRONMENTS UNDER DYNAMIC HYDROLOGIC FLUX CONDITIONS

During the intense hydrologic shift to losing conditions in late July, porewater samples collected using peepers show SO_4^{2-} concentrations increase dramatically in all sampled locations; dissolved sulfide concentrations also become much more variable. Samples collected using Rhizon samplers show porewater chemistry returns to similar values reported in previous months, suggesting rapid rates of S-cycling. This rapid cycling of S, combined with changes and accumulation of S-intermediates, and a lack of large-scale alteration of Fe-minerals in the sediment, indicate "cryptic" cycling of S may be a primary driver of large-scale geochemical conditions in the subsurface of Second Creek.

2.5.2 IMPACT OF SULFATE-LOADING ON SUBSURFACE GEOCHEMISTRY

Contrary to previous assumptions incorporated into biophysical models which predicted Fe monosulfide acted as an overwhelming sink for excess S, these results show that S intermediates (especially ZVS) comprise the primary pool of S in the subsurface of Second Creek. The dynamic redox conditions present in the subsurface caused by rapid fluctuations in hydrologic flux may allow short-term formation of Fe monosulfide and ZVS during reducing conditions; however, under weakly oxidizing conditions, Fe monosulfides in the sediment may alter to form inorganic monosulfides (i.e. pyrite) and ferrihydrite, or form ZVS and ferrihydrite; additionally, ZVS may form thiosulfate (equation 18 & 19). When redox conditions return to favoring reduction, the ferrihydrite previously produced may oxidize sulfide formed through MSR, producing ZVS; this would explain the lack of ferrihydrite in Fe K-edge EXAFS, the generally high fraction of ZVS in S-XANES, and the mix of Fe monosulfide, inorganic disulfide, and thiosulfate in S-XANES.

2.5.3 FUTURE WORK

While results of this research have confirmed the relationship between hydrologic flux and subsurface geochemical interactions, and found that S intermediates, especially ZVS, are major sinks for excess SO_4^{2-} and sulfide, rather than Fe monosulfide, further investigation may clarify and further confirm the results of this study. Characterization of minerals in the sediments using X-ray diffraction may allow for the confirmation of minerals identified using Fe K-edge EXAFS as well as detection of non-Fe-bearing minerals. S-XANES characterization of sediments collected during the month of July will allow for an understanding of S cycling and fixation immediately following rapid changes in hydrologic flux and subsurface redox. Measurement of total S will allow for quantification of S compounds, allowing for comparisons of S accumulation between sampling times and comparisons between total S and total Fe.

3. Comparison of S and Fe Biogeochemical Cycling in High and Moderate SO_4^{2-}-Containing Environmental Systems.

3.1 BACKGROUND

Two sites were compared for this study: Second Creek; a heavily impacted riparian wetland system near Hoyt Lakes, Minnesota and Sand River; a less-impacted river in northern Minnesota located downstream from Minntac Tailings Basin Cell One (figure 28). The primary sampling site at Sand River was located about ten miles downstream off Highway 169, about 6 miles east of Britt, Minnesota. Surface water SO_4^{2-} concentrations are significantly lower than those measured at Second Creek, with average concentrations of about 50ppm. While SO_4^{2-} concentrations at Sand River are higher than the concentration recommended by the MPCA, they are significantly lower than those measured at Second Creek and wild rice is harvested from this system annually; therefore, this site serves as a 'less-impacted' river system to compare spatiotemporal cycling of Fe, C, and S.

3.2 METHODS

3.2.1 SITES AND FIELD SAMPLING

Three sampling locations were chosen at Sand River to transect an inlet on the north river bank, the center of the river channel, and an inlet on the south river bank (figure 28). Sediment cores were collected in July, August, and October of 2018 using an HTH gravity corer. Each sediment core was flash-frozen with dry ice, transferred to a portable glove bag purged with nitrogen gas, and sampled in the field. Each core was sampled at two intervals at depths of approximately 4cm and 15 cm. Sediment samples were collected for measurement of acid-volatile sulfides, solid Fe, and DNA extractions. Five mL of 1% (w/w) zinc chloride was added to AVS samples for preservation. Approximately five to ten grams of sediment were collected in 40mL I-Chem™ clear VOA glass vials with 0.125in septa for all samples except the DNA samples which were collected in 2.5mL centrifuge tubes. All samples were sealed in mylar bags with an AnaeroPack® satchet, stored on dry ice, and moved to a -80°C freezer until analysis. Porewater and surface water samples were also collected from each sampling location using the methods outlined in section 2.2.1.

Piezometers and stream gauges were deployed at Sand River to record hydrologic conditions throughout the field season. Two piezometers were installed: one near the south inlet and one near the north inlet (Figure 28).

3.2.2 SAMPLE ANALYSIS

Solid Fe from Sand River sediments was measured using a hydrochloric acid extraction method modified from *Bhattacharyya et al., 2018*. While this method does not result in the dissolution of most crystalline Fe phases, it does allow for speciated Fe measurements (ferric vs. ferrous Fe). Two different concentrations of hydrochloric acid (0.1M & 6M) were added stepwise

to understand the extent of sediment Fe reactivity. Sediment samples were prepared as in the dithionite extraction, but instead of adding the dithionite solution, 10.00mL of 0.1M hydrochloric acid was added to the falcon tube followed by inversion. The tube was stored benchtop for 24 hours, followed by centrifugation at 4,700rpm for 5 minutes. The supernatant was extracted using a 15mL syringe and pressed through a 45µm syringe filter and the filtered supernatant was stored under refrigeration for later analysis. 10.00mL of 6M hydrochloric acid was then added to the retained, unreacted sediment followed by inversion and a 24-hour reaction period. The sample was centrifuged at 4,700rpm, and the supernatant was filtered using a 45µm syringe filter. 40µL of the 0.1M extracted supernatant and the 6M supernatant were added to separate UV-vis cuvettes followed by 1.00mL of a 0.005M ferrozine, 2.5M ammonium acetate solution and 1.00mL nanopure water. The samples reacted for 25 minutes followed by measurement on a Cary 60 UV-vis spectrophotometer at 562nm wavelength to measure ferrous Fe. Following the UV-vis measurement, 40µL of a 0.2M hydroxylamine hydrochloride, 0.1M hydrochloric acid solution was added to each cuvette. After 10 minutes the standards were run again on the UV-vis spectrophotometer to measure total Fe. The concentration of ferric Fe is calculated by subtracting the concentration of ferrous Fe from the measured total Fe. AVS measurements were performed as outlined in 2.2.2.

Aqueous geochemical samples were analyzed as outlined in section 2.2.3.

3.3 RESULTS

3.3.1 PHYSICAL HYDROLOGY

Vertical hydraulic gradient data for the piezometer in the north inlet of Sand River (SRN) is shown in figure 29 and head difference data for the piezometer in the south inlet (SRS) is shown in figure 30. Daily precipitation data for the Sand River field site are shown in Figure 31.

Vertical hydraulic gradient data was unable to be calculated for piezometer SRS because the depth of the piezometer screen was not measured; head difference has been calculated instead. The hydrology data suggest that downward flux conditions persist in the north and south inlets of Sand River throughout the field season, with some slight variability during the month of September.

3.3.2 GEOCHEMICAL TRENDS OF THE SURFACE WATER, POREWATER, AND SEDIMENTS

pH

Trends of pH with depth at Sand River and Second Creek are similar, showing little variability with season and decreasing with depth into the sediment. pH is slightly lower in Sand River than in Second Creek, with a maximum of 7.4 and 8.3 respectively, and a minimum of 6.5 at both locations (Figure 32). The pH of the north inlet and channel of Sand River are similar, while the pH of the south inlet is slightly higher with increasing depth into the porewater (Figure 33).

Dissolved Sulfate

Chemical analysis of the surface waters at the north and south inlet of Sand River measured lower concentrations of SO_4^{2-} (2±1 and 3.0±0.8mg/L, respectively) compared to the main channel (55±8mg/L). Concentrations of SO_4^{2-} in the surface water of Second Creek were much higher than those measured at Sand River, with average concentrations of 310±10mg/L measured throughout the field season.

Concentrations of SO_4^{2-} in the porewater at Sand River rapidly decrease with increasing depth in the north inlet and south inlet during all sampling times (Figures 34, 35, and 36). On average, concentrations of porewater SO_4^{2-} are slightly lower in the north and south inlets during

the month of August (0.7±0.2 and 0.31±0.03mg/L, respectively) compared to concentrations measured in October (1.1±0.1 and 0.4±0.2mg/L, respectively). In the channel, porewater SO_4^{2-} concentrations decrease rapidly to an average concentration of 1.5±0.5 below the sediment-water interface during the month of August. Peepers collected in the channel in October had been disturbed, and the data was not able to be utilized.

Concentrations of dissolved SO_4^{2-} are very low in the porewater of Sand River compared to the porewater of Second Creek (figures 15 to 17). While SO_4^{2-} concentrations below the sediment-water interface at Sand river generally level off to concentrations <1mg/L, concentrations of SO_4^{2-} at Second Creek remain elevated, even at depth, ranging from ~14 to ~50 mg/L.

Dissolved Sulfide

Measurements of dissolved sulfide in the sediment porewater of Sand River are plotted in figure 37. Measurements of dissolved sulfide in porewater collected using rhizon samplers in June are similar to those measured in August in the north inlet, with average concentrations of 0.112±0.003mg/L in the upper interval and 0.09±0.02mg/L in the lower interval. All three sampling locations had similar average concentrations of dissolved sulfide in August, with 0.14±0.08mg/L measured in the south inlet, 0.15±0.06mg/L measured in the channel, and 0.2±0.1mg/L measured in the north inlet. Peeper sulfide samples were not collected during the month of October, but rhizon samples indicate concentrations of dissolved sulfide were comparable to August in the south inlet and channel, but higher in the upper sampling interval of the north inlet, reaching a maximum concentration of 0.554mg/L.

Concentrations of dissolved sulfide in the porewater of Sand River are comparable to those measured in the porewater of Second Creek. Second Creek had an average porewater

sulfide concentration of 0.17mg/L which is only slightly higher than Sand River's overall average of 0.16mg/L, despite Second Creeks much higher concentrations of dissolved SO_4^{2-} in the surface water and porewater.

Dissolved Iron

Concentrations of dissolved ferrous and ferric Fe were measured in the porewater of all three locations at Sand River during the month of August (Figure 38). Average concentrations of dissolved Fe in all three locations were similar, with 600±100µM (302.1-813.2 µM range) measured in the north inlet, 600±200µM (277.7-1004.9 range) in the channel, and 600±200µM (121.0-842.4µM range) measured in the south inlet. Ferrous Fe is the dominant Fe-species at nearly all depths and locations, comprising 94±9% of the total Fe fraction. Dissolved Fe concentrations are low in the surface water (<5µM) but increase rapidly below the sediment-water interface.

Concentrations of dissolved Fe in the porewater of Sand River are much higher than concentrations measured in the porewater of the channel at Second Creek (150±90µM) and slightly higher than in the wetlands (400±200µM). The fractional percent of ferrous Fe is similar in the porewater of Sand River to the east and west wetlands of Second Creek (91±6% and 90±5%, respectively), and higher than Second Creek's channel (80±10%).

Total Extractable Fe

Concentrations of extractable Fe are depicted in figures 39, 40, and 41. Extractable Fe content is the highest in the lower sediments collected in the channel of Sand River, with an average concentration of 300±200µmol Fe/g. Fe content is lower in the sediments in the upper sampling interval, with an average concentration of 140±20µmol Fe/g. Extractable Fe content is lowest in the north inlet, with an average of 90±30µmol Fe/g in the upper sediment interval and

120±70µmol F/g in the lower sediment interval. The extractable Fe content in the south inlet is reversed with respect to the channel and north inlet, with a lower concentration of extractable Fe in the lower sampling interval (84.4µmol Fe/g) and elevated Fe in the upper sediment interval (221.8µmol Fe/g).

Ferrous and Ferric Fe Fractions in the Sediments

Ferrous Fe comprises 70±10% of the total Fe present in the sediments collected from the north inlet at Sand River. In the channel, ferrous Fe is the primary Fe-species in the upper sediment interval (59±7%); however, in the lower sediment interval, the ferrous Fe fraction decreases to 40±20%. In the south inlet, ferrous Fe is decreased in the upper sediment interval (27%), and slightly elevated in the lower interval (64%).

The Fe from Sand River sediments were extracted using two different concentrations of acid: 0.1M HCl was used to measure the 'easily extracted' fraction of Fe and 6M HCl was used to measure the remaining HCl extractable Fe fraction. In the north inlet, easily extracted ferrous Fe comprises a small fraction of the total ferrous Fe measured during the month of July, with only 18.9% in the upper sediment interval and 20.7% in the lower sediment interval. In August, the easily extractable ferrous Fe fraction increases to 47.8% in the upper sediment interval and decreases to 12.4% in the lower interval. In October, the easily extractable ferrous Fe fraction increases to 73.1% and 74.6% in the upper and lower sediment intervals, respectively.

The easily extracted ferric Fe fraction comprises a small amount of total ferric Fe measured in the north inlet with an overall average of 13±8%. The easily extracted ferric Fe fraction is highest in July with 28.6% and 16.7% in the upper and lower sediment intervals, respectively. In August, both the upper and lower sediment intervals have decreased easily extracted ferric Fe fractions, with 14.2% measured in the upper sediment interval and 9.4%

measured in the lower sediment interval. The easily extracted ferric Fe fraction continues to decrease in October, with only 0.2% measured in the upper sediment interval and 10.9% measured in the lower interval.

In the channel, the easily extracted ferrous Fe comprises a large fraction of total ferrous Fe, with 74.4% and 97.1% in the August upper and lower sediment intervals, respectively. This fraction decreases in October, with 56.6% of the total ferrous Fe extracted easily in the upper sediment interval and 47.5% in the lower interval.

The easily extracted ferric Fe fraction is low in the upper sediment interval of the channel with no easily extracted ferric Fe present in August and only 6% of the total Fe was easily extracted in October. In the lower sediment interval, 24.5% of the extractable ferric Fe was easily extracted in August, and only 9% was easily extracted in October.

41.0% of the ferrous Fe in the upper interval of the south inlet is easily extracted during the month of October; 14.8% of the ferrous Fe is easily extracted in the lower sediment interval. The fraction of easily extracted ferric Fe is low in the upper sediment interval (9.0%) and none of the ferric Fe is easily extracted in the lower interval.

Extractions of Fe in the sediments of Second Creek were performed using a dithionite extraction, which should allow for extraction of more crystalline Fe-phases than the HCl extraction technique used to extract Fe from the sediments of Sand River, but the dithionite extraction does not allow for distinctions between ferrous and ferric Fe. Despite the wider range of Fe minerals extracted from Second Creek samples, the lower sediment interval in the channel of sand river had much more extractable Fe than sediment measured in any of the Second Creek sediments. The east wetland, channel, and west wetland of Second Creek had average measured

sediment Fe concentrations of 160.0, 139.8, and 136.2µmol Fe/g, which are far lower than the 300µmol Fe/g average measured in the lower sediment interval of Sand River.

Acid Volatile Sulfides

Results of AVS measurements from sediments collected from the north inlet, channel, and south inlet of Sand River are plotted in figures 42, 43, and 44, respectively. AVS content is generally low in Sand River with respect to other SO_4^{2-}-impacted systems, with an overall range of 0.56-13.05µmol S/g. In July, the north inlet AVS content is similar in the upper (5±3µmol S/g) and lower (4±1µmol S/g) sediment intervals. In August, AVS content in the north inlet is elevated in the upper sediment interval (5±1µmol S/g) and decreased in the lower interval (3±1µmol S/g). In October, the upper and lower sediment intervals of the north inlet both contain low amounts of sulfide, with 1.06 and 1.54µmol S/g, respectively.

In the channel, AVS content is elevated in the upper sediment interval (13.05µmol S/g) during the month of August and decreased in the lower interval (1.68µmol S/g). Both the upper and lower sediment intervals contain low amounts of AVS in the channel during the October sampling trip, with 1.4±0.5 and 1.2±0.6µmol S/g measured in the upper and lower sediment intervals, respectively.

The south inlet contains low amounts of sulfide during the August sampling trip, with 0.56µmol S/g measured in the upper sediment interval and 0.76µmol S/g measuring in the lower interval.

Acid-volatile sulfide content in the sediment of Sand River are far lower than those measured in the sediment of Second Creek. The east wetland, channel, and west wetland of Second Creek contained 94.9, 51.1, and 53.8µmol S/g on average, respectively. These measurements are more than an order of magnitude higher than average values in the north inlet,

channel, and south inlet of Sand River (3.2, 4.3, and 0.7µmol S/g, respectively). Ratios of Fe:AVS in the sediments collected from Sand River are far higher than the Fe:AVS ratio in the sediments of Second Creek, and the trends of total Fe with depth do not seem to reflect the trends of AVS content with depth at Sand River, as they do for Second Creek.

3.4 DISCUSSION

3.4.1 BIOGEOCHEMICAL CYCLING OF FE AND S

While porewater dissolved sulfide concentrations are comparable between Second Creek and Sand River, concentrations of surface and porewater SO_4^{2-} and AVS content are much higher at Second Creek and concentrations of porewater and sediment Fe are generally higher at Sand River. Simulations from Pollman *et al.*, 2017 found a relationship between concentrations of surface water SO_4^{2-}, sediment Fe, TOC, and porewater sulfide with increased concentrations of sediment Fe resulting in lower concentrations of porewater sulfide (through the production of dissolved Fe and subsequent formation of Fe sulfide minerals), and increased concentrations of TOC, and surface water SO_4^{2-} resulting in increased concentrations of dissolved sulfide by facilitating MSR.

The higher concentrations of dissolved SO_4^{2-} and the lower concentrations of sediment Fe at Second Creek relative to Sand River suggest that porewater sulfide concentrations should be higher at Second Creek than at Sand River if TOC concentrations are comparable between the two sites. Since porewater sulfide concentrations are similar between the two sites, this may suggest that TOC content is lower in the subsurface of Sand River than Second Creek, resulting in incomplete or limited MSR. This could explain the higher concentrations of dissolved SO_4^{2-} in the sediment porewater and the abundance of intermediate organic S-species (e.g. organic monosulfides) in the subsurface of Second Creek.

Despite the elevated concentrations of SO_4^{2-} in the channel of Sand River, AVS content decreases throughout the field season. This may imply that, like at Second Creek, Fe monosulfide minerals are not the primary sink for excess SO_4^{2-} in this system. The low concentrations of dissolved SO_4^{2-}, dissolved sulfide, and AVS may suggest that S intermediates (e.g. ZVS, thiosulfate, organic sulfides) comprise a larger pool of S than previously expected. The constant downward flux of oxygenated surface water into the subsurface coupled with the availability of weakly-crystalline and dissolved Fe in the subsurface may facilitate the production of S intermediates rather than the precipitation of Fe monosulfides. Alternatively, the constant downward flux of oxygenated surface water may result in the conversion of Fe monosulfide to Fe disulfides (i.e. pyrite), as shown in equation 36. This would decrease the amount of sediment sulfide detected in AVS measurements while also depleting AVS concentrations throughout the season.

3.4.2 FUTURE WORK

Quantification of sediment Fe from sediments collected from Second Creek using the same method used to extract Fe from Sand River sediments may provide a better comparison and allow for a more thorough understanding of Fe-bearing mineral phases in the subsurface. Utilizing XAS characterization to study sediments from Sand River will provide information related to Fe mineral formation and changes in S oxidation state in the porewater and sediments. This will elucidate the role of "cryptic" S cycling at Sand River and allow for a more thorough comparison between these two sites. Additionally, measurement of TOC in the sediments of both systems could be used to confirm the relationship between dissolved sulfide, TOC, dissolved SO_4^{2-}, and sediment Fe suggested from models by Pollman *et al.*, 2017.

Continued monitoring of Sand River and Second Creek may allow for more opportunities to identify differences and similarities between the two sites, especially during short-term

fluctuations of hydrologic flow. During the 2018 field season, the sites monitored at Sand River were continuously losing systems; if losing conditions were to suddenly intensify, the resulting changes in geochemical conditions could be compared to the changes observed during the hydrologic shift observed at Second Creek in July 2017. Continued observations and sample collection would also provide more porewater and sediment geochemical data, allowing for more thorough comparisons and identification of both long-term and short-term relationships between hydrology, SO_4^{2-} loading, and subsurface biogeochemistry.

4. Summary of Geochemistry of Wild Rice Waters

4.1 BACKGROUND

Surface water samples, hydrology data, and sediment cores were collected from six lake and river systems in northern Minnesota and Wisconsin during the summer and fall of 2018 as part of the University of Minnesota's Grand Challenges *Kawe Gidaa-Naanaagadawendaamin Manoomin* project. This project was designed with three primary objectives:

1) The development of respectful, reciprocal working relationships between the University of Minnesota and Tribal nations.
2) Identification of concerns regarding wild rice growth, health, and anthropogenic and ecological impacts.
3) Collaboration between Tribal nations and the University to utilize understanding of biophysical processes influencing wild rice to implement better protection for wild rice.

Through collaboration with Tribal partners, nine water bodies were selected for preliminary biophysical surveying during the 2018 field season based on Tribal concerns, wild rice abundance, and previous studies/monitoring. Six sites were selected for detailed geochemical analysis. Of these sites, three were found to have abundant wild rice growing at the time of

sampling (Clam Lake, Perch Lake, and Sand River). The other three sites (Big Rice Lake, Lake A, and Twin Lakes) had little to no wild rice growth, despite reports of historic growth. Biophysical monitoring of these sites provided an opportunity to identify potential biophysical or ecological issues different sites may be facing, development of analytical methods for studying the biogeochemistry of the sediments, surface, and porewater, and further develop relationships between the University and Tribal partners.

4.2 METHODS

4.2.1 SITES AND FIELD SAMPLING

Sample Collection

Surface water samples and sediment cores were collected from six lake and river systems in northern Minnesota and Wisconsin during the summer and fall of 2018 as part of the University of Minnesota's Grand Challenges *Kawe Gidaa-Naanaagadawendaamin Manoomin* project. Of these sites, three were found to have abundant wild rice growing at the time of sampling (Clam Lake, Perch Lake, and Sand River). The other three sites (Big Rice Lake, Lake A, and Twin Lakes) had little to no wild rice growth, despite reports of historic growth.

Surface water samples were collected as outlined in 2.1.2. Sediment cores were collected from each site using an HTH gravity corer. Several sediment cores were collected for porewater extraction using Rhizon samplers, as described in 2.1.2. Porewater samples were collected for measurement of dissolved sulfide (preserved with 1mL 1% (w/w) zinc chloride), alkalinity, and bulk cations and anions. The Rhizon samplers extracted porewater from the top (0-10cm) sediment interval and the lower (13-23cm) interval. Porewater samples were stored on wet ice during transport, then transferred to refrigeration until analysis. 'Peepers' were deployed and sampled at one of the lakes in this study, Sand River. Peepers were deployed and sampled as outlined in 3.2.1.

Sediment samples were collected by flash-freezing a portion of the sediment cores using dry ice, then subsampling the cores in a portable glove bag purged with nitrogen gas in the field. The cores were subsampled at two depths; shallow sediment samples were collected at ~4cm depth and deeper samples were collected at ~15cm depth. Sediment samples were collected for measurement of acid volatile sulfides, solid-phase Fe, and DNA extractions. The AVS and solid Fe samples were collected and stored in 40mL I-Chem™ clear VOA glass vials with 0.125in septa and the DNA samples were collected in 2.5mL centrifuge tubes. All sediment samples were sealed in mylar bags with an AnaeroPack® satchet, stored on dry ice, and moved to a -80°C freezer until analysis.

Project Sites

Clam Lake

Clam Lake is a lake in northwestern Wisconsin, about 2.5 miles from Siren, Wisconsin. Historically, Clam Lake had been Wisconsin's most productive wild rice lake, with nearly 10,000 pounds harvested in 1997; however, over the following decade, wild rice yields began to decline (Caithamer, 2011). This decline has been attributed to an increase in carp population which impedes wild rice growth by destroying young plants through foraging and decreasing water clarity (Johnson, 2010). The carp population has decreased in recent years through temporary barriers and netting and wild rice growth has been improving. Sediment, porewater, and surface water samples were collected in September 2018 from the southern shore of the lake (Figure 45). Hydrologic monitoring equipment was not deployed at this site.

Perch Lake

Perch Lake is within the Fond du Lac Reservation near Cloquet, Minnesota and the south basin of this lake is the most productive wild rice lake in the Stoney Brook watershed. Two wild

rice management efforts have improved wild rice productivity in the last 20 years. The first was a series of water control structures that were constructed throughout the watershed in the late 1990s to manage hydrological extremes that resulted from extensive ditching in the early 1900s. The second is an ongoing program to remove competing native vegetation that began in the late 2000s. Fond du Lac Resource Management has over 20 years of water quality data on Perch Lake and is partnering with the US Geological Survey to complete a hydrologic model and watershed plan for the Stoney Brook watershed. Fond du Lac also has its own federally approved water quality standards, including a 10mg/L limit for sulfate. Sediment, porewater, and surface water samples were collected near a boat launch on the southeast shore of the lake in August and September 2018 (Figure 46). A piezometer and a stream gauge were deployed at this site during the field sampling trip in August; they were removed in late September.

Sand River

Sand River is in northern Minnesota; its headwaters originate from Twin Lakes which is down-gradient from Minntac Tailings Basin Cell One. This location is of interest because SO_4^{2-} concentrations have been measured above the 10mg/L standard in the surface water, but wild rice growth is unimpaired. Sediment cores were collected for porewater extraction and sediment sampling during the months of July, August, and October 2018. Peepers were sampled during the August and October sampling trips. Sediment, porewater, and surface water samples were collected from an inlet on the northern shore of the river, an inlet on the southern shore of the river, and from the center of the channel between these two points (Figure 28). Stream gauges and piezometers were installed at the north and south shore sampling sites. The monitoring equipment was installed near the north shore in early July, and near the south shore in early August; they were removed in late October.

Big Rice Lake

Big Rice Lake is located 4 miles north of Britt, Minnesota. It has served as a major research site for wild rice restoration and archaeological evidence has suggested that wild rice has actively been harvested at this site for hundreds to thousands of years (DNR, 2013). Sediment cores were collected from the eastern side of the lake for sediment sampling and porewater collection during the months of June and July 2018 (Figure 47). A piezometer was installed at a lake inlet on the east side of the lake in late June; it was removed in late September. The 1854 Treaty Authority had installed a stream gauge on the southeast side of the lake.

Lake A

Lake A is in an undisclosed location and had abundant wild rice historically; however, recently, wild rice growth has ceased. Porewater samples were collected from sediment cores taken from an access point in October (Figure 48). The sediment from this system is highly unconsolidated, making sediment sampling difficult. Additionally, sediment vials were broken during transport, therefore, no sediment geochemistry data is available from this system. No hydrologic monitoring equipment was installed at this site.

Twin Lakes

Twin Lakes is in Brittmount County, Minnesota, near a Minntac tailings basin. Elevated SO_4^{2-} concentrations have been measured in the surface water. Changes in water quality and quantity from Minntac tailing basin releases has resulted in a loss in wild rice at this location. Sediment cores and surface water was collected from the western side of the west lake during June, 2018 and cores and surface water was collected from the western side of the west lake, the inlet on the south side of the west lake, the south side of the east lake, and the outlet on the

northern side of the east lake during September, 2018 (Figure 48). A stream gauge and a piezometer were installed near the geochemical sampling site in late June.

Geochemical Analysis

Sediment samples were analyzed as outlined in 3.2.2. Porewater and surface water samples were analyzed as outlined in 2.2.3.

4.3 RESULTS

4.3.1 CHEMISTRY OF SURFACE WATER AND SEDIMENT POREWATER

Surface water and porewater measurements for dissolved phosphate, nitrite and nitrate, SO_4^{2-}, and sulfide are depicted in figures 49, 50, 51, and 52, respectively. Measurement results for all bulk cations, anions, and sulfide are reported in tables 4, 5, 6 and 7. The results of AVS, porewater sulfide, phosphate, and nitrite and nitrate measurements differ from measurements undertaken by the MPCA; however, this is likely due to differences in measurement techniques.

Big Rice Lake: Phosphate

In June, concentrations of dissolved phosphate increase from the upper interval of sediment porewater (0.4±0.4mg/L average; 0.008 to 0.886mg/L range) into the lower interval of sediment porewater (0.83±0.7mg/L average; 0.767 to 0.909mg/L range). In July, concentrations of phosphate increase from the surface water (0.0895±0.0005mg/L average; 0.089 to 0.09mg/L range) into the upper interval of sediment porewater (1.6±0.1mg/L average; 1.535 to 1.749mg/L range), then decrease slightly into the lower sampling interval (1.4±0.1 average; 1.217 to 1.499mg/L range). Compared to the other sites incorporated in this study, concentrations of dissolved phosphate are low to moderate at Big Rice Lake with an overall average porewater concentration of 1.1±0.5mg/L.

Lake A: Phosphate

Concentrations of dissolved phosphate at Lake A are very low relative to other sites included in this study; three of the five collected samples were below the detection limit of the instrument. The two porewater samples that had measurable concentrations, contained only 0.06±0.03mg/L phosphate (0.03 to 0.094mg/L range).

Clam Lake: Phosphate

In September, dissolved phosphate concentrations at Clam Lake increase from 0.088±0.004mg/L (0.085 to 0.092mg/L range) in the surface water to 11±2mg/L (9.393 to 12.737mg/L range) in the upper sediment porewater interval. In the lower porewater interval, concentrations of dissolved phosphate decrease to 4.6±0.8mg/L (3.839 to 5.398mg/L range). Clam Lake has elevated concentrations of phosphate in its porewater compared to the other sites incorporated in this study, with an overall average porewater concentration of 8±4mg/L.

Perch Lake: Phosphate

Like Lake A, Perch Lake has very low concentrations of phosphate in the surface water and porewater. In August, the surface water reaches an average concentration of 0.1±0.1mg/L (0.025 to 0.228mg/L range). Dissolved phosphate concentrations decrease into the upper sediment interval to a concentration of 0.008±0.006 (0.001 to 0.014mg/L range). Only one of the duplicate porewater samples collected at the lower porewater interval had concentrations above the instrument's limit of detection; this samples had a measured concentration of 0.003mg/L. In September, only two of the 6 samples collected had detectable phosphate concentrations: one of the surface water duplicates (0.075mg/L) and one of the duplicate porewater samples from the lower sediment interval (0.015mg/L).

Sand River: Phosphate

In the north inlet of Sand River, concentrations of dissolved phosphate are low in the surface water in June (0.04±0.01mg/L average; 0.03 to 0.58mg/L range), elevated during the month of August (0.461mg/L), and low again in October (0.079±0.002mg/L average; 0.077 to 0.081mg/L range). In the porewater, dissolved phosphate concentrations are elevated in the upper sediment interval during the months of July (4±1mg/L average; 2.21 to 4.817mg/L range) and October (2±1mg/L average; 1.368 to 3.573mg/L range), but decreased in August (0.049mg/L). In July, porewater concentrations decrease with depth slightly to an average concentration of 3.1±0.6mg/L (2.477 to 3.719mg/L range) in the lower sediment interval. In October, porewater concentrations of dissolved phosphate increase to 3±1mg/L (1.85 to 4.075mg/L range) in the lower sediment interval.

Twin Lakes: Phosphate

At the west bank sampling location at Twin Lakes ('W'), surface water concentrations of dissolved phosphate are low, ranging from 0.02 to 0.034mg/L (0.027±0.007mg/L average) in July and with a concentration of 0.076mg/L in September (duplicate surface water sample was below detection). In the upper porewater interval, phosphate concentrations increase to 1.2±0.2mg/L (0.945 to 1.426mg/L range) in July, and to 0.19±0.03mg/L (0.16 to 0.226mg/L range) in September. In the lower porewater interval, concentrations increase to 0.849mg/L in September.

At the 'WR' sampling location at Twin Lakes, surface water concentrations of dissolved phosphate are low (0.075mg/L; duplicate surface water samples were below detection), but concentrations increase greatly in the porewater. The concentration of dissolved phosphate in the upper porewater sampling interval ranged from 3.997 to 4.585mg/L (4.3±0.3mg/L average) and

the concentration in the lower porewater interval had a concentration of 2.072mg/L (only a single lower porewater interval was obtained from this location).

Big Rice Lake: Nitrite and Nitrate

The concentration of dissolved nitrite and nitrate in the surface water during the month of July was 0.23mg/L (the duplicate surface water sample concentration was below detection). The concentration of nitrite and nitrate in the upper porewater interval was elevated, with respect to the surface water, with an average concentration of 0.46±0.09mg/L (0.37 to 0.56mg/L range) in June and 0.32±0.08mg/L (0.24 to 0.40mg/L range) in July. Concentrations of nitrite and nitrate are similar in the lower porewater interval with an average concentration of 0.380±0.006mg/L (0.37 to 0.39mg/L range) in June and 0.46±0.02mg/L (0.44 to 0.49mg/L range) in July. Concentrations of dissolved nitrite and nitrate were elevated at this site with respect to the other sites incorporated in this study.

Lake A: Nitrite and Nitrate

Concentrations of dissolved nitrite and nitrate were below detection in the surface water at Lake A. In the upper porewater interval, the concentration of dissolved nitrite and nitrate ranged from 0.367 to 0.384mg/L (0.376±0.009mg/L). In the lower porewater interval, the concentration of dissolved nitrite and nitrate was 0.368mg/L (the concentration of nitrite and nitrate in the duplicate porewater sample was below detection). Measured concentrations of dissolved nitrite and nitrate were low to average at Lake A with respect to concentrations measured in the other sites included in this study.

Clam Lake: Nitrite and Nitrate

Both surface water samples collected from Clam Lake during the September sampling trip were below detection. Of the two upper porewater interval samples collected, one was below

detection and the other had a concentration of 0.375mg/L. In the lower porewater interval at Clam Lake, the concentration of nitrite and nitrate ranged from 0.368 to 0.372mg/L (0.370±0.002mg/L). Measured concentrations of dissolved nitrite and nitrate were low to average at Clam Lake with respect to concentrations measured in the other sites included in this study.

Perch Lake: Nitrite and Nitrate

Concentrations of dissolved nitrite and nitrate were elevated in the surface water of Perch Lake during the month of August, ranging from 0.597 to 1.396mg/L (1.0±0.4mg/L average), but lower during the month of September, with a measured concentration of 0.347mg/L (the duplicate surface water sample was below detection). Nitrite and nitrate concentrations decreased into the upper porewater interval in August, with values ranging from 0.3778 to 0.380mg/L (0.379±0.001mg/L average), and increased in September, with values ranging from 0.373 to 0.446mg/L (0.41±0.04mg/L average). In the deeper porewater interval, nitrite and nitrate concentrations remain relatively constant in August, with an average concentration of 0.375±0.006mg/L (0.369 to 0.380mg/L range), and decrease slightly in September, with a concentration of 0.366mg/L.

Sand River: Nitrite and Nitrate

Concentrations of dissolved nitrite and nitrate are similar in the surface, upper porewater interval and lower porewater interval for each month at Sand River. In July, average concentrations of dissolved nitrite and nitrate are 0.24±0.02mg/L. In August, average concentrations increase to 0.38±0.03mg/L. In October, dissolved nitrite and nitrate concentrations decrease to 0.08±0.01mg/L.

Twin Lakes: Nitrite and Nitrate

In the west bank sampling location at Twin Lakes (location 'W'), the concentration of dissolved nitrite and nitrate in the surface water ranged from 0.218 to 0.224mg/L (0.221±0.003mg/L average) in July and increased slightly in September to a range of 0.265 to 0.266 (0.266±0.001mg/L average). In the upper porewater interval, the measured concentration for the July sample was 0.244mg/L (duplicate porewater sample was below detection), and the measured concentration for the September sample was 0.370mg/L (duplicate porewater sample was below detection).

In the 'WR' sampling location, the concentration of nitrite and nitrate ranged from 0.351 to 0.355mg/L (0.353±0.002mg/L average). The measured concentration of nitrite and nitrate in the upper porewater interval was 0.448mg/L (duplicate porewater sample was below detection), and the deeper porewater interval had a measured concentration of 0.371mg/L.

Big Rice Lake: Sulfate

Concentrations of dissolved SO_4^{2-} in the surface of Big Rice lake were elevated during the July sampling period, with concentrations ranging from 36.717 to 36.736mg/L (36.727±0.009mg/L average). SO_4^{2-} concentrations decreased into the subsurface, with 1.5±0.5mg/L (1.009 to 1.939mg/L range) measured in the upper porewater interval in June, and 0.8±0.2mg/L (0.667 to 0.998mg/L range) measured in July. Concentrations of dissolved SO_4^{2-} remained low with respect to surface water concentrations in the lower porewater interval, with 1.2±0.2mg/L (1.058 to 1.429mg/L range) SO_4^{2-} measured in June and 1.4±0.2mg/L (1.215 to 1.641mg/L) measured in July.

Lake A: Sulfate

Dissolved SO_4^{2-} concentrations in the surface of Lake A were measured to be 2.371mg/L (only a single sample was collected, so no range data is available). SO_4^{2-} concentrations decreased slightly in the upper porewater interval, ranging from 1.403 to 1.599mg/L (1.5±0.1mg/L average). Dissolved SO_4^{2-} concentrations increased to 3.8±0.3mg/L (3.508 to 4.175mg/L range) in the deeper porewater interval.

Clam Lake: Sulfate

Concentrations of dissolved SO_4^{2-} in the surface and porewater of Clam Lake are low relative to the other sites included in this study with a measured concentration of 0.81±0.04mg/L in the surface water (0.768 to 0.856mg/L range), 1.00±0.05mg/L (1.557 to 1.585mg/L range) in the upper porewater interval, and 1.06±0.07mg/L (0.988 to 1.131mg/L range) in the lower porewater interval.

Perch Lake: Sulfate

Concentrations of dissolved SO_4^{2-} in Perch Lake are slightly elevated in the August sampling interval relative to September. Surface water SO_4^{2-} concentrations in August are 2.5±0.7mg/L (1.745 to 3.159mg/L range), 1.5±0.3mg/L (1.774 to 1.184mg/L range) in the upper porewater interval, and 3.2±0.9mg/L (2.291 to 4.065mg/L range) in the lower porewater interval. In September, concentrations of dissolved SO_4^{2-} decrease to 0.26±0.01mg/L in the surface water, 0.89±0.02mg/L in the upper porewater interval, and 0.89±0.01mg/L in the lower porewater interval.

Sand River: Sulfate

Trends of dissolved SO_4^{2-} in the surface and porewater of Sand River are outlined in section 2.3.2.

Twin Lakes: Sulfate

Concentrations of dissolved SO_4^{2-} in Twin Lakes are elevated with respect to other sites included in this study. Concentrations of dissolved SO_4^{2-} are highest in sampling location 'W' with an overall average concentration of 230±80mg/L. SO_4^{2-} in the porewater of this location are comparable to those measured in the surface. In location 'WR', concentrations of SO_4^{2-} in the surface are elevated (116±2mg/L) and decrease into the subsurface (7±4mg/L). The surface water in location 'OUT' was elevated, with a concentration of 80.0mg/L. The surface water in location 'IN' was low compared to other locations, with a measured concentration of 2.7mg/L.

Big Rice Lake: Sulfide

Dissolved sulfide concentrations in the upper sampling interval of Big Rice lake were low with respect to other systems included in this study, with an average concentration of 0.02±0.01mg/L (0.0045 to 0.03mg/L range). Of the duplicate samples collected from the lower sediment interval, one was below detection, and the other had elevated concentrations of dissolved SO_4^{2-} with respect to the upper sample (0.219mg/L).

Clam Lake: Sulfide

Dissolved sulfide concentrations in the upper and lower sampling intervals of Clam Lake are similar, with 0.21±0.06mg/L measured in the upper interval and 0.2±0.1mg/L measured in the lower interval.

Perch Lake: Sulfide

Samples for measurement of dissolved sulfide were only collected from the upper interval of the sediments in Perch Lake. Concentrations of dissolved sulfide were average relative to other sites included in this study with an average concentration of 0.4±0.2mg/L.

Sand River: Sulfide

Trends of dissolved sulfide in the surface and porewater of Sand River are outlined in section 3.3.2.

Twin Lakes: Sulfide

Concentrations of dissolved sulfide in the porewater of Twin Lakes are highly variable and elevated with respect to other sites in location 'W'. In the upper sampling interval, the average dissolved sulfide concentration was 30±20mg/L. The concentrations in the lower sediment interval are 20±10mg/L. Dissolved sulfide concentrations in location 'WR' are lower, with 0.96mg/L measured in the upper sampling interval and 1.98mg/L measured in the lower sampling interval.

4.3.2 SPECIATION OF SOLID IRON AND SULFUR IN THE SEDIMENTS

Results from extractions of ferrous and ferric Fe from sediments collected from Big Rice Lake, Clam Lake, Perch Lake, and locations 'W' and 'WR' from Twin Lakes are depicted in figures 54, 55, 56, 57, and 58, respectively; raw data is shown in tables 8 and 9. Ferrous and ferric Fe extraction data from the north inlet, channel and south inlet of Sand River are depicted in figures 39, 40, and 41, respectively; raw data is shown in table 9. Results of measurements of acid-volatile sulfides from sediments collected during the 2018 field season are depicted in figure 54.

Big Rice Lake: Sediment Iron

Extractions of Fe in the sediment of Big Rice Lake show that approximately 50% of solid-phase Fe is composed of ferrous Fe, while the lower sediment interval contains about 66 to 73% ferrous Fe. A small fraction of the total ferrous Fe is easily extractable, with >80 of the ferrous Fe removed during the 6M HCl extraction step. Ferric Fe is similar, with nearly 90% of the ferric Fe fraction requiring the 6M HCl extraction step. Total Fe concentrations are low to average with respect to other sites included in this study.

Clam Lake: Sediment Iron

The extractable Fe in the sediment of Clam Lake is elevated in the lower sediment interval, reaching the highest concentration of any site included in this study. Majority of the Fe in the sediments is present as ferrous Fe, comprising >80% of the total Fe in the upper sediment interval and >90% in the lower sediment interval. More than 85% of the total ferrous Fe is easily extracted; conversely, <9% of the ferric Fe is easily extracted.

Perch Lake: Sediment Iron

Most of the total extractable Fe in the sediments of Perch Lake is present as ferrous Fe, comprising >80% of the total Fe. >90% of the ferrous Fe in sediment samples collected during the August sampling trip is easily extracted; this amount drops to ~75% in September. No ferric Fe was measured in the 0.1M HCl extraction samples, indicating none of the ferric Fe is easily extracted.

Sand River: Sediment Iron

Trends of extractable Fe measurements from sediments collected at the Sand River site are outlined in section 3.3.2.

Twin Lakes: Sediment Iron

Extractable Fe in the sediments of location 'W' at Twin Lakes are highly variable with depth and time. Fe in the upper sediment interval in July contain an elevated fraction of ferric Fe (~62%). Total Fe concentration decreases from the upper sediment interval to the lower interval, decreasing from ~70µmol Fe/g to ~50µmol Fe/g. In September, total extractable Fe concentrations are elevated to >150µmol Fe/g in the upper sediment interval, with ferrous Fe comprising 97% of the total extracted Fe. In the lower sediment interval in samples collected during the September sampling trip, the total Fe concentration decreases to ~41µmol Fe/g, with ferrous Fe comprising 93% of the total Fe.

Big Rice Lake: Acid-Volatile Sulfides

In June, AVS content at Big Rice Lake increases with depth, rising from 0.7±0.2µol sulfide/g (0.542 to 0.892µmol sulfide/g range) in the upper sediment interval to 9±5µmol sulfide/g (3.398 to 14.221µmol sulfide/g range). AVS content is less variable with depth in July; AVS measurements in the upper sediment interval detected 0.86±0.04µmol sulfide/g (0.821 to 0.902µmol sulfide/g range) and 1.0±0.3µmol sulfide/g (0.725 to 1.345µmol sulfide/g range) in the lower sediment interval.

Clam Lake: Acid-Volatile Sulfides

Measurements of AVS in the sediment of Clam Lake detected little variability with depth and low concentrations relative to other sites incorporated in this study. The upper sediment interval contained 1.1±0.4µmol sulfide/g (0.714 to 1.501µmol sulfide/g range) and the lower sediment interval contained 1.0±0.4µmol sulfide/g (0.641 to 1.347µmol sulfide/g range).

Perch Lake: Acid-Volatile Sulfides

AVS content in the sediment of Perch Lake increased with depth during the August sampling interval, increasing from 0.608µmol sulfide/g in the upper interval to 2.107µmol sulfide/g in the lower interval (duplicate samples were not collected during this sampling interval). In September, AVS content was relatively constant, with 0.35±0.08µmol sulfide/g (0.267 to 0.425µmol sulfide/g range) measured in the upper interval and 0.4±0.2µmol sulfide/g (0.211 to 0.563µmol sulfide/g range) measured in the lower sediment interval.

Sand River: Acid Volatile Sulfides

Trends of acid-volatile sulfide measurements in the sediment of Sand River are outlined in section 3.3.2.

Twin Lakes: Acid Volatile Sulfides

Little variability in AVS content was observed with increasing depth during the July sampling trip to the west bank of Twin Lakes (location 'W'), with 5.9±0.5µmol sulfide/g (5.415 to 6.404µmol sulfide/g range) in the upper sediment interval and 6.325µmol sulfide/g in the deeper sediment interval. In September, AVS content increased to 12±4µ sulfide/g (8.048 to 15.352µmol sulfide/g range) in the upper sediment interval, but the lower sediment interval decreased with respect to the July sampling interval with a range of 2.168 to 6.111µmol sulfide/g (4±2µmol sulfide/g average). At location 'WR' of Twin Lakes, AVS content in the upper sediment interval was measured to be 3±2µmol sulfide/g (1.377 to 4.490µmol sulfide/g range). AVS content decreased to 0.430µmol sulfide/g in the lower sediment interval.

4.4 FUTURE WORK

Plans to continue to monitor wild rice bodies through The University of Minnesota's Grand Challenges *Kawe Gidaa-Naanaagadawendaamin Manoomin* project in 2019 are currently under development. Monitoring throughout the 2018 field season has developed a baseline

understanding of geochemical and hydrologic conditions at each site, so more focused observations can be implemented during future studies. The development of analytical techniques used to characterize and measure various minerals and analytes have been developed and tested; these methods can now be employed to efficiently and effectively identify geochemical trends at each site during future observations.

Tables

WEST WETLAND							CHANNEL							EAST WETLAND						
		Depth (cm)	Fe(II) conc. (μM)	Fe(III) conc. (μM)	Total Fe (μM)	%Fe(II)			Depth (cm)	Fe(II) conc. (μM)	Fe(III) conc. (μM)	Total Fe (μM)	%Fe(II)			Depth (cm)	Fe(II) conc. (μM)	Fe(III) conc. (μM)	Total Fe (μM)	%Fe(II)
JULY	Peeper #3	3.12	240.9	39.6	280.5	86%	JULY	Peeper #3	-4.68	2.9	0.0	2.9	100%	JULY	Peeper #1	6.24	518.7	19.8	538.5	96%
		7.80	350.6	31.5	382.1	92%			0.00	126.6	0.0	126.6	100%			10.92	633.5	46.5	680.0	93%
		12.48	382.1	40.0	422.1	91%			4.68	31.0	1.0	32.0	97%			15.60	398.0	12.6	410.6	97%
		17.16	519.2	43.7	562.9	92%			14.04	116.7	28.6	145.3	80%			20.28	248.4	9.7	258.1	96%
		21.84	521.0	37.9	558.9	93%			17.16	126.3	21.2	147.5	86%			24.96	233.0	11.7	244.7	95%
		26.52	743.3	60.8	804.1	92%			20.28	103.6	53.6	157.2	66%			29.64	305.7	23.1	328.8	93%
		31.20	1002.0	126.0	1128.0	89%			24.96	95.8	34.8	130.6	73%			34.32	310.2	32.2	342.4	91%
		35.88	560.9	73.2	634.1	88%			29.64	87.9	48.0	135.9	65%			39.00	227.7	36.3	264.0	86%
		40.56	470.2	49.2	519.4	91%			34.32	75.3	31.1	106.4	71%			43.68	212.1	21.4	233.5	91%
		45.24	558.8	63.2	622.0	90%		Peeper #4	-6.24	0.0	6.5	6.5	0%	JULY	Peeper #2	1.56	832.2	38.0	870.2	96%
		49.92	335.5	36.3	371.8	90%			0.00	0.0	0.0	0.0	0%			6.24	803.6	25.3	828.9	97%
	Peeper #4	3.12	349.2	28.8	378.0	92%			4.68	309.7	117.4	427.1	73%			10.92	508.5	21.0	529.5	96%
		7.80	319.7	29.7	349.4	91%			9.36	253.9	47.5	301.4	84%			15.60	452.2	45.0	497.2	91%
		12.48	344.1	53.1	397.2	87%			14.04	167.6	56.4	224.0	75%			20.28	523.5	36.7	560.2	93%
		17.16	372.5	49.2	421.7	88%			18.72	124.6	28.8	153.4	81%			24.96	441.4	37.3	478.7	92%
		21.84	329.9	58.4	388.3	85%			23.40	169.8	74.8	244.6	69%			29.64	440.8	58.7	499.5	88%
		26.52	582.1	124.9	707.0	82%			28.08	120.1	63.1	183.2	66%			34.32	495.8	43.6	539.4	92%
		31.20	461.8	76.8	538.6	86%			32.76	125.0	41.2	166.2	75%			39.00	565.3	73.2	638.5	89%
		35.88	278.2	55.4	333.6	83%										43.68	406.2	43.4	449.6	90%
		40.56	248.7	41.9	290.6	86%														
		45.24	209.7	53.6	263.3	80%														
		49.92	221.6	39.0	260.6	85%														
AUGUST	Peeper #5	-1.56	235.3	27.1	262.4	90%	AUGUST	Peeper #5	0.00	9.6	0.0	9.6	100%	AUGUST	Peeper #3	-6.24	0.4	2.9	3.3	12%
		3.12	577.0	5.0	582.0	99%			4.68	55.0	2.6	57.6	95%			-1.56	1.3	7.9	9.2	14%
		7.80	633.0	60.0	693.0	91%			9.36	81.4	4.6	86.0	95%			3.12	370.6	20.5	391.1	95%
		12.48	407.1	57.9	465.0	88%			14.04	47.8	0.1	47.9	100%			7.80	502.1	27.0	529.1	95%
		17.16	240.9	38.2	279.1	86%			18.72	43.5	0.0	43.5	100%			12.48	535.7	33.5	569.2	94%
		21.84	290.9	52.4	343.3	85%			23.40	45.2	9.2	54.4	83%			17.16	299.7	39.9	339.6	88%
		26.52	204.2	29.4	233.6	87%			28.08	46.1	0.5	46.6	99%			21.84	173.6	33.9	207.5	84%
		31.20	213.9	39.7	253.6	84%		Peeper #6	-6.24	11.2	17.6	28.8	39%			26.52	168.4	21.5	189.9	89%
		37.44	219.5	37.4	256.9	85%			-1.56	0.0	0.0	0.0	0%			31.20	122.6	25.2	147.8	83%
		45.24	334.6	34.7	369.3	91%			3.12	140.7	20.8	161.5	87%			35.88	83.5	24.4	107.9	77%
		49.92	302.8	31.2	334.0	91%			7.80	129.9	53.7	183.6	71%			40.56	68.4	18.7	87.1	79%
	Peeper #6	-1.56	19.1	60.5	79.6	24%			12.48	50.4	19.5	69.9	72%			45.24	47.7	26.2	73.9	65%
		3.12	429.8	7.8	437.6	98%			17.16	90.1	26.4	116.5	77%							
		9.36	642.4	14.4	656.8	98%			21.84	80.7	39.1	119.8	67%							
		17.16	557.1	18.1	575.2	97%			26.52	77.7	49.2	126.9	61%							
		21.84	598.7	28.5	627.2	95%														
		26.52	499.2	30.8	530.0	94%														
		31.20	418.1	36.7	454.8	92%														
		35.88	362.8	41.4	404.2	90%														
		37.44	277.6	15.0	292.6	95%														
		43.68	209.8	110.1	319.9	66%														
		49.92	258.3	27.5	285.8	90%														
OCTOBER	Peeper #7	-6.24	2.1	0.7	2.8	75%	OCTOBER	Peeper #7	-12.50	0.0	0.4	0.4	0%	OCTOBER	Peeper #4	-4.68	14.6	9.5	24.1	61%
		-1.56	0.0	0.0	0.0	0%			-7.80	0.0	0.2	0.2	0%			-1.56	400.3	20.1	420.4	95%
		3.12	186.2	16.5	202.7	92%			-4.65	0.0	0.0	0.0	0%			3.12	511.8	39.7	551.5	93%
		7.80	267.5	20.8	288.3	93%			1.56	51.8	16.2	68.0	76%			7.80	403.5	20.8	424.3	95%
		12.48	228.0	21.7	249.7	91%			6.24	152.6	18.2	170.8	89%			12.48	343.0	17.5	360.5	95%
		17.16	174.0	8.8	182.8	95%		Peeper #8	-23.40	2.2	0.0	2.2	100%			17.16	266.5	13.3	279.8	95%
		23.40	132.9	15.0	147.9	90%			-18.72	0.0	2.4	2.4	0%			21.84	235.8	26.0	261.8	90%
		28.08	139.2	7.3	146.5	95%			-14.04	0.0	0.0	0.0	0%			26.52	147.1	13.1	160.2	92%
		31.20	114.2	6.9	121.1	94%			-9.36	2.5	0.0	2.5	100%			31.20	179.6	21.8	201.4	89%
		35.88	129.7	9.0	138.7	94%			-3.12	0.0	0.0	0.0	0%			35.88	204.1	15.4	219.5	93%
	Peeper #8	-17.16	0.0	0.0	0.0	0%			1.56	313.1	20.9	334.0	94%			40.56	161.9	20.2	182.1	89%
		-12.48	0.0	0.0	0.0	0%			6.24	143.6	28.1	171.7	84%			45.24	138.2	19.3	157.5	88%
		-7.80	0.0	0.0	0.0	0%														
		-3.12	0.0	0.0	0.0	0%														
		1.56	181.4	23.0	204.4	89%														
		6.24	241.4	24.4	265.8	91%														

Table 1: Concentrations of dissolved Fe in pore-water collected during the 2017 field season at Second Creek. West wetland data is reported on the left, channel data is reported in the center, and east wetland data is reported on the right. Depth is reported as depth into the subsurface, with 0 as the sediment-water interface and negative values corresponding to measurements of surface water intervals above the sampling location. West wetland peepers 3, 5, and 7, channel peepers 3, 5, and 7, and east wetland peepers 1, 3, and 4 are plotted in figure 14.

			Goethite	2-line Ferrihydrite	Ferric Citrate	Hematite	Biotite	Ferrous Chloride	Ferrous Sulfate	Vivianite	Siderite	Chalcopyrite	Pyrite	Pyrrhotite	Mackinawite
CHANNEL	[illegible]	top	0.0%	0.0%	11.1%	0.0%	18.7%	33.9%	4.9%	0.0%	0.0%	0.0%	3.0%	0.0%	28.3%
		middle	0.0%	16.9%	10.5%	0.0%	17.8%	19.1%	10.7%	0.0%	0.0%	0.0%	0.0%	1.9%	23.1%
		bottom	0.0%	24.3%	0.0%	7.4%	17.2%	13.2%	0.0%	0.0%	0.0%	0.0%	6.1%	11.0%	20.8%
	[illegible]	top	0.0%	0.0%	19.2%	0.0%	26.2%	0.0%	24.4%	0.0%	0.0%	0.0%	0.0%	15.2%	15.0%
		middle	0.0%	0.0%	27.9%	0.0%	51.5%	0.0%	0.0%	0.0%	0.0%	0.0%	0.0%	0.0%	20.6%
		bottom	0.0%	0.0%	25.7%	0.0%	25.2%	0.0%	19.2%	0.0%	0.0%	0.0%	0.0%	9.6%	20.3%
	[illegible]	top	0.0%	0.0%	23.0%	0.0%	38.3%	0.0%	0.0%	0.0%	2.7%	0.0%	5.8%	0.0%	30.2%
		middle	0.0%	0.0%	12.0%	0.0%	18.4%	15.1%	5.2%	0.0%	0.0%	0.0%	0.0%	13.8%	35.6%
		bottom	0.0%	0.0%	15.1%	6.0%	16.8%	0.0%	14.3%	0.0%	0.0%	0.0%	0.0%	10.3%	37.5%
	[illegible]	top	0.0%	0.0%	16.9%	0.0%	24.2%	0.0%	19.5%	0.0%	0.0%	0.0%	3.8%	13.4%	22.3%
		middle	0.0%	0.0%	22.1%	0.0%	38.8%	0.0%	0.0%	0.0%	0.0%	0.0%	10.1%	0.0%	29.0%
		bottom	0.0%	0.0%	28.5%	5.5%	20.3%	0.0%	22.6%	0.0%	0.0%	0.0%	0.0%	10.2%	12.9%
EAST WETLAND	[illegible]	top	0.0%	0.0%	12.5%	0.0%	20.2%	0.0%	22.7%	0.0%	0.0%	0.0%	0.0%	22.3%	22.3%
		middle	25.3%	0.0%	8.2%	0.0%	33.5%	0.0%	16.9%	0.0%	0.0%	0.0%	0.0%	0.0%	16.1%
		bottom	0.0%	0.0%	28.4%	0.0%	25.4%	22.4%	7.1%	0.0%	0.0%	6.7%	0.0%	0.0%	10.2%
	[illegible]	top	0.0%	0.0%	16.2%	0.0%	20.3%	0.0%	19.1%	0.0%	0.0%	0.0%	3.8%	7.8%	32.9%
		middle	0.0%	0.0%	25.7%	0.0%	25.2%	0.0%	19.2%	0.0%	0.0%	0.0%	0.0%	9.6%	20.3%
		bottom													
	[illegible]	top	0.0%	0.0%	0.0%	0.0%	2.0%	16.5%	27.6%	0.0%	0.0%	3.5%	0.4%	7.9%	42.2%
		middle													
		bottom	7.0%	0.0%	10.7%	0.0%	15.3%	34.9%	0.0%	0.0%	0.0%	0.0%	2.5%	0.0%	29.7%
	[illegible]	top	6.9%	0.0%	16.4%	0.0%	16.7%	16.3%	8.1%	0.0%	0.0%	0.0%	0.0%	9.3%	26.4%
		middle	21.8%	0.0%	8.0%	0.0%	19.7%	20.2%	0.0%	0.0%	0.0%	13.0%	1.8%	0.0%	15.6%
		bottom	0.0%	22.2%	8.6%	0.0%	13.9%	14.4%	0.0%	0.0%	0.0%	15.0%	7.9%	18.0%	0.0%
WEST WETLAND	[illegible]	top	0.0%	0.0%	7.4%	0.0%	10.0%	21.4%	26.3%	0.0%	0.0%	0.0%	0.0%	1.0%	33.9%
		middle	0.0%	0.0%	26.3%	0.0%	26.5%	0.0%	10.0%	0.0%	0.0%	0.0%	0.0%	9.5%	27.7%
		bottom	18.1%	0.0%	0.0%	0.0%	10.9%	23.0%	0.0%	0.0%	0.0%	8.3%	1.7%	7.6%	30.4%
	[illegible]	top	0.0%	0.0%	21.3%	0.0%	22.6%	24.4%	0.0%	0.0%	0.0%	12.2%	10.9%	0.0%	8.4%
		middle													
		bottom	0.0%	0.0%	35.4%	0.0%	31.6%	15.6%	0.0%	0.0%	0.0%	0.0%	8.1%	1.6%	7.6%
	[illegible]	top	0.0%	0.0%	0.0%	0.0%	8.3%	10.5%	50.3%	0.0%	0.0%	0.0%	0.0%	9.6%	21.4%
		middle	0.0%	0.0%	4.0%	0.0%	29.6%	18.5%	0.0%	23.8%	0.0%	3.8%	8.2%	6.5%	5.6%
		bottom	0.0%	0.0%	25.0%	0.0%	30.5%	18.3%	0.0%	0.0%	0.0%	0.0%	5.3%	7.1%	13.9%
	[illegible]	top	0.0%	0.0%	12.0%	0.0%	10.0%	18.4%	17.1%	0.0%	0.0%	7.8%	3.8%	10.4%	20.4%
		middle	0.0%	0.0%	16.8%	0.0%	12.5%	17.8%	14.1%	0.0%	0.0%	0.0%	3.2%	8.3%	27.3%
		bottom	0.0%	0.0%	30.3%	0.0%	34.2%	12.7%	5.8%	0.0%	0.0%	0.0%	8.8%	0.0%	8.2%

Table 2: LCF fit results for Fe K-edge EXAFS samples. Sample intervals 'top', 'middle', and 'bottom' refer to sediment depth intervals of ~4cm, ~10cm, and ~20cm respectively, in relation to the depth below the sediment-water interface. LCF results are expressed as mass concentration (wt % Fe) for Fe-containing components in bulk sediment samples with the sum of all Fe species normalized to 100%.

			Inorganic Sulfate	Thiosulfate	Organic Monosulfide	Organic Disulfide	Sulfur	Iron Disulfide	Copper-Iron Disulfide	Iron Monosulfide
CHANNEL	June	top	0.0%	7.3%	0.0%	0.0%	32.2%	0.0%	36.8%	23.8%
		middle	17.4%	40.2%	31.0%	0.0%	11.4%	0.0%	0.0%	0.0%
		bottom	6.0%	30.2%	0.0%	0.0%	35.4%	0.0%	28.5%	0.0%
	August	top	6.5%	10.6%	0.0%	0.0%	44.5%	0.0%	25.3%	13.3%
		middle	8.7%	12.7%	11.1%	0.0%	68.2%	0.0%	0.0%	0.0%
		bottom	4.7%	10.8%	8.6%	0.0%	68.6%	0.0%	7.5%	0.0%
	October	top	0.0%	5.9%	0.0%	0.0%	39.9%	0.0%	29.7%	24.7%
		middle								
		bottom	11.2%	16.9%	17.7%	0.0%	37.0%	0.0%	16.5%	0.0%
EAST WETLAND	June	top	0.0%	0.0%	0.0%	0.0%	16.2%	0.0%	54.9%	28.9%
		middle	31.6%	16.1%	31.8%	0.0%	20.5%	0.0%	0.0%	0.0%
		bottom	62.6%	19.2%	10.9%	0.0%	7.3%	0.0%	0.0%	0.0%
	August	top	0.0%	9.6%	7.3%	0.0%	55.2%	0.0%	16.0%	11.9%
		middle								
		bottom	12.1%	22.0%	14.5%	0.0%	40.2%	0.0%	0.0%	11.3%
	October	top	12.7%	11.3%	10.0%	0.0%	49.2%	0.0%	16.4%	0.0%
		middle	31.3%	44.2%	36.8%	0.0%	0.0%	0.0%	0.0%	0.0%
		bottom								
WEST WETLAND	June	top	0.0%	9.1%	6.2%	0.0%	50.5%	0.0%	23.7%	10.5%
		middle	0.0%	14.7%	15.4%	0.0%	42.8%	0.0%	26.1%	0.0%
		bottom	0.0%	13.1%	12.6%	0.0%	50.8%	0.0%	22.7%	0.0%
	August	top	11.7%	14.9%	10.7%	0.0%	46.6%	0.0%	15.6%	0.0%
		middle	15.8%	25.4%	31.1%	0.0%	27.6%	0.0%	0.0%	0.0%
		bottom								
	October	top	0.0%	8.6%	0.0%	0.0%	43.9%	0.0%	26.7%	21.0%
		middle								
		bottom	0.0%	18.9%	13.9%	0.0%	0.0%	50.0%	0.0%	16.8%

Table 3: LCF fit results for S-XANES samples. Sample intervals 'top', 'middle', and 'bottom' refer to sediment depth intervals of ~4cm, ~10cm, and ~20cm respectively, in relation to the depth below the sediment-water interface. LCF results are expressed as mass concentration (wt % S) for S-containing components in bulk sediment samples with the sum of all S species normalized to 100%.

Site Name	Month	Core ID	Sampled Interval	Anions (mg/L)						Cations (mg/L)			
				Phosphate	Chloride	Nitrite	Bromide	Nitrate	Sulfate	Sodium	Potassium	Magnesium	Calcium
BIG RICE LAKE	JUNE	E	TOP	0.89	1.31	b.d.	0.63	1.57	1.01	6.44	1.94	4.27	12.05
			BOTTOM	0.91	301.79	b.d.	b.d	1.58	1.06	6.10	4.09	8.56	28.31
		F	TOP	0.01	2.78	b.d.	0.91	2.36	1.94	24.98	2.42	6.49	16.89
			BOTTOM	0.77	2.71	b.d.	b.d	1.63	1.43	81.97	0.78	2.03	6.31
	JULY	G	TOP	1.54	2.25	0.26	0.42	0.65	0.67	21.79	6.25	20.36	59.54
			BOTTOM	1.22	3.40	0.13	0.77	1.88	1.64	11.34	2.60	8.20	28.95
		K	TOP	1.75	1.86	0.10	0.67	1.55	1.00	4.65	4.44	11.70	35.69
			BOTTOM	1.50	3.35	b.d.	0.78	1.86	1.22	13.48	3.23	12.10	33.24
		SURFACE WATER		0.09	32.98	b.d.	0.63	0.98	36.74	25.20	5.18	72.35	57.44
				0.09	33.08	b.d.	0.63		36.72	3.70	4.15	22.05	16.00
Lake A	OCTOBER	A	TOP	0.03	3.97	b.d.	0.61	1.62	1.40	8.17	2.51	3.45	10.07
			BOTTOM	0.09	1.61	b.d.	b.d	1.55	4.17	2.30	1.20	5.33	19.84
		F	TOP	b.d.	4.90	b.d.	b.d	1.55	1.60	3.37	1.06	3.81	17.39
			BOTTOM	b.d.	1.45	b.d.	b.d		3.51	2.40	0.60	6.01	28.46
		SURFACE WATER		b.d.	4.69	b.d.	b.d		2.37			n.d.	
CLAM LAKE	SEPTEMBER	I	TOP	9.39	6.41	b.d.	0.70	1.59	0.95	6.15	8.18	14.21	63.74
			BOTTOM	3.84	4.04	b.d.	0.69	1.57	1.13	4.12	10.12	20.13	95.33
		J	TOP	12.74	10.24	b.d.	0.66		1.05	9.55	11.00	12.94	59.09
			BOTTOM	5.40	3.13	b.d.	0.71	1.56	0.99	2.64	7.72	21.75	104.06
		SURFACE WATER		0.09	5.03	b.d.	b.d		0.86			n.d.	
				0.09	5.45	b.d.	b.d		0.77			n.d.	
PERCH LAKE	AUGUST	F	TOP	0.00	2.82	b.d.	0.66	1.60	1.18	10.92	1.08	14.04	34.42
			BOTTOM	b.d.	2.59	b.d.	0.63	1.56	2.29	7.27	1.42	16.06	42.18
		I	TOP	0.01	2.84	b.d.	b.d	1.61	1.77	11.80	1.28	13.28	32.24
			BOTTOM	0.00	4.29	b.d.	0.63	1.61	4.07	7.69	2.07	16.07	41.07
		SURFACE WATER		0.23	11.17	0.79	b.d	1.46	1.75			n.d.	
				0.03	17.48	b.d.	0.95	5.90	3.16			n.d.	
	SEPTEMBER	J	TOP	b.d.	8.22	b.d.	0.63	1.58	0.88	3.82	1.32	6.79	24.02
			BOTTOM	b.d.	7.51	b.d.	0.62	1.55	0.90	3.16	1.82	9.43	33.07
		X	TOP	b.d.	8.27	b.d.	0.62	1.88	0.91	6.00	1.82	8.31	28.23
			BOTTOM	0.02	7.84	b.d.	0.62	1.55	0.88	3.39	1.67	8.59	30.96
		SURFACE WATER		0.08	7.54	b.d.	b.d	1.47	0.27	4.73	0.61	9.32	25.01
				b.d.	6.97	b.d.	b.d		0.25	4.89	0.74	9.34	25.03

Table 4: Bulk anion and cation data collected from Big Rice Lake, Lake A, Clam Lake, and Perch Lake during the 2018 field season. All values reported in mg/L. "b.d." indicates measurement was below detection limit of instrument. "n.d." indicates no data is currently available. "Sampled Interval" refers to the interval of the core that the Rhizon™ sampler had been inserted into; 'TOP' refers to the ~0-10cm interval (where 0 is the sediment-water interface) and 'BOTTOM' refers to the ~13-23cm interval.

Site Name	Month	SAMPLE LOCATION	Core ID	Sampled Interval	Anions (mg/L)						Cations (mg/L)			
					Phosphate	Chloride	Nitrite	Bromide	Nitrate	Sulfate	Sodium	Potassium	Magnesium	Calcium
SAND RIVER	JULY	NORTH INLET	A	TOP	4.817	5.738	0.259	0.406	0.635	1.057	30.175	9.985	70.96	42.685
				BOTTOM	3.719	6.428	0.261	0.415	0.789	0.824	24.5	5.65	25.05	23.745
			K	TOP	2.21	8.633	0.254	0.425	0.632	4.741	12.245	6.685	18.26	33.235
				BOTTOM	2.477	7.278	0.240	0.420	0.611	1.367	29.255	6.225	16.44	29.845
			SURFACE WATER		0.03	1.356	0.231	b.d.	0.658	1.535	0.735	b.d.	b.d.	bd
					0.058	1.381	0.240	b.d.	0.833	1.577	29.695	11.29	68.13	46.645
	AUGUST	CHANNEL	F	TOP	1.355	26.012	b.d	0.769	1.564	6.417	14.587	5.718	38.295	42.320
				BOTTOM	0.319	24.737	b.d	0.816	1.566	1.352	13.542	5.028	28.492	40.880
			H	TOP	0.323	25.368	b.d	0.772	1.566	6.629	15.424	4.209	27.513	32.922
				BOTTOM	0.169	27.033	b.d	0.816	1.564	2.142	13.276	4.476	23.856	39.960
			SURFACE WATER		0.021	40.803	b.d	0.986	1.631	44.939	7.4658	0.5106	11.3528	13.0134
					0.103	129.119	b.d	1.650	1.452	67.841	13.2848	1.242	25.4288	23.4462
		NORTH INLET	H	TOP	0.049	6.149	b.d	0.622	1.571	5.800	14.173	2.295	5.824	7.507
			SURFACE WATER		n.d.	3.306	b.d	b.d	1.505	3.840	2.3092	0.6716	2.4242	5.3406
					0.461	1.102	b.d	b.d	1.431	0.713	2.3	0.667	2.2954	4.6644
		SOUTH INLET	F	TOP	n.s.	13.303	b.d	0.865	1.904	1.935	17.654	2.258	21.165	24.497
			I	TOP	0.028	9.012	b.d	0.692	1.571	1.336	9.494	8.565	21.648	29.445
				BOTTOM	0.355	15.231	b.d	0.790	1.562	1.394	12.521	11.376	32.094	45.618
			SURFACE WATER		0.193	17.167	b.d	0.976	6.759	2.195	7.682	0.4554	11.385	13.1054
					0.112	3.420	b.d	b.d	1.552	3.886	7.5716	0.552	11.0308	13.2296
	OCTOBER	CHANNEL	K	TOP	0.149	23.385	b.d	0.259	0.436	27.734	17.3604	2.2034	22.034	25.9578
				BOTTOM	0.15	26.957	b.d	0.359	0.310	3.740	12.9858	2.737	20.8426	40.066
			I	TOP	0.223	24.402	b.d	0.362	0.397	0.884	25.8612	1.8998	31.5652	36.9058
				BOTTOM	0.136	25.690	b.d	0.329	0.371	0.663	13.6528	2.6174	27.2412	42.9962
			SURFACE WATER		0.098	23.835	b.d	0.259	0.306	53.167	14.5268	1.3708	27.2596	17.0568
					0.084	24.052	b.d	0.252	0.308	53.674	14.3888	1.3202	27.7702	17.1994
		NORTH INLET	K	TOP	1.368	9.480	b.d	0.159	0.308	3.715	7.1392	1.2696	8.234	15.019
				BOTTOM	1.85	6.757	b.d	0.166	0.296	2.427	4.3516	1.0764	8.1098	15.6722
			P	TOP	3.573	7.229	b.d	0.147	0.338	1.526	15.2536	1.38	9.476	17.0062
				BOTTOM	4.075	5.406	b.d	0.187	0.294	0.789	5.2992	1.5364	11.5736	22.5538
			SURFACE WATER		0.081	5.871	b.d	b.d.	0.343	1.491	3.6662	0.4968	2.3368	4.9404
					0.077	5.903	b.d	b.d.	0.352	1.500	3.703	0.4876	2.3874	4.9358
		SOUTH INLET	H	TOP	0.776	12.322	b.d	0.194	0.355	0.770	22.1996	4.2642	23.7084	29.9368
				BOTTOM	2.274	17.411	b.d	0.259	0.301	0.810	13.1698	3.6248	22.977	32.6784
			X	TOP	0.213	11.870	b.d	0.189	0.443	3.155	13.386	3.4362	17.388	22.3974
				BOTTOM	1.385	16.749	b.d	0.240	0.287	0.889	13.3952	4.186	21.0956	32.0804
TWIN LAKES	JULY	W	F	TOP	1.426	n.s.	n.s.	n.s.	n.s.	n.s.	11.33	5.155	17.86	31.07
			X	TOP	0.945	28.334	0.261	0.644	0.681	111.400	53.21	7.16	117.72	94.725
			SURFACE WATER		0.02	1.325	0.236	b.d.	0.604	1.573	50.82	6.975	130.455	102.87
					0.034	22.542	0.222	0.565	0.649	118.174	4.355	3.63	28.165	26.62
	SEPTEMBER	W	F	TOP	0.16	38.953	b.d	0.872	1.562	310.352	28.709	2.553	107.120	82.621
			E	TOP	0.226	37.942	b.d	0.858	b.d	330.585	29.049	2.636	108.348	83.674
				BOTTOM	0.849	38.802	b.d	0.902	b.d	317.219	28.741	3.110	118.358	92.313
			SURFACE WATER		b.d.	33.560	b.d	1.020	1.122	197.885			n.m.	
					0.076	33.710	b.d	1.020	1.125	197.050			n.m.	
		OUT	SURFACE		b.d.	19.871	b.d	0.786	1.491	79.980			n.m.	
		WR	C	TOP	3.997	22.098	b.d	0.932	1.896	6.636	22.752	5.106	46.115	44.165
				BOTTOM	2.072	13.233	b.d	0.769	1.566	2.277	11.790	5.083	38.070	46.101
			B	TOP	4.585	23.427	b.d	0.837	b.d	11.604	22.798	5.364	45.683	44.160
			SURFACE WATER		0.075	24.745	b.d	0.838	1.500	118.407			n.m.	
					b.d.	24.584	b.d	0.838	1.484	114.569	43.9714	3.4822	113.2014	84.755
		N	SURFACE		n.m.	17.508	b.d	0.974	5.876	2.724			n.m.	

Table 5: Bulk anion and cation data from porewater collected using Rhizon samplers at Sand River and Twin Lakes during the 2018 field season. All values reported in mg/L. "b.d." indicates measurement was below detection limit of instrument. "n.d." indicates no data is currently available. "n.s." indicates insufficient porewater was collected to perform the measurement. "Sampled Interval" refers to the interval of the core that the Rhizon™ sampler had been inserted into; 'TOP' refers to the ~0-10cm interval (where 0 is the sediment-water interface) and 'BOTTOM' refers to the ~13-23cm interval. See figures X and X for specific sampling locations.

Location	Month	Sampling Location	Core ID	Interval	Sulfide Conc. (mg/L)
Big Rice Lake	July	-	A	top	0.0045
		-		bottom	b.d.
		-	T	top	0.03
		-		bottom	0.219
Clam Lake	September	-	A	top	0.1305
		-		bottom	0.1695
		-	G	top	0.216
		-		bottom	0.3585
		-	X	top	0.2955
		-		bottom	0.099
Perch Lake	August	-	G	top	0.5085
		-	I	top	0.2055

Table 6: Dissolved sulfide data from porewater collected using Rhizon samplers in Big Rice Lake, Clam Lake, and Perch Lake during the 2018 field season. All values reported in mg/L. "b.d." indicates measurement was below detection limit of instrument. "Interval" refers to the interval of the core that the Rhizon™ sampler had been inserted into; 'TOP' refers to the ~0-10cm interval (where 0 is the sediment-water interface) and 'BOTTOM' refers to the ~13-23cm interval. See figures 45, 46, and 47 for specific sampling locations.

Location	Month	Sampling Location	Core ID	Interval	Sulfide Conc. (mg/L)
Sand River	July	North Inlet	J	top	0.1155
				bottom	0.111
			F	top	0.1095
				bottom	0.063
	August	Channel	D	top	0.1095
				bottom	0.1275
			A	top	0.159
				bottom	0.0885
		North Inlet	F	top	0.0855
				bottom	0.1515
			J	top	0.0705
				bottom	0.1215
		South Inlet	D	top	0.1455
				bottom	0.042
	October	Channel	G	top	0.1335
				bottom	0.096
		North Inlet	I	top	0.5535
			F	top	0.4455
		South Inlet	K	top	0.2595
				bottom	0.126
			I	top	0.0915
				bottom	0.228
Twin Lakes	July	W	B	top	6.225
				bottom	16.695
			H	top	43.305
				bottom	10.455
	September	W	B	top	7.365
				bottom	37.245
			A	top	56.25
				bottom	13.785
		WR	D	top	2.505
				bottom	1.98
			E	top	1.755
				bottom	0.96

Table 7: Dissolved sulfide data from porewater collected using Rhizon samplers in Sand River and Twin Lakes during the 2018 field season. All values reported in mg/L. "Interval" refers to the interval of the core that the Rhizon™ sampler had been inserted into; 'TOP' refers to the ~0-10cm interval (where 0 is the sediment-water interface) and 'BOTTOM' refers to the ~13-23cm interval. See figures 28 and 49 for specific sampling locations.

Site Name	Month	Core ID	Sampled Interval	µmol Sulfide/ gram sediment	Extractable Iron (µmol Fe/gram sediment)				
					0.1M HCl		6M HCl		Total Iron
					Ferrous Fe	Ferric Fe	Ferrous Fe	Ferric Fe	
BIG RICE LAKE	June	C	TOP	0.542	6.99	1.38	20.76	25.20	54.33
			BOTTOM	14.221	9.54	2.59	56.12	21.08	89.33
		Y	TOP	0.892	12.45	1.23	37.51	50.69	101.87
			BOTTOM	3.398	38.11	5.71	38.98	35.35	118.15
	July	F*	TOP	0.821	6.66	1.85	42.22	36.00	86.73
			BOTTOM	1.345	4.68	3.27	28.96	18.60	55.51
		F	TOP	0.902	5.77	4.96	20.68	30.53	61.94
			BOTTOM	0.725	8.04	b.d.	30.31	5.08	43.43
CLAM LAKE	Sept.	H	TOP	0.714	148.18	b.d.	18.19	9.46	175.83
			BOTTOM	0.641	447.58	b.d.	63.92	33.84	545.33
		F	TOP	1.501	32.10	2.16	11.72	37.81	83.79
			BOTTOM	1.347	262.91	b.d.	32.99	13.41	309.31
PERCH LAKE	Aug.	K	TOP	0.608	47.14	b.d.	16.17	12.41	75.72
			BOTTOM	2.107	50.18	b.d.	18.47	8.88	77.53
	Sept.	P	TOP	0.425	52.37	b.d.	4.35	21.39	78.11
			BOTTOM	0.563	81.07	b.d.	6.59	10.09	97.75
		G	TOP	0.267	44.70	b.d.	9.33	5.85	59.89
			BOTTOM	0.211	38.88	b.d.	16.62	12.23	67.74

Table 8: Sediment composition data for Big Rice Lake, Clam Lake, and Perch Lake from the 2018 field season. AVS data is reported as µmol sulfide per gram sediment and extractable Fe data is reported as µmol Fe per gram sediment. 'TOP' sampled interval refers to the sediment sample collected from ~4cm from the top of the sediment cores; 'BOTTOM' sampled interval refers to the sediment sample collected from ~20cm from the top of the sediment cores. "b.d." indicates the measurement was below the detection limit of the instrument.

Site Name	Month	Sample Location	Core ID	Sampled Interval	µmol Sulfide/ gram sediment	Extractable Iron (µmol Fe/gram sediment)				
						0.1M HCl		6M HCl		Total Iron
						Ferrous Fe	Ferric Fe	Ferrous Fe	Ferric Fe	
SAND RIVER	July	North Inlet	X	TOP	7.511	8.78	10.92	b.d.	6.77	26.47
				BOTTOM	5.156	6.30	4.11	24.29	34.75	69.45
			G	TOP	2.324	8.40	8.96	36.82	42.81	96.98
				BOTTOM	3.127	8.49	7.72	32.49	24.11	72.82
	August	North Inlet	K	TOP	6.281	37.01	3.86	28.27	24.69	93.84
				BOTTOM	3.566	56.02	7.71	196.81	b.d.	260.54
			I	TOP	4.278	25.15	4.17	39.52	23.94	92.78
				BOTTOM	1.469	16.39	2.43	33.89	23.49	76.20
		Channel	K	TOP	13.046	66.14	b.d.	22.71	88.98	177.83
				BOTTOM	1.675	105.16	3.17	48.69	149.93	306.94
		South Inlet	F	TOP	0.559	25.16	3.36	35.66	157.63	221.82
				BOTTOM	0.763	40.01	2.26	14.26	27.90	84.43
	October	North Inlet	J	TOP	1.067	52.46	0.17	20.11	38.45	111.18
				BOTTOM	1.540	43.83	3.00	28.39	22.45	97.66
		Channel	H	TOP	1.841	59.89	b.d.	25.50	39.88	125.27
				BOTTOM	0.574	33.81	2.34	55.18	517.17	608.50
			P	TOP	0.917	31.89	2.90	44.85	51.06	130.70
				BOTTOM	1.794	40.85	b.d.	27.49	25.73	94.07
TWIN LAKES	July	W	A	TOP	6.404	13.60	2.17	23.93	23.83	63.53
				BOTTOM	6.325	6.42	b.d.	36.83	4.72	47.96
			D	TOP	5.415	20.89	2.57	25.64	23.93	73.01
	September	W	F	TOP	8.048	120.24	b.d	12.70	2.82	135.77
				BOTTOM	6.111	67.05	b.d	4.79	2.90	74.74
			A	TOP	15.352	148.62	1.35	20.33	2.96	173.26
				BOTTOM	2.168	0.10	b.d	b.d	b.d	0.10
		WR	H	TOP	4.490	153.24	b.d	22.47	15.22	190.93
				BOTTOM	3.203	130.73	9.22	11.61	15.91	167.47
			G	TOP	1.377	39.38	b.d	6.80	8.34	54.52
				BOTTOM	0.430	39.10	b.d	6.58	15.14	60.82

Table 9: Sediment composition data for Sand River and Twin Lakes from the 2018 field season. AVS data is reported as µmol sulfide per gram sediment and extractable Fe data is reported as µmol Fe per gram sediment. 'TOP' sampled interval refers to the sediment sample collected from ~4cm from the top of the sediment cores; 'BOTTOM' sampled interval refers to the sediment sample collected from ~20cm from the top of the sediment cores. "b.d." indicates the measurement was below the detection limit of the instrument. See Figures X and X for specific sample locations.

Figures

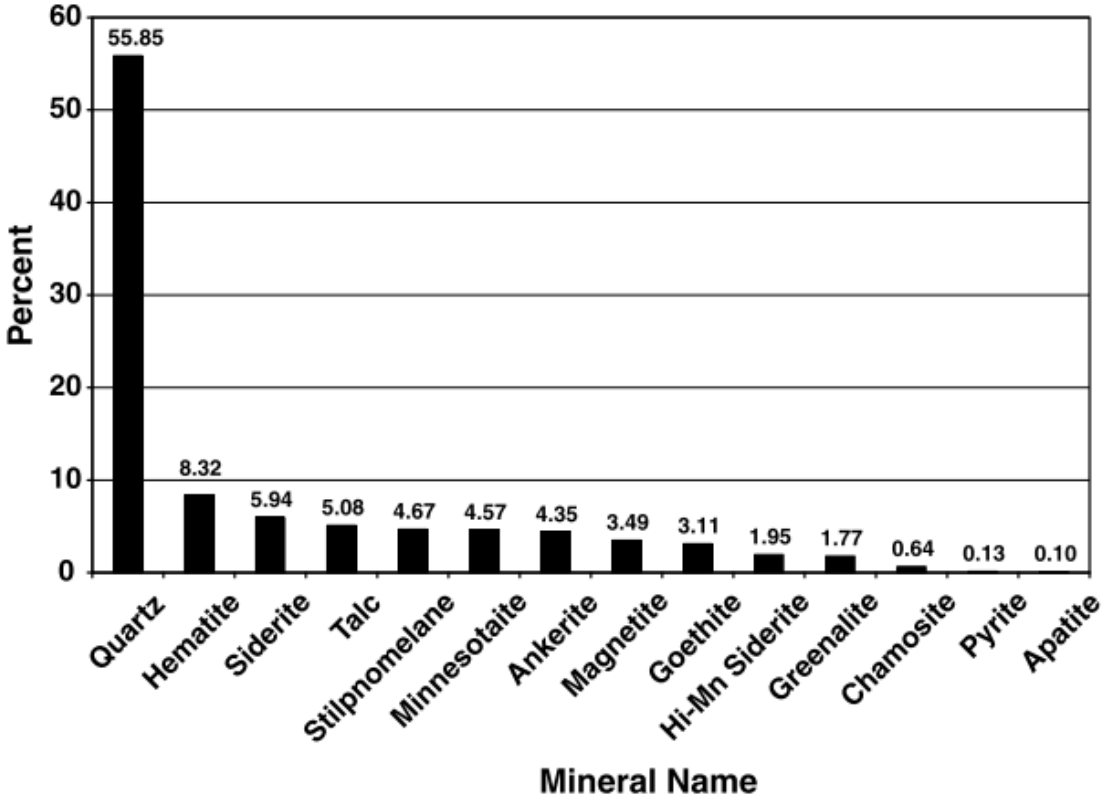

Figure 1: Course tailings sample mineralogy from Zanko *et al.*, 2008. Percentages are averaged from 18 samples obtained from multiple mining locations in northern Minnesota.

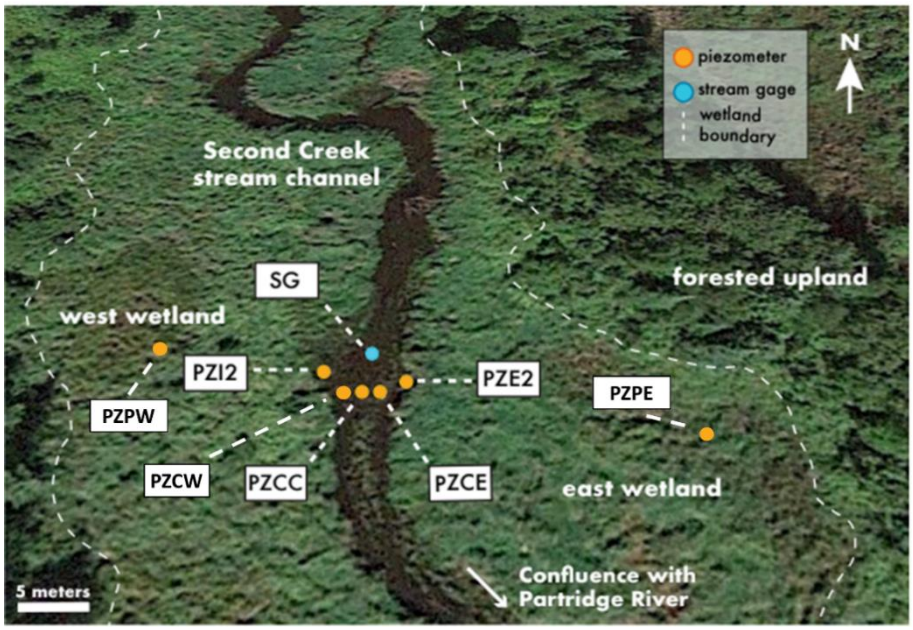

Figure 2: Site map showing locations of hydrologic monitoring equipment during the 2017 field season at Second Creek. Piezometer locations are depicted by orange circles, and the channel stream gauge is represented by the blue circle. The dotted white line shows the boundary of the wetland flanking Second Creek. Adapted from Yourd, 2017 and Fadely, 2018.

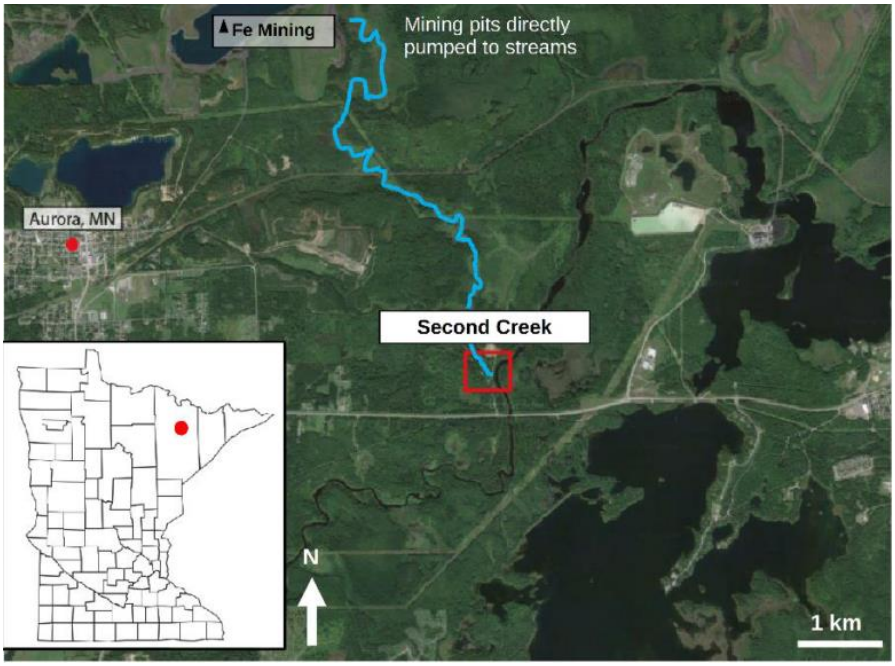

Figure 3: Regional map of Second Creek (study site denoted by red box). Stream (blue line) flows north (from mining pits) to south. From Yourd, 2017.

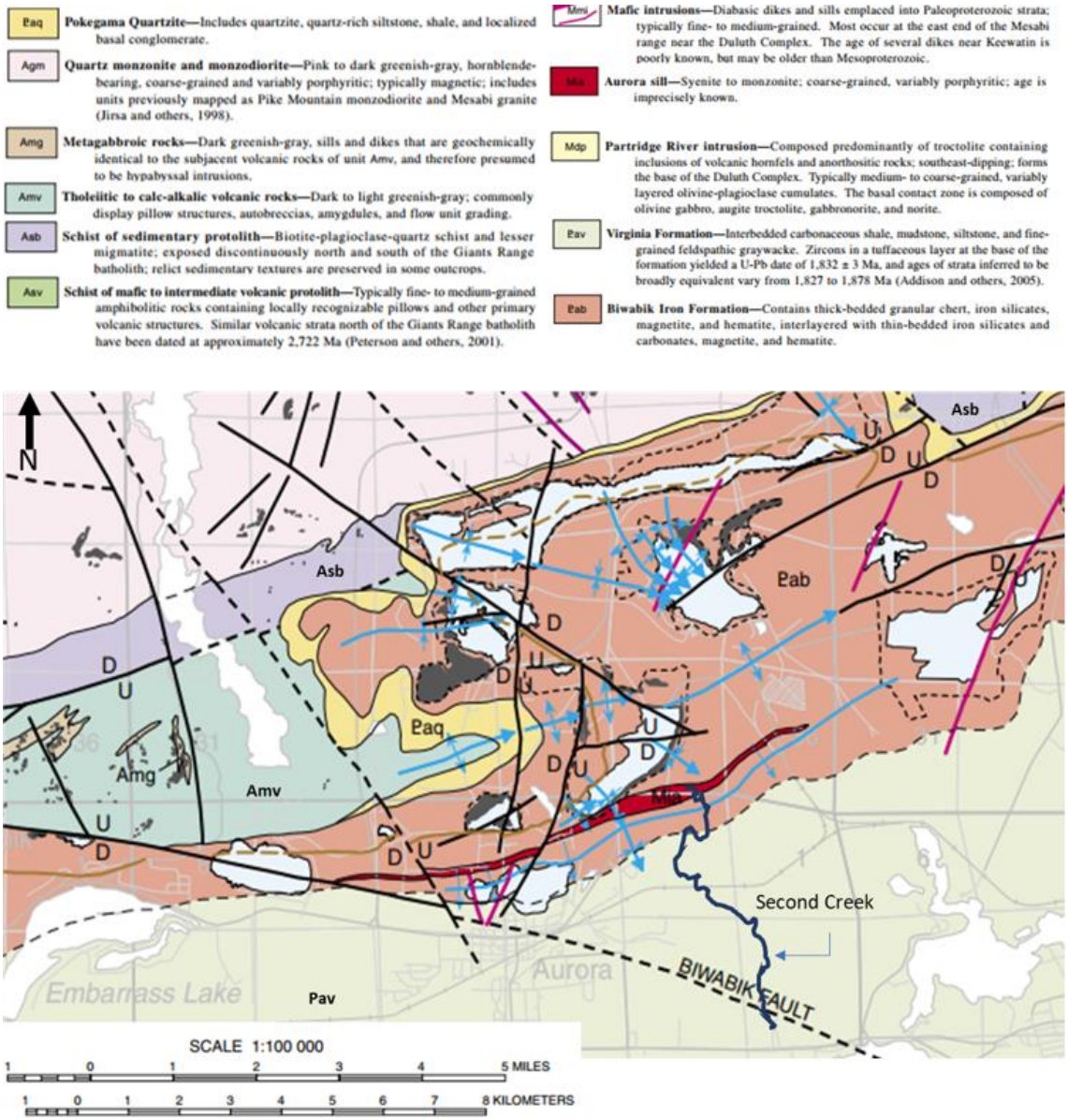

Figure 4: Regional bedrock map for Second Creek field site. Modified from Jirsa *et al.*, 2005.

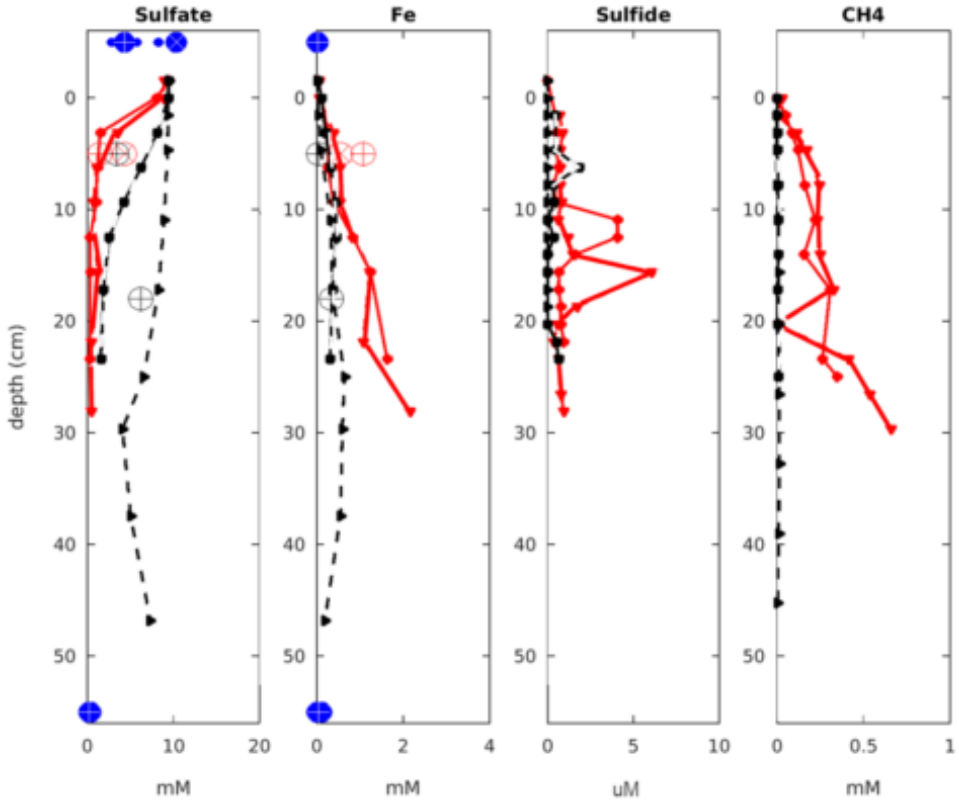

Figure 5: Results of geochemical analyses from porewater samples collected from 'peepers' installed in the main channel (dashed lines) and west wetland (solid lines) of Second Creek during the 2016 field season. Geochemical results from samples collected using Rhizon samplers in channel and west wetland cores are depicted by black and red crossed circles respectively. Surface water and groundwater data are depicted by blue circles at the top and bottom of the profiles, respectively. From Yourd, 2017.

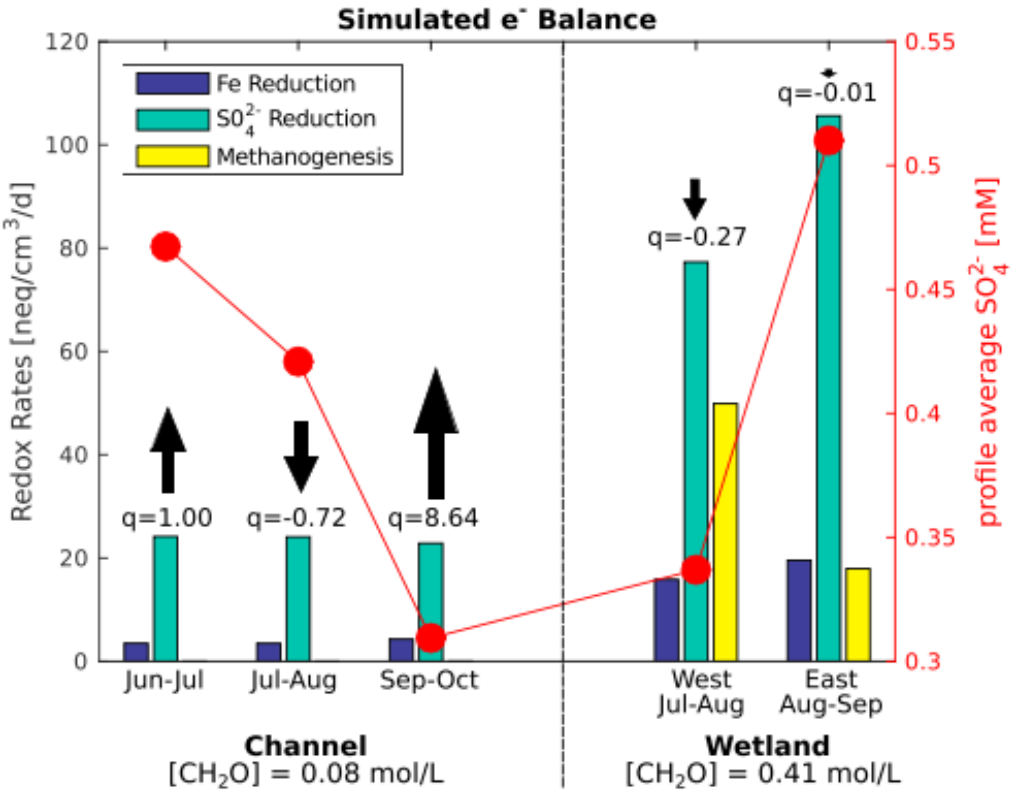

Figure 6: Simulated e^- redox rates (left axis) derived from reactive transport model for 5 different scenarios (channel pre-flood, flood, and post-flood; flooded east and west wetlands). Red dots show average simulated concentrations (right axis) over 2.5m soil profiles over the 30-day simulation period. Modeled hydrologic flux rates (q) and concentrations of organic C (CH_2O) are also depicted. The results of this model are supported by field observations and geochemical analyses. From Ng *et al.*, 2017.

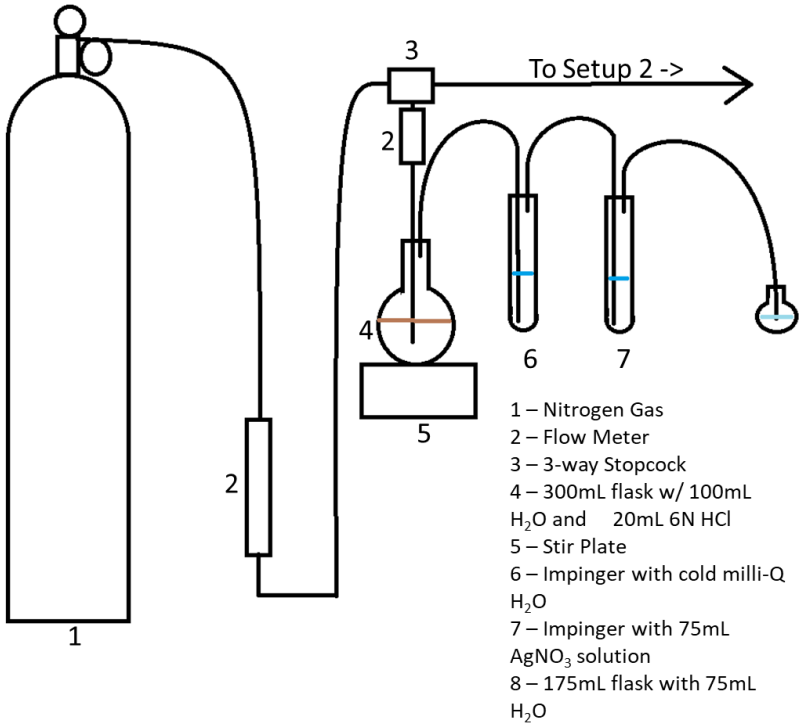

Figure 7: Schematic depicting setup used for measurement of acid volatile sulfides. Adapted from Allen *et al.*, 1993.

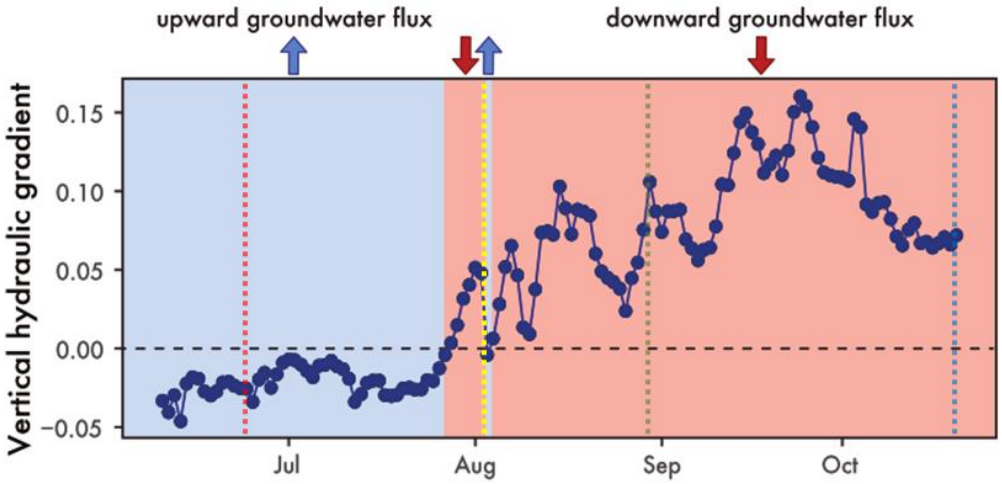

Figure 8: Vertical hydraulic gradient data collected from the east piezometer in the channel of Second Creek (piezometer PZCE) during the 2017 field season. Red shaded areas indicate downward groundwater flux while blue shaded regions indicate upward groundwater flux. Approximate geochemical sampling times are indicated by dashed red, yellow, green, and blue lines to represent the June, July, August, and October sampling times, respectively. Modified from Fadely, 2018.

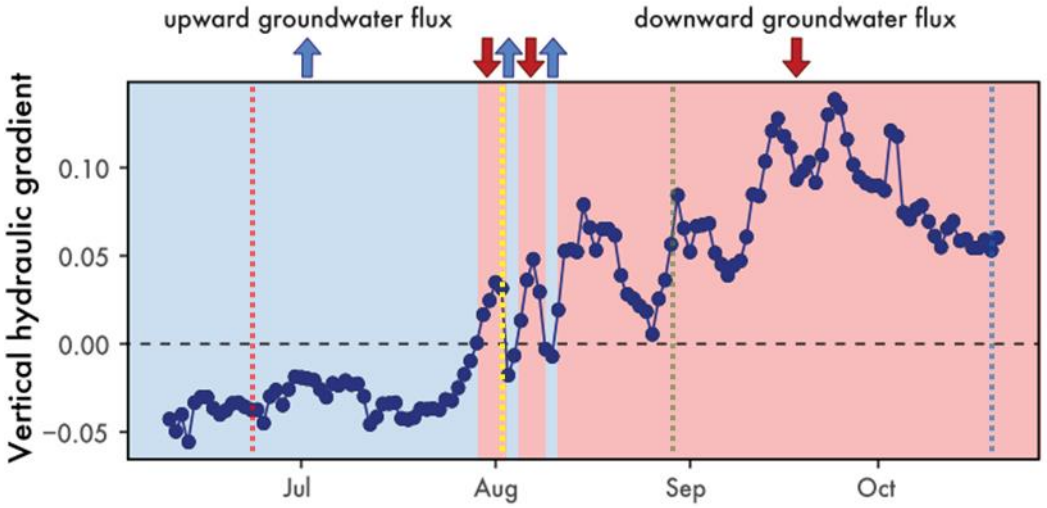

Figure 9: Vertical hydraulic gradient data collected from the center piezometer in the channel of Second Creek (piezometer PZCC) during the 2017 field season. Red shaded areas indicate downward groundwater flux while blue shaded regions indicate upward groundwater flux. Approximate geochemical sampling times are indicated by dashed red, yellow, green, and blue lines to represent the June, July, August, and October sampling times, respectively. Modified from Fadely, 2018.

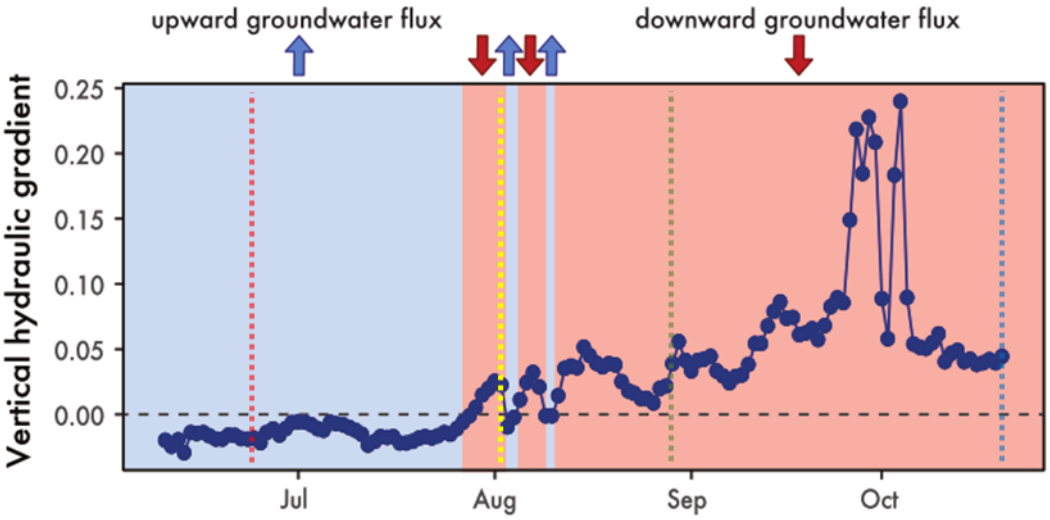

Figure 10: Vertical hydraulic gradient data collected from the piezometer in the east wetland at Second Creek (piezometer PZE2) during the 2017 field season. Red shaded areas indicate downward groundwater flux while blue shaded regions indicate upward groundwater flux. Approximate geochemical sampling times are indicated by dashed red, yellow, green, and blue lines to represent the June, July, August, and October sampling times, respectively. Modified from Fadely, 2018.

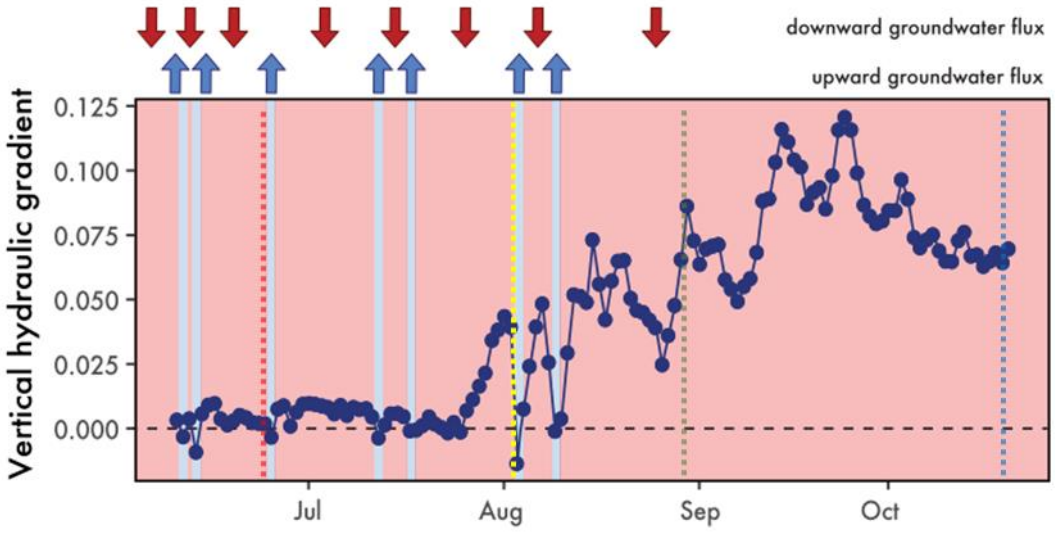

Figure 11: Vertical hydraulic gradient data collected from the piezometer in the west wetland at Second Creek (piezometer PZI2) during the 2017 field season. Red shaded areas indicate downward groundwater flux while blue shaded regions indicate upward groundwater flux. Approximate geochemical sampling times are indicated by dashed red, yellow, green, and blue lines to represent the June, July, August, and October sampling times, respectively. Modified from Fadely, 2018.

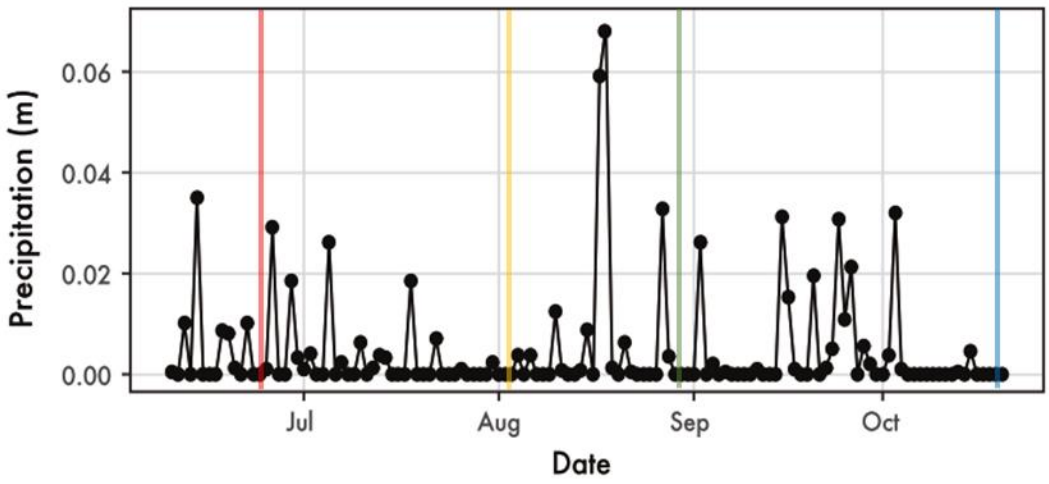

Figure 12: Daily precipitation data for Second Creek Field site during 2017 field season. Measurements obtained from nearby city (Embarrass, MN). Approximate geochemical sampling times are indicated by red, yellow, green, and blue lines to represent the June, July, August, and October sampling times, respectively. Modified from Fadely, 2018.

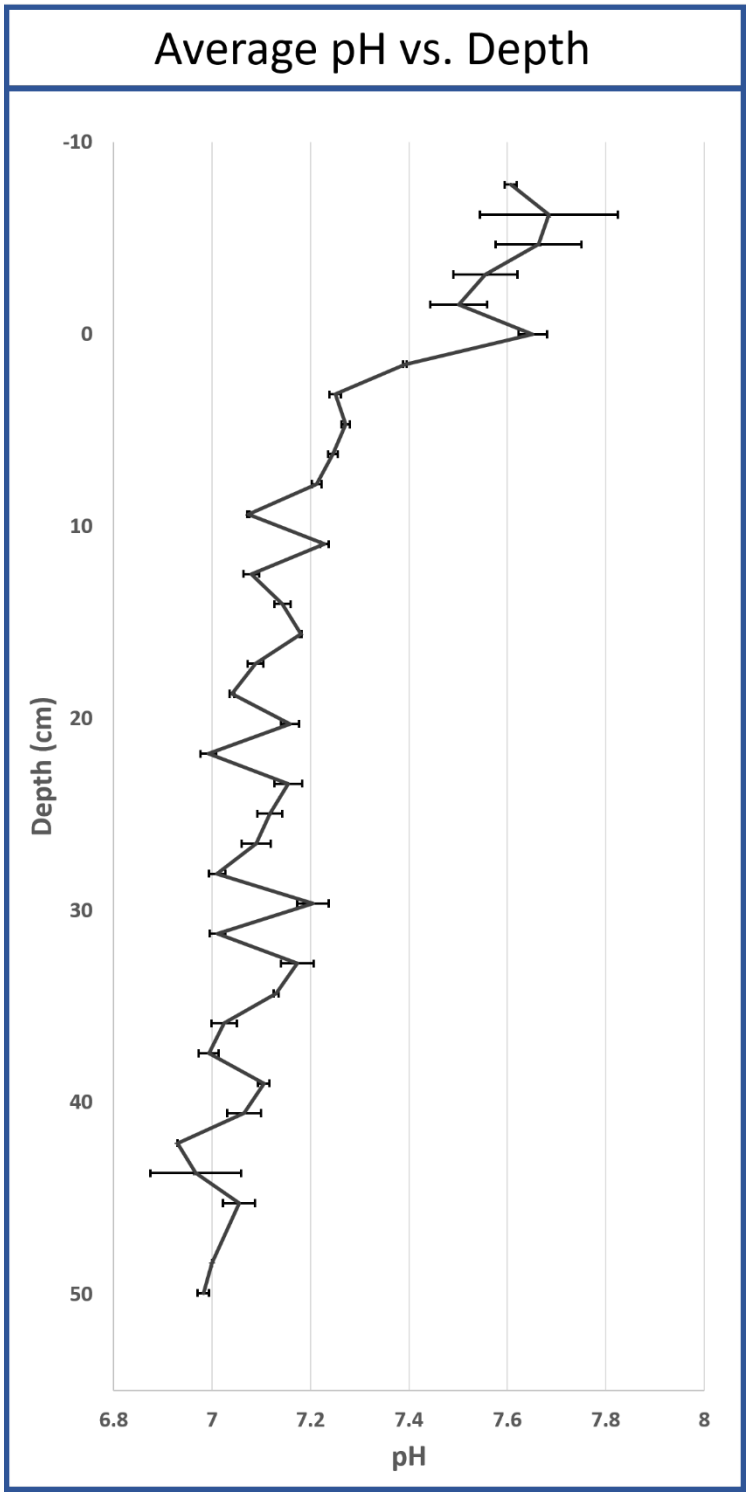

Figure 13: Average pH with depth at Second Creek. Plotted values represent cumulative average for each depth from all sampled peepers. Error bars represent standard deviation for each depth. Zero depth marks the sediment-water interface with increasing depth values indicating deeper sediment depth.

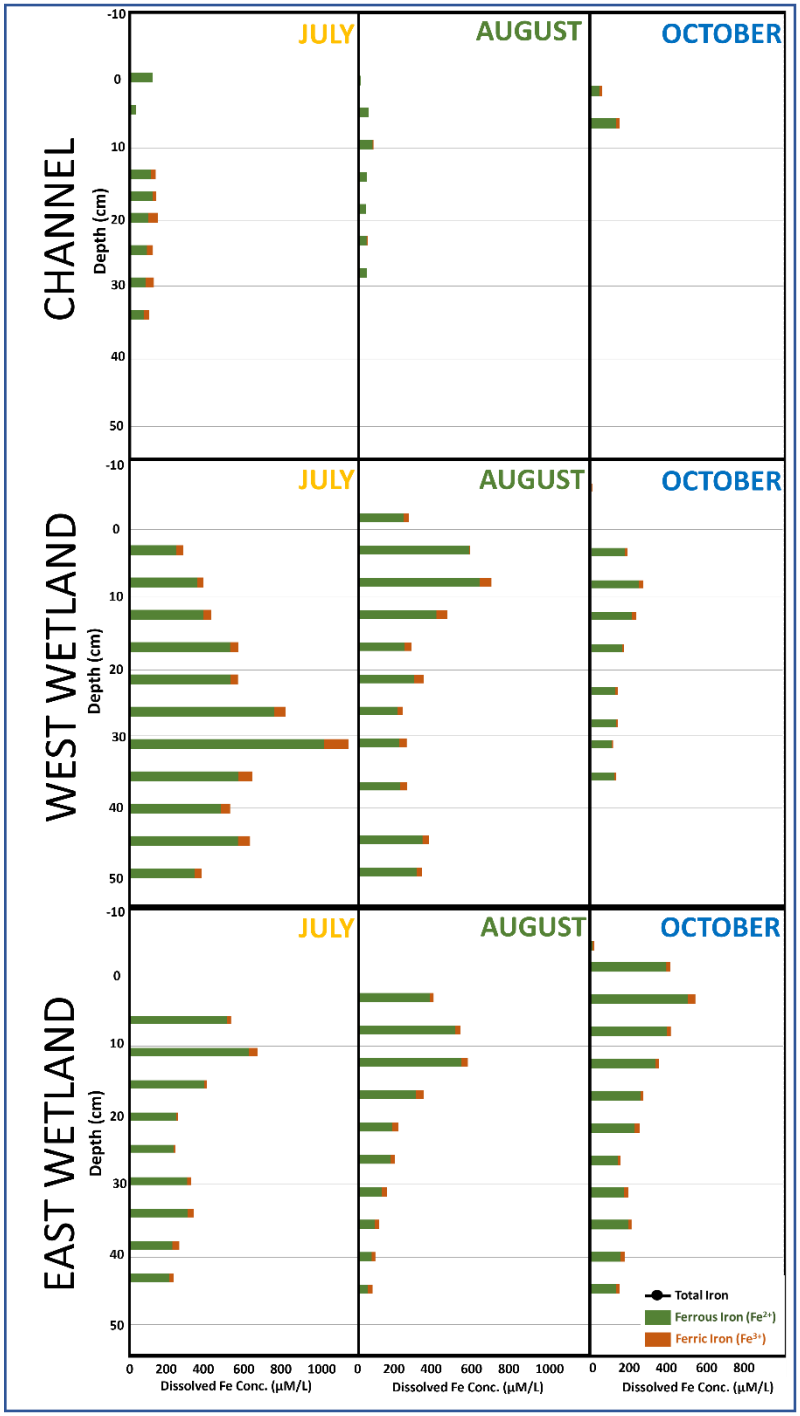

Figure 14: Select porewater Fe speciation and concentration as a function of depth (see table 1 for all Fe speciation data). Channel data is plotted in the top row, west wetland data is plotted in the middle row, and east wetland data is plotted in the bottom row. Fe measurements from porewater collected in July, August, and October are plotted in the left, center, and right columns respectively. Measured ferrous Fe (Fe^{2+}) concentrations are denoted by green bars and measured ferric Fe (Fe^{3+}) concentrations are denoted by orange bars.

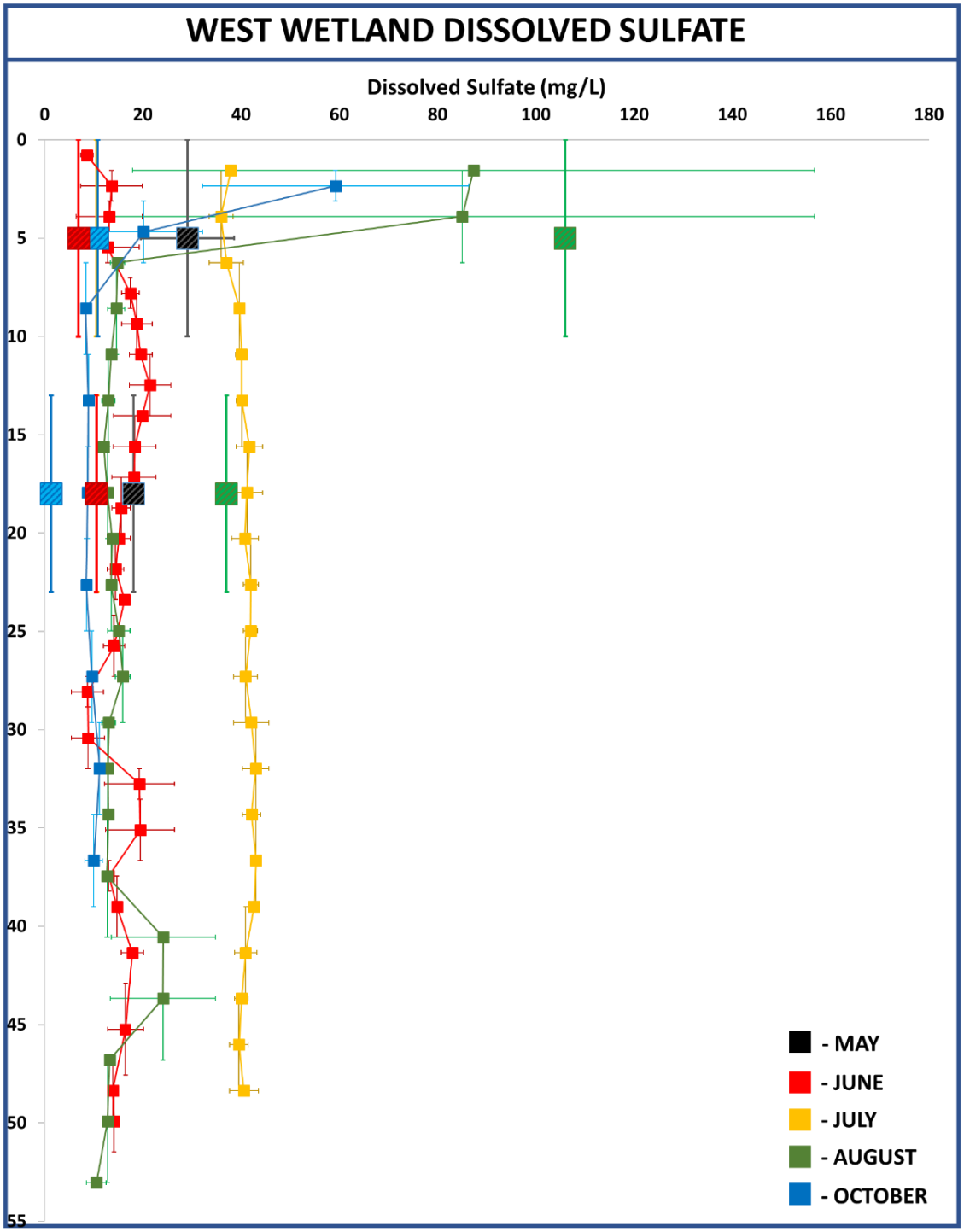

Figure 15: Dissolved SO_4^{2-} concentration versus depth for west wetland at Second Creek. Small solid squares represent 'peeper' data; error bars represent standard deviation for averaged duplicate peepers. Porewater samples collected using Rhizon™ samplers denoted by large patterned squares; horizontal error bars represent standard deviation for duplicate Rhizon™ samples while vertical error bars represent sampling range of sampler. May, June, July, August, and October sampling periods represented by black, red, yellow, green, and blue squares, respectively.

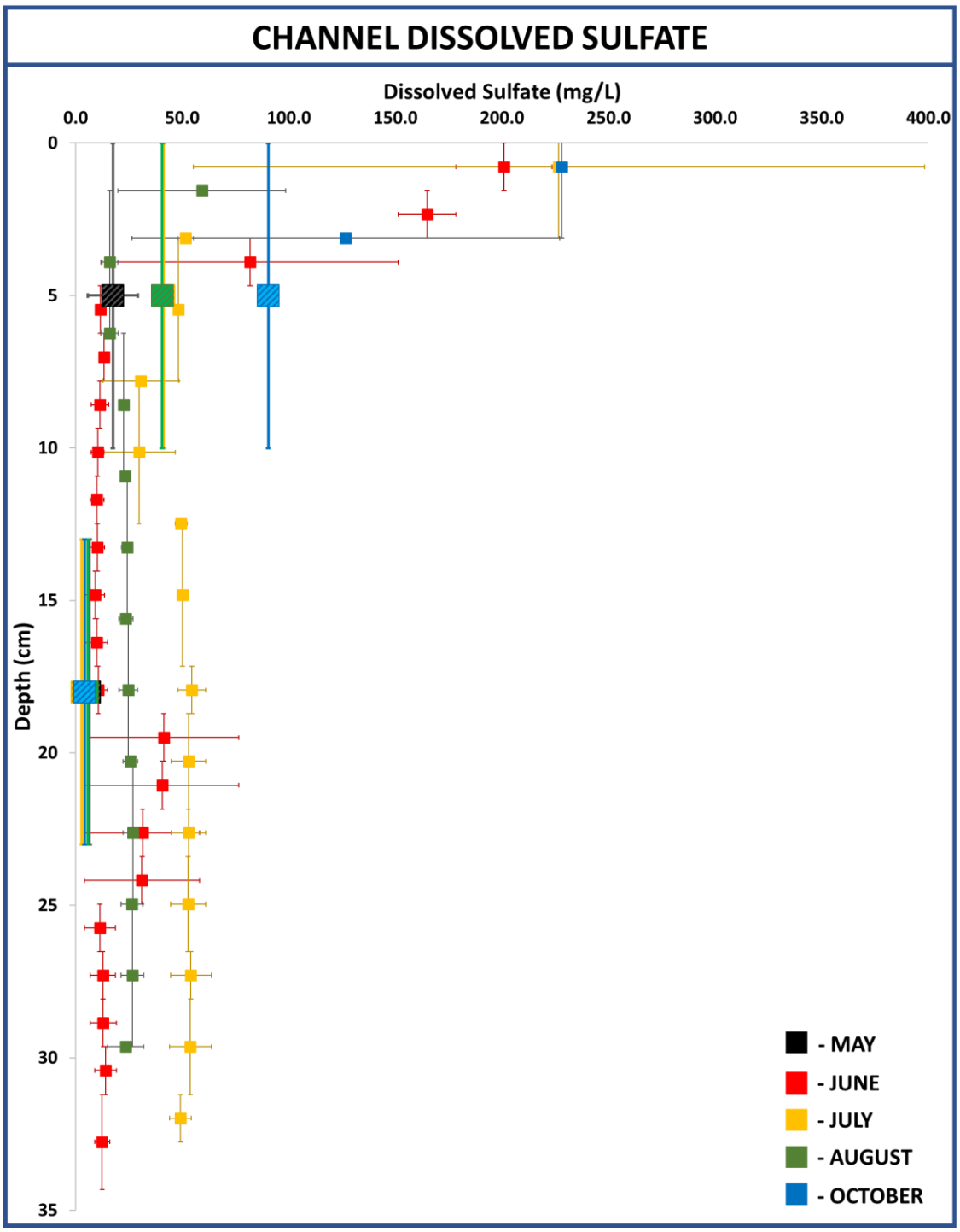

Figure 16: Dissolved SO_4^{2-} concentration versus depth for channel at Second Creek. Small solid squares represent 'peeper' data; error bars represent standard deviation for averaged duplicate peepers. Porewater samples collected using Rhizon™ samplers denoted by large patterned squares; horizontal error bars represent standard deviation for duplicate Rhizon™ samples while vertical error bars represent sampling range of sampler. May, June, July, August, and October sampling periods represented by black, red, yellow, green, and blue squares, respectively.

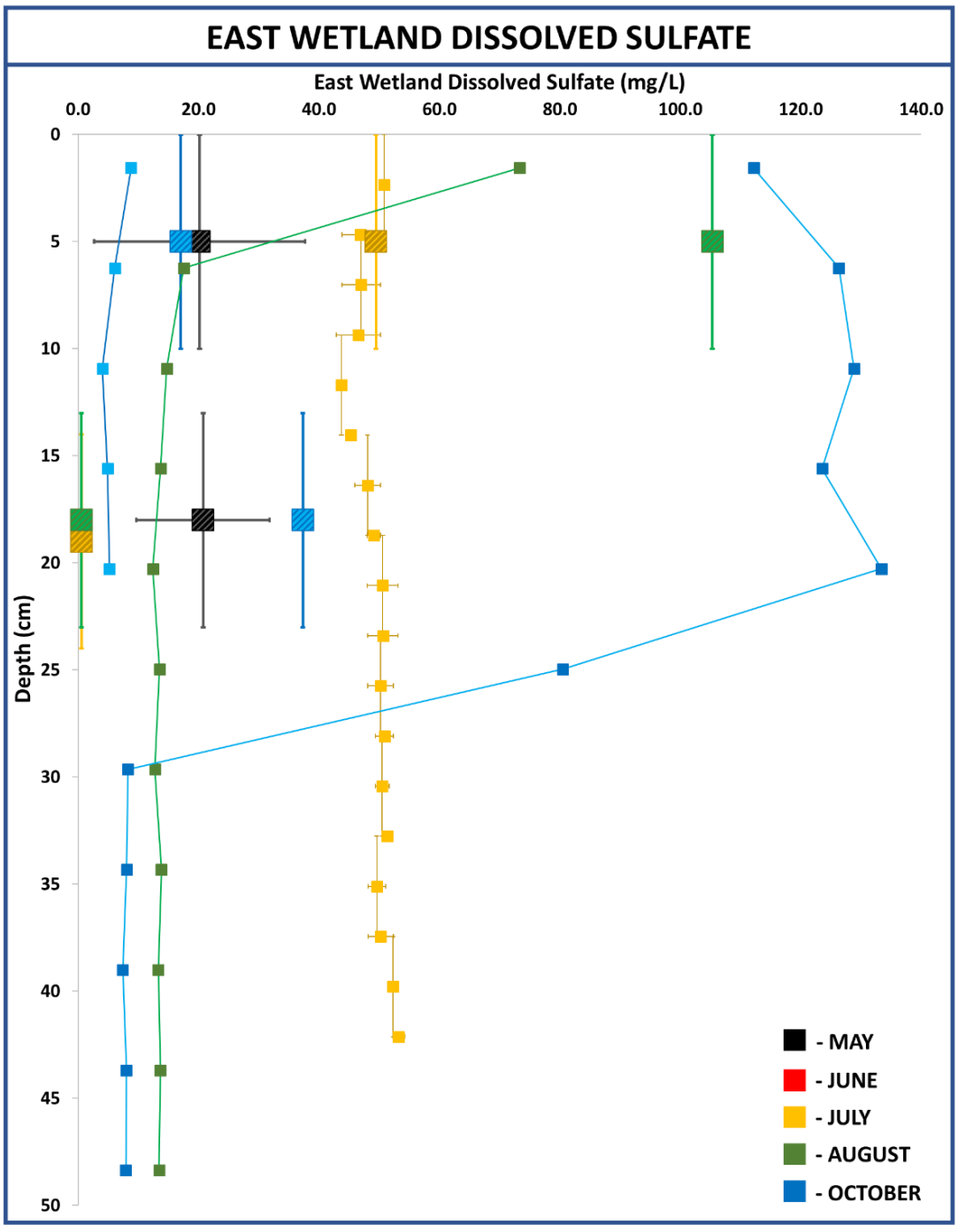

Figure 17: Dissolved SO_4^{2-} concentration versus depth for east wetland at Second Creek. Small solid squares represent 'peeper' data; error bars represent standard deviation for a veraged duplicate peepers. Porewater samples collected using Rhizon™ samplers denoted by large patterned squares; horizontal error bars represent standard deviation for duplicate Rhizon™ samples while vertical error bars represent sampling range of sampler. May, June, July, August, and October sampling periods represented by black, red, yellow, green, and blue squares, respectively. For October samples, duplicate peeper data has been plotted individually due to high variability between sampled locations. Only one peeper was sampled in August at this location, so no statistical information is available for individual datapoints.

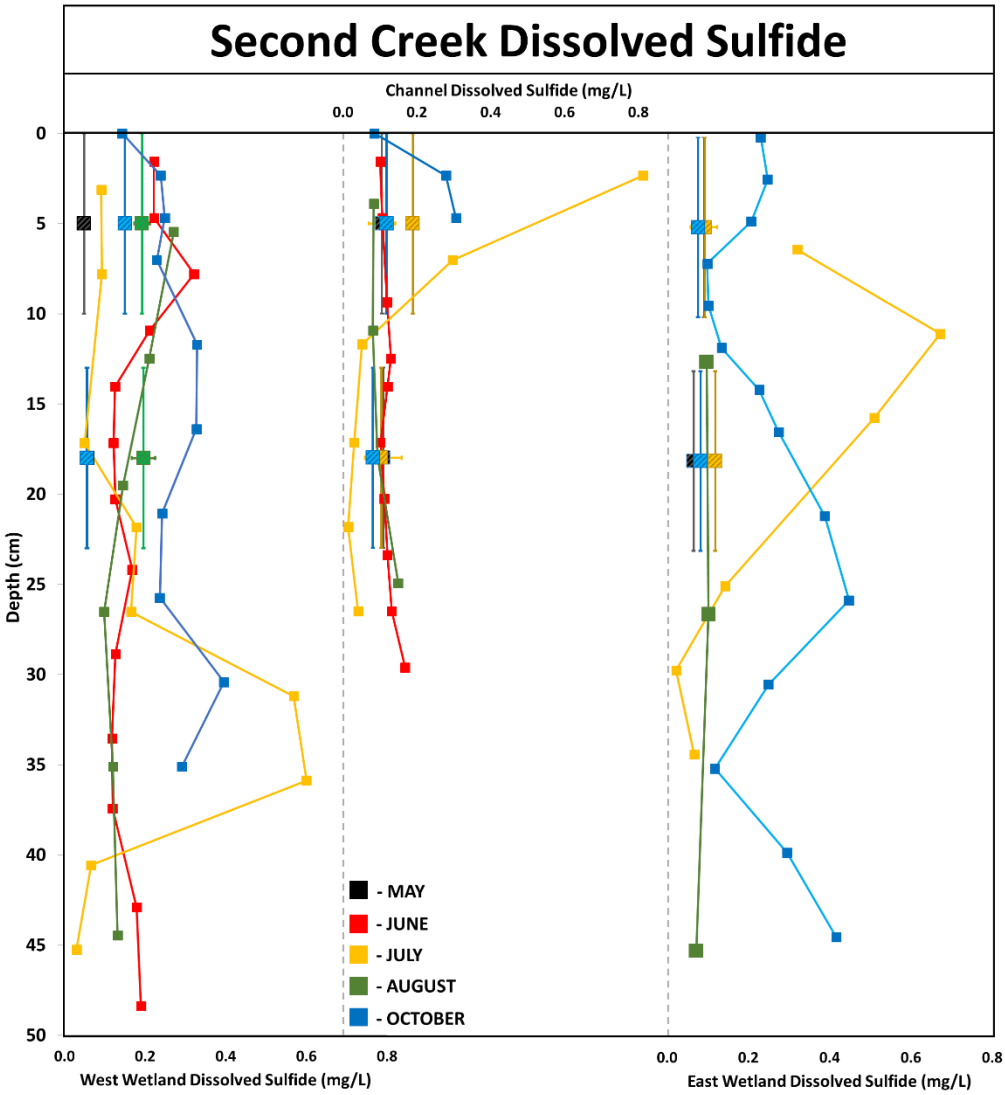

Figure 18: Dissolved sulfide concentrations in the west wetland (left), channel (center), and east wetland (right) in porewater collected using rhizon samplers (large, patterned squares) and peepers (smaller squares). Samples were collected during the months of May (black), June (red), July (yellow), August (green), and October (blue). All plotted values are averaged between duplicate rhizon samplers or peepers. Error bars on rhizon sample points indicate standard deviation from averaged values. Error bars are not depicted for peeper samples for visual simplicity, but these values were generally less than ±20%.

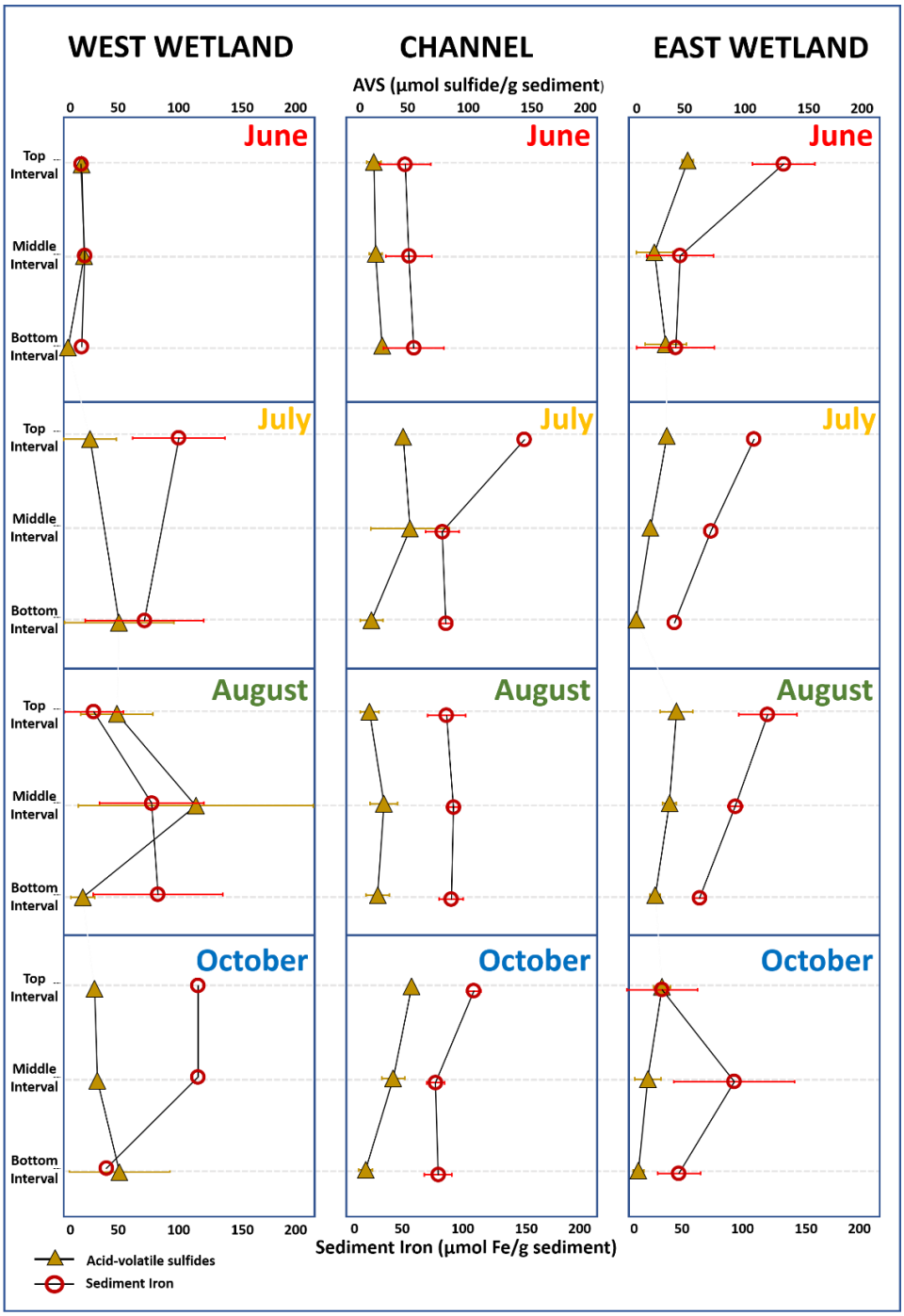

Figure 19: Measurement of solid-phase Fe and acid volatile sulfide (AVS) fraction in sediments collected from the west wetland, channel, and east wetland (left to right, respectively) of Second Creek during the 2017 field season. June data are plotted at the top followed by July and August in the center and October at the bottom. Sediment Fe is denoted as open red circles and AVS fraction is denoted by yellow triangles. The 'Top Interval', 'Middle Interval', and 'Bottom Interval' axis corresponds to sampling intervals of approximately 4cm, 10cm, and 20cm respectively. Error bars represent standard deviation between duplicate cores.

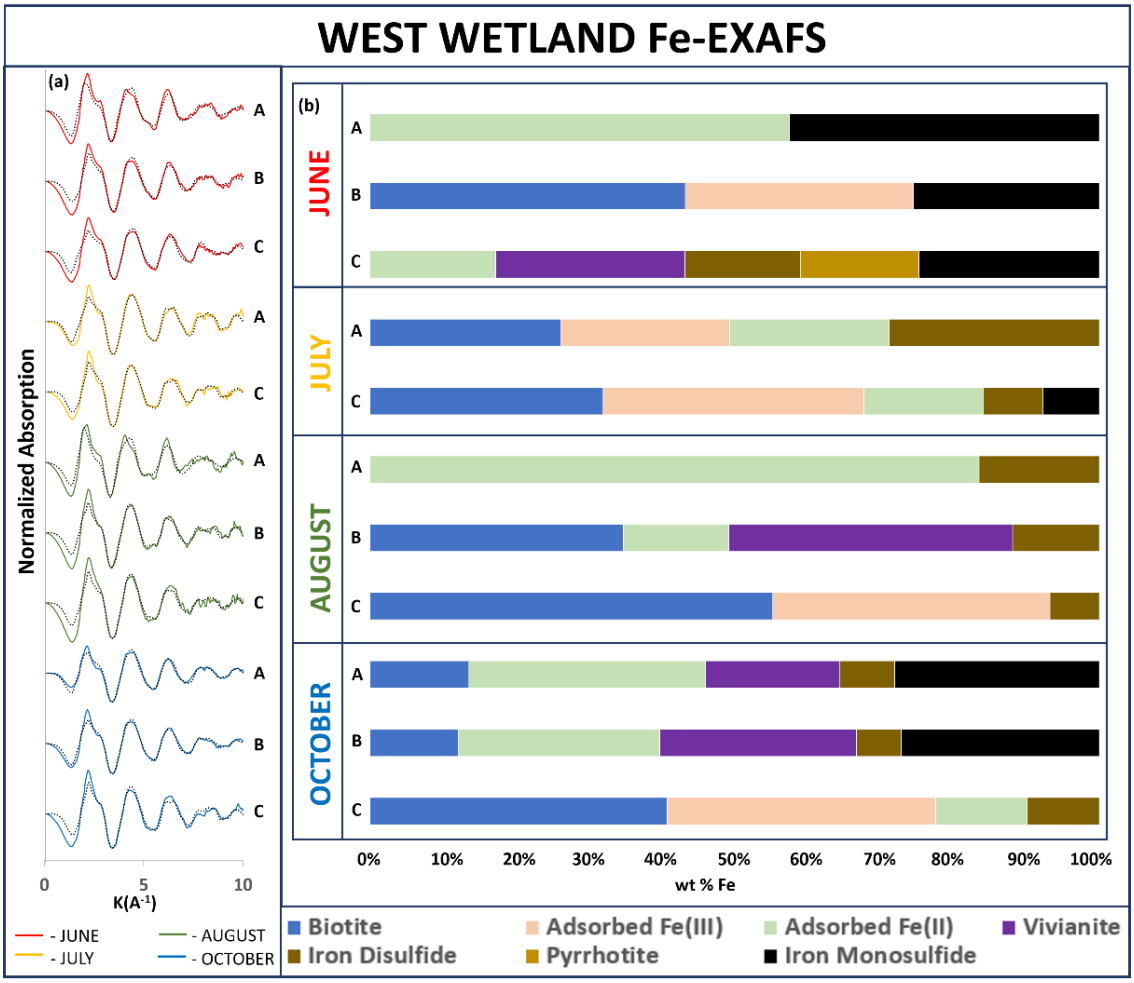

Figure 20: Fe K-edge X-ray absorption spectroscopy data from sediments collected from the west wetland at Second Creek. The 'A', 'B', and 'C' denotations refer to the top (~4cm), middle (~10cm), and bottom (~20cm) sampling intervals. (a) Experimental k^2-weighted EXAFS spectra for June (red), July (yellow), August (green), and October (blue) and linear combination fits (gray dotted line); (b) LCF results expressed as mass concentration (wt % Fe) for Fe-containing components in bulk sediment samples with the sum of all Fe species normalized to 100%.

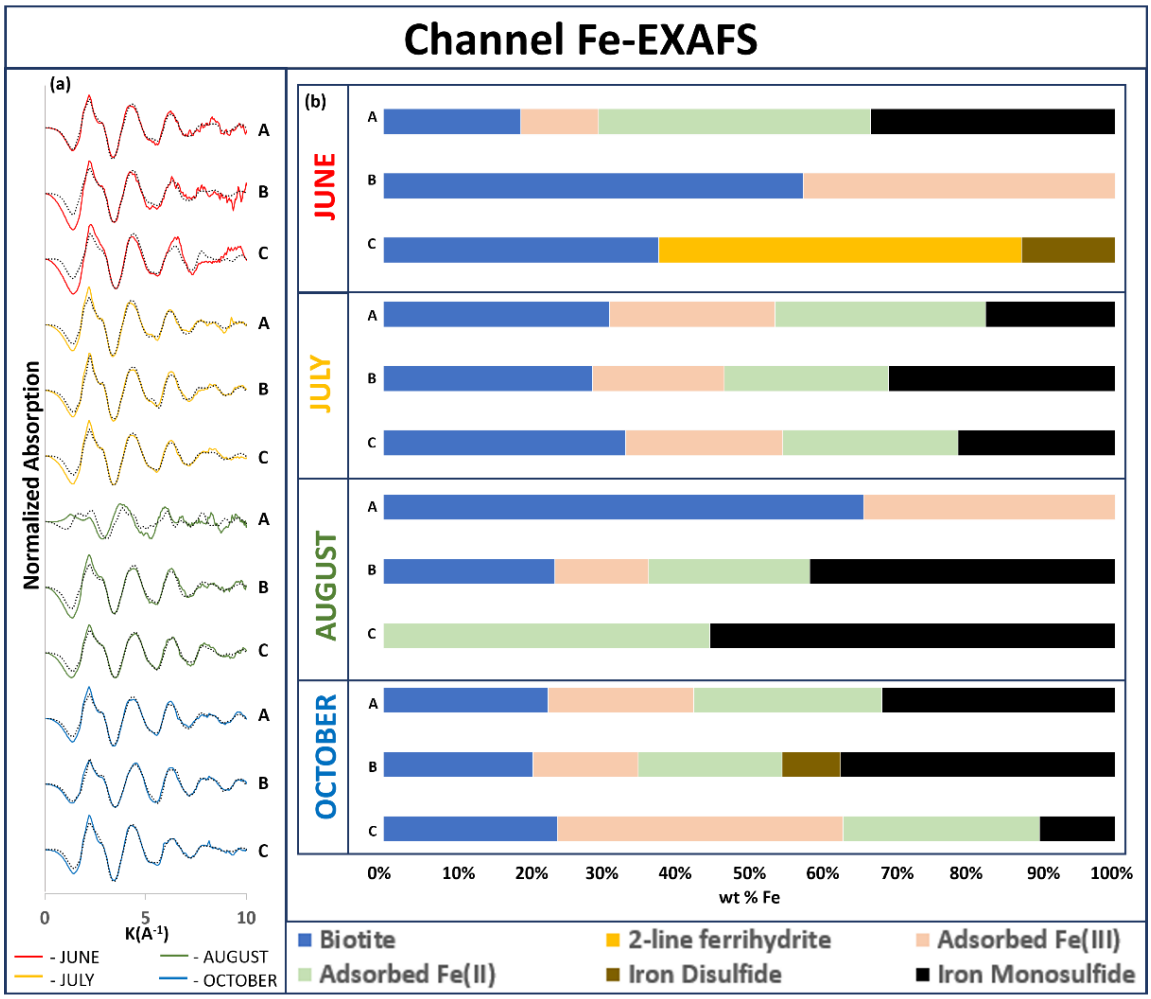

Figure 21: Fe K-edge X-ray absorption spectroscopy data from sediments collected from the channel at Second Creek. The 'A', 'B', and 'C' denotations refer to the top (~4cm), middle (~10cm), and bottom (~20cm) sampling intervals. (a) Experimental k^2-weighted EXAFS spectra for June (red), July (yellow), August (green), and October (blue) and linear combination fits (gray dotted line); (b) LCF results expressed as mass concentration (wt % Fe) for Fe-containing components in bulk sediment samples with the sum of all Fe species normalized to 100%.

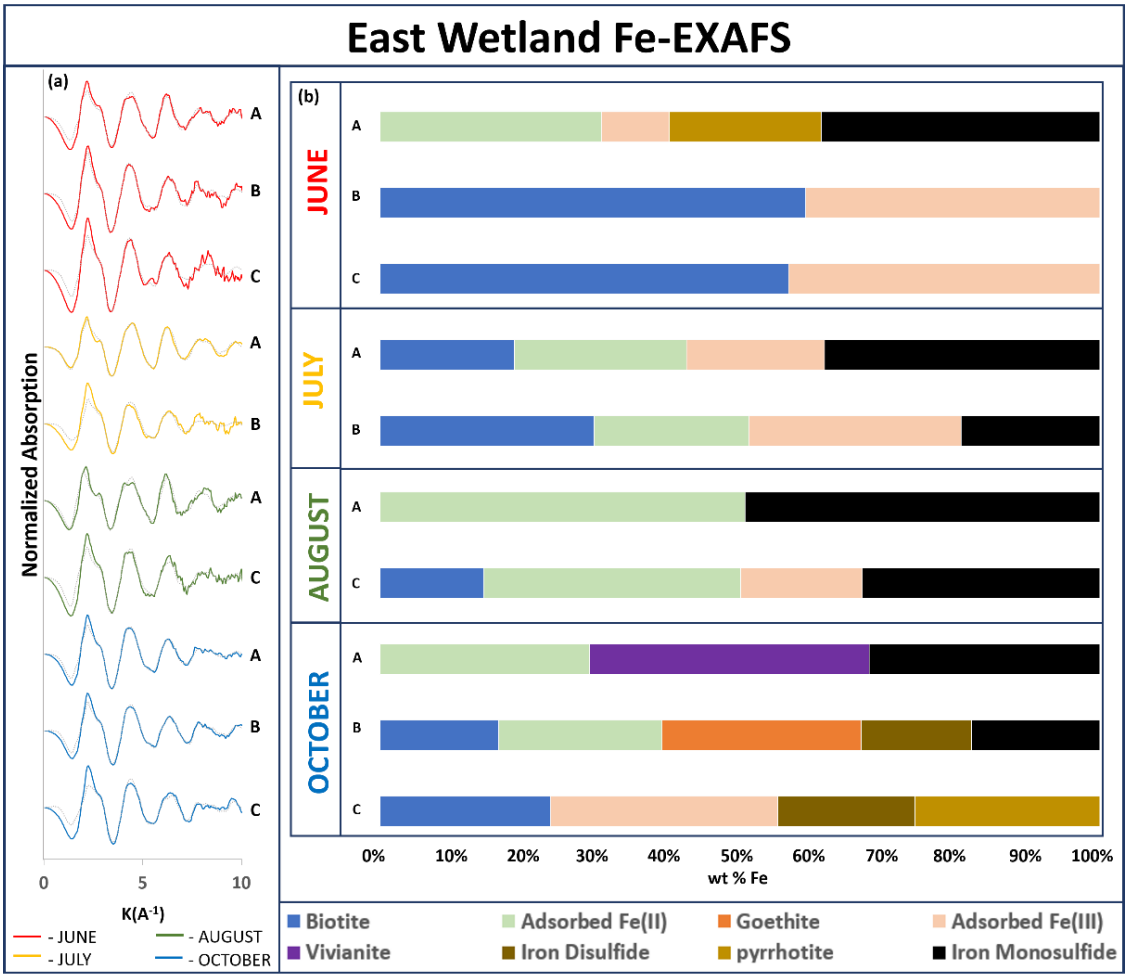

Figure 22: Fe K-edge X-ray absorption spectroscopy data from sediments collected from the east wetland at Second Creek. The 'A', 'B', and 'C' denotations refer to the top (~4cm), middle (~10cm), and bottom (~20cm) sampling intervals. (a) Experimental k^2-weighted EXAFS spectra for June (red), July (yellow), August (green), and October (blue) and linear combination fits (gray dotted line); (b) LCF results expressed as mass concentration (wt % Fe) for Fe-containing components in bulk sediment samples with the sum of all Fe species normalized to 100%.

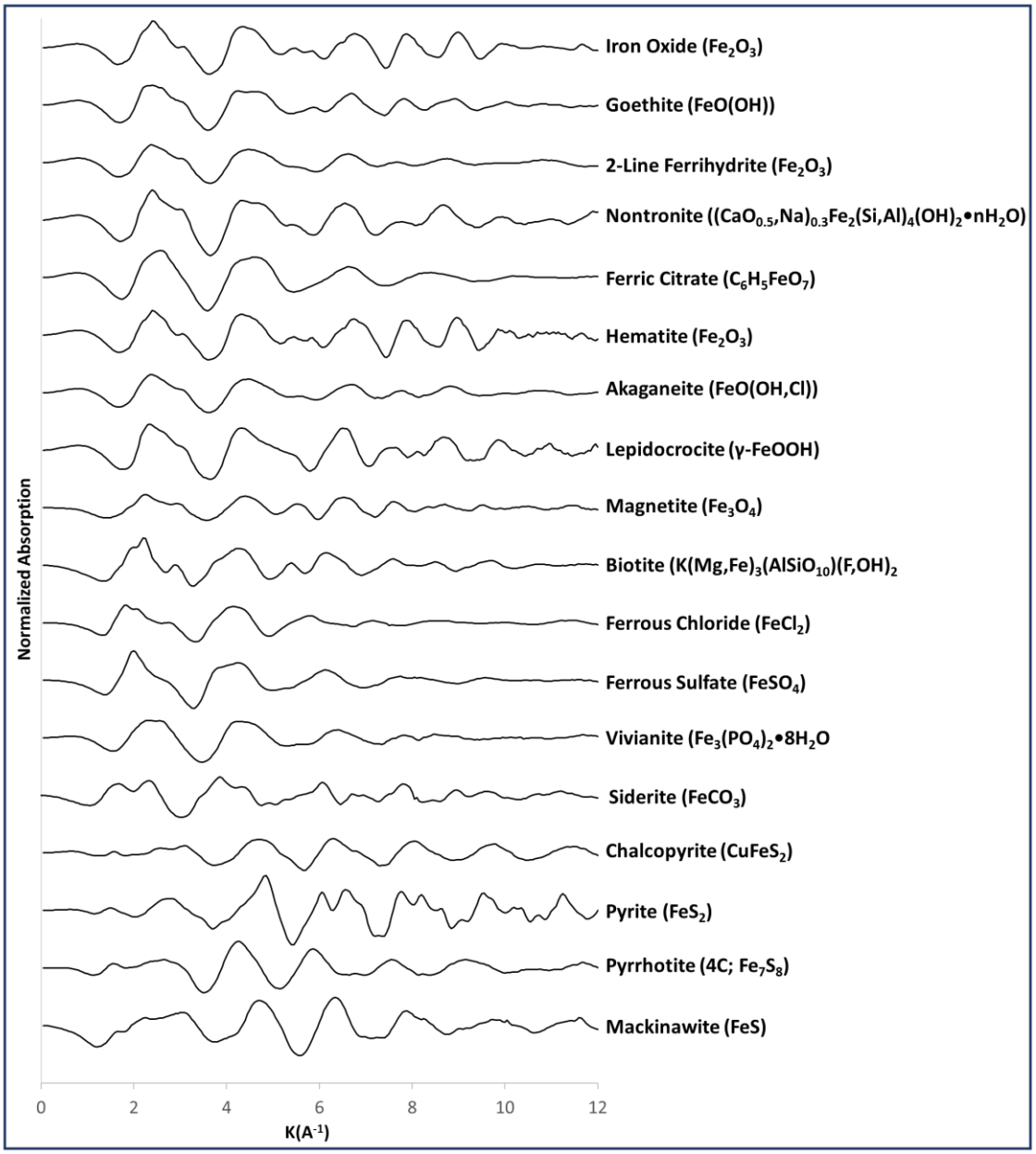

Figure 23: Normalized Fe-EXAFS spectra of reference standards used to perform linear combination fits. Raw XANES spectra of mackinawite courtesy of Dr. Brandy Toner.

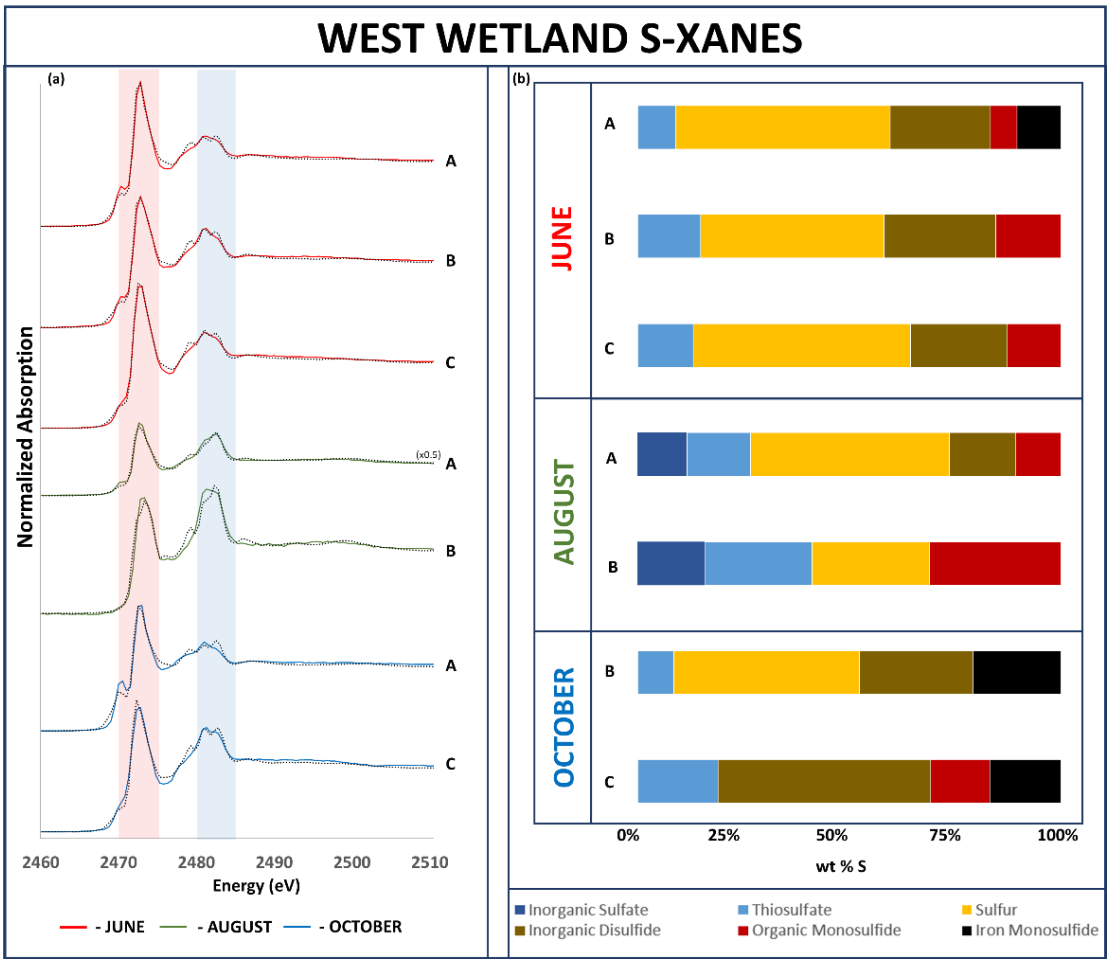

Figure 24: S K-edge X-ray absorption spectroscopy data from sediments collected from the west wetland at Second Creek. The 'A', 'B', and 'C' denotations refer to the top (~4cm), middle (~10cm), and bottom (~20cm) sampling intervals. (a) Experimental k^2 weighted XANES spectra for June (red), August (green), and October (blue) and linear combination fits (gray dotted lines); (b) LCF results expressed as mass concentrations (wt % S) for S-containing components in bulk sediment samples with the sum of all S species normalized to 100%. "(x0.5)" indicates the normalized absorption peak intensity was scaled down by a factor of two. The red shaded region denotes expected eV range for reduced S compounds (2470 - 2475eV) and blue shaded region denotes expected eV range for oxidized S compounds (2480 -2485eV).

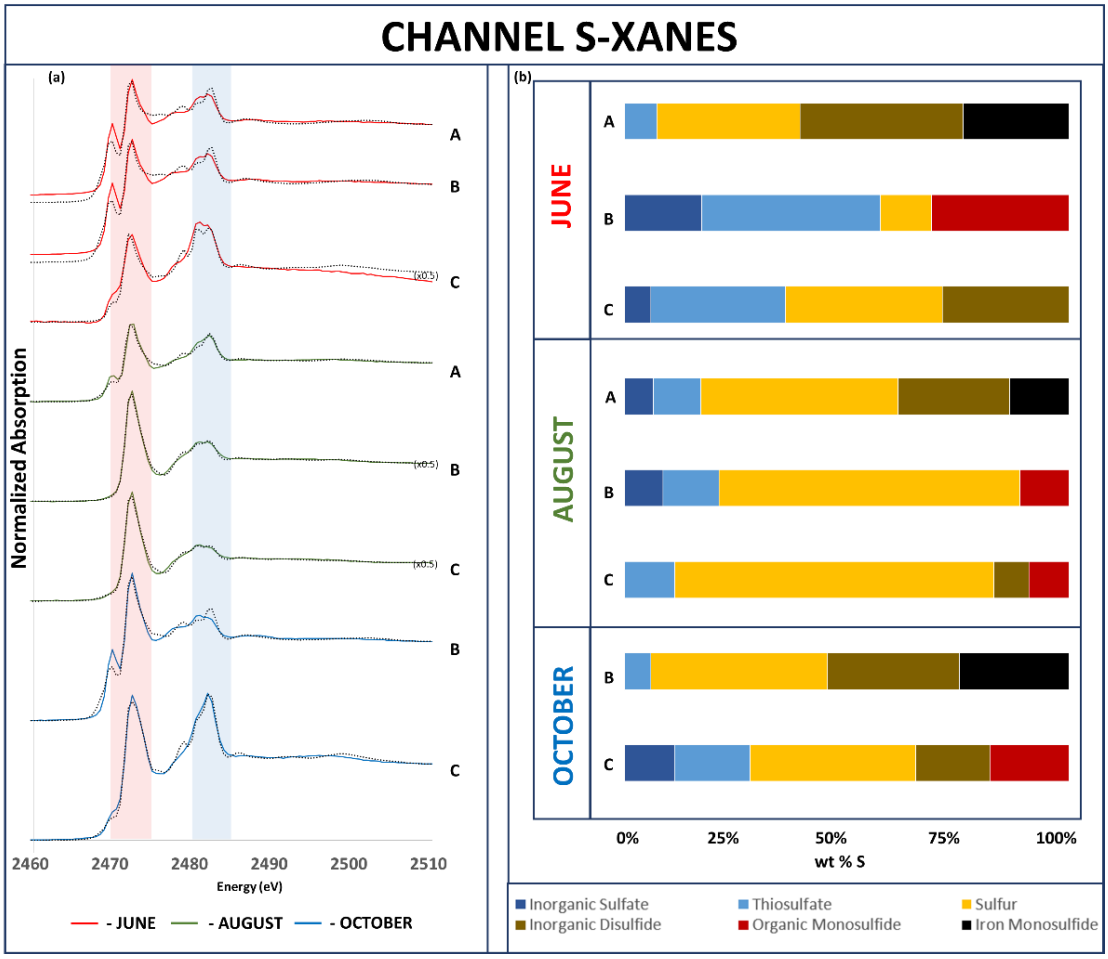

Figure 25: S K-edge X-ray absorption spectroscopy data from sediments collected from the channel at Second Creek. The 'A', 'B', and 'C' denotations refer to the top (~4cm), middle (~10cm), and bottom (~20cm) sampling intervals. (a) Experimental k^2 weighted XANES spectra for June (red), August (green), and October (blue) and linear combination fits (gray dotted lines); (b) LCF results expressed as mass concentrations (wt % S) for S-containing components in bulk sediment samples with the sum of all S species normalized to 100%. "(x0.5)" indicates the normalized absorption peak intensity was scaled down by a factor of two. The red shaded region denotes expected eV range for reduced S compounds (2470-2475eV) and blue shaded region denotes expected eV range for oxidized S compounds (2480-2485eV).

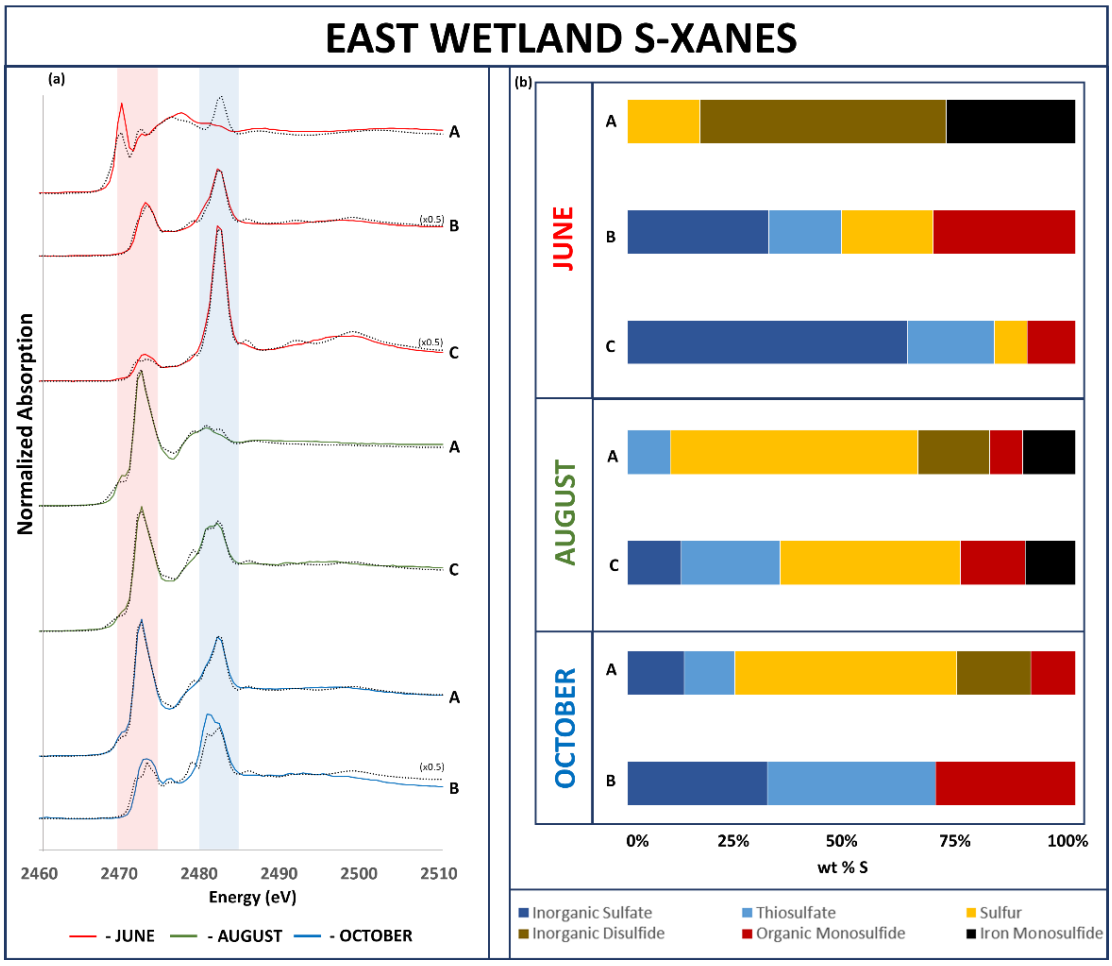

Figure 26: S K-edge X-ray absorption spectroscopy data from sediments collected from the east wetland at Second Creek. The 'A', 'B', and 'C' denotations refer to the top (~4cm), middle (~10cm), and bottom (~20cm) sampling intervals. (a) Experimental k^2 weighted XANES spectra for June (red), August (green), and October (blue) and linear combination fits (gray dotted lines); (b) LCF results expressed as mass concentrations (wt % S) for S-containing components in bulk sediment samples with the sum of all S species normalized to 100%. "(x0.5)" indicates the normalized absorption peak intensity was scaled down by a factor of two. The red shaded region denotes expected eV range for reduced S compounds (2470-2475eV) and blue shaded region denotes expected eV range for oxidized S compounds (2480-2485eV).

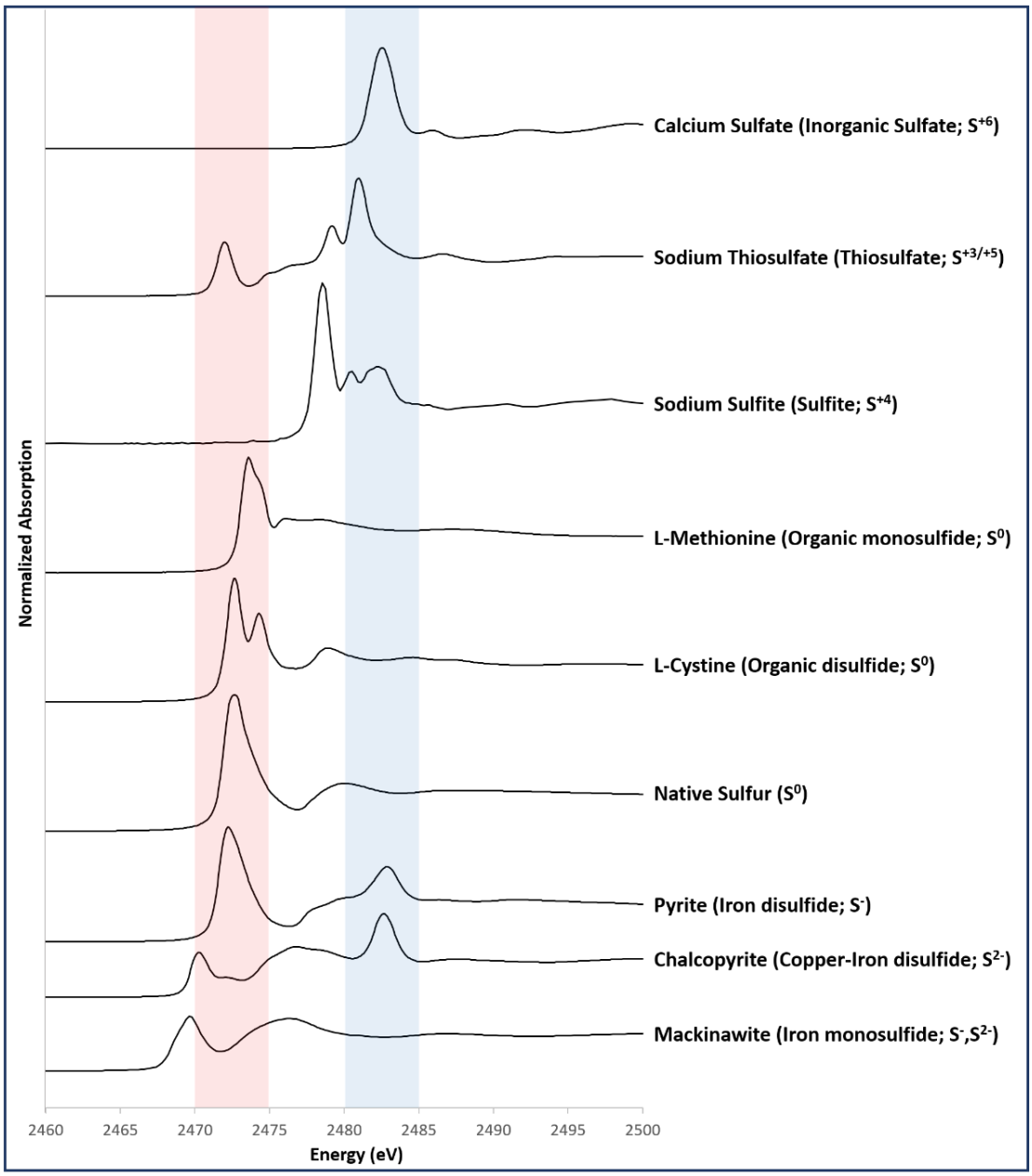

Figure 27: Normalized S-XANES spectra of reference standards used to perform linear combination fits. The eV range for reduced sulfide components (2470-2475eV) is highlighted with red, while the eV range for oxidized sulfide components (2480-2485eV) is highlighted with blue. Raw XANES spectra of mackinawite and sodium sulfite courtesy of Dr. Brandy Toner.

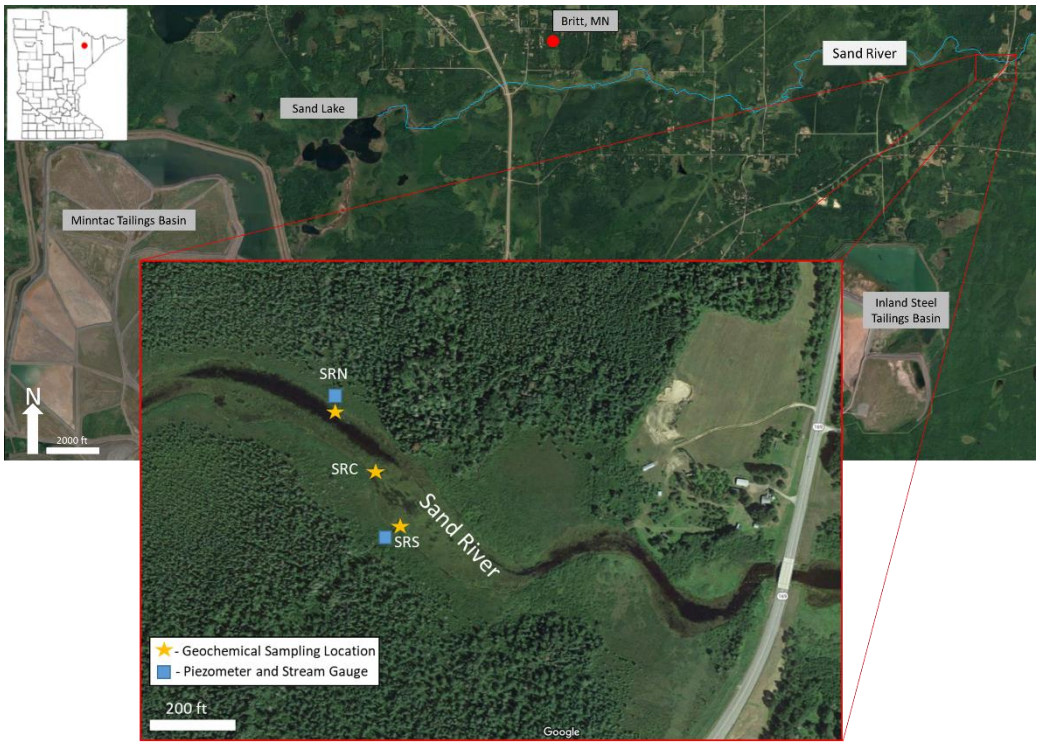

Figure 28: Regional Map showing Sand River field site location and setting (background). Site map showing close-up of field site (foreground). Geochemical sampling sites depicted by gold stars. Piezometer locations depicted by blue squares. Images acquired and modified from Google Earth on 15 Nov. 2018.

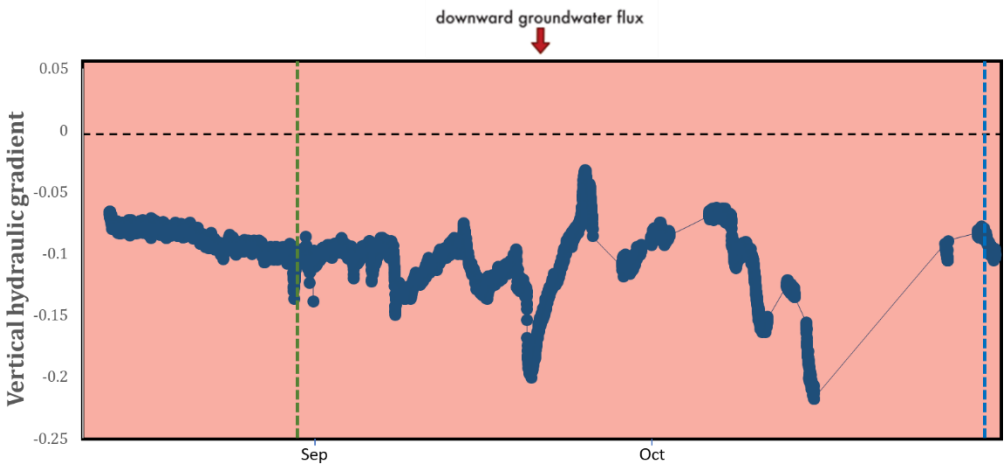

Figure 29: Vertical hydraulic gradient data collected from the piezometer in the north inlet at Sand River (piezometer SRN) during the 2018 field season. Approximate geochemical sampling times are indicated by dashed green, and blue lines to represent the August and October sampling times, respectively. Negative vertical hydraulic gradient suggests a downward flux of water into the subsurface.

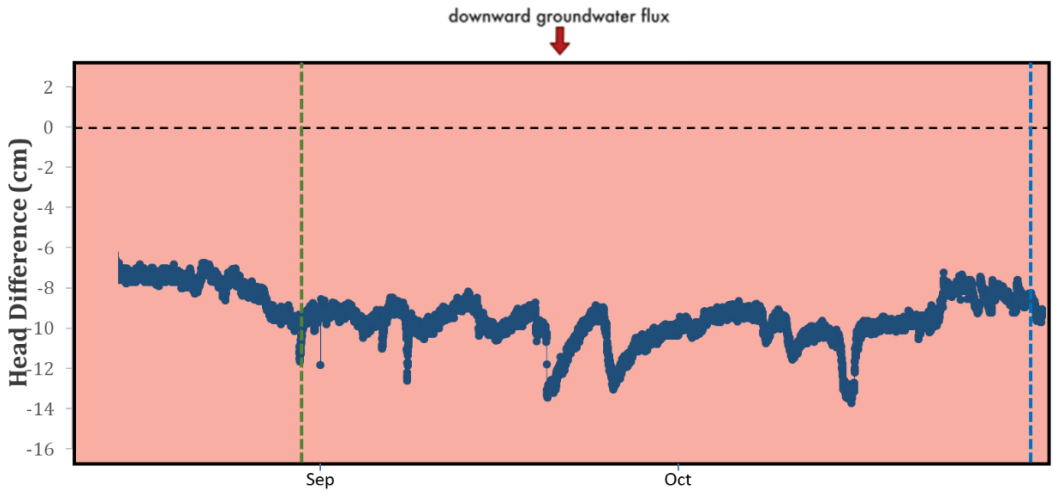

Figure 30: Head difference data collected from the piezometer in the south inlet at Sand River (piezometer SRS) during the 2018 field season. Approximate geochemical sampling times are indicated by dashed green, and blue lines to represent the August and October sampling times, respectively. Negative head difference suggests a flux of water into the subsurface.

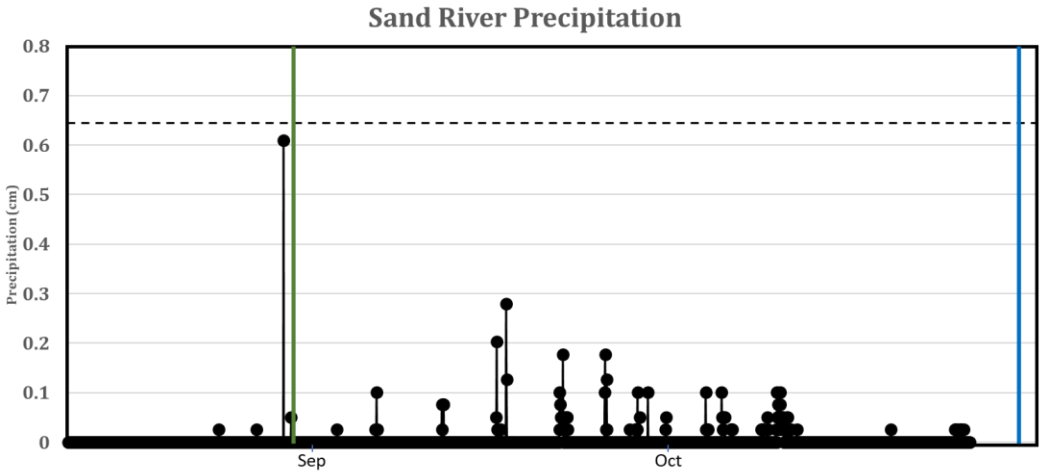

Figure 31: Daily precipitation data for the Sand River field site during 2018 field season. Approximate geochemical sampling times are indicated by green and blue lines to represent the August and October sampling times, respectively.

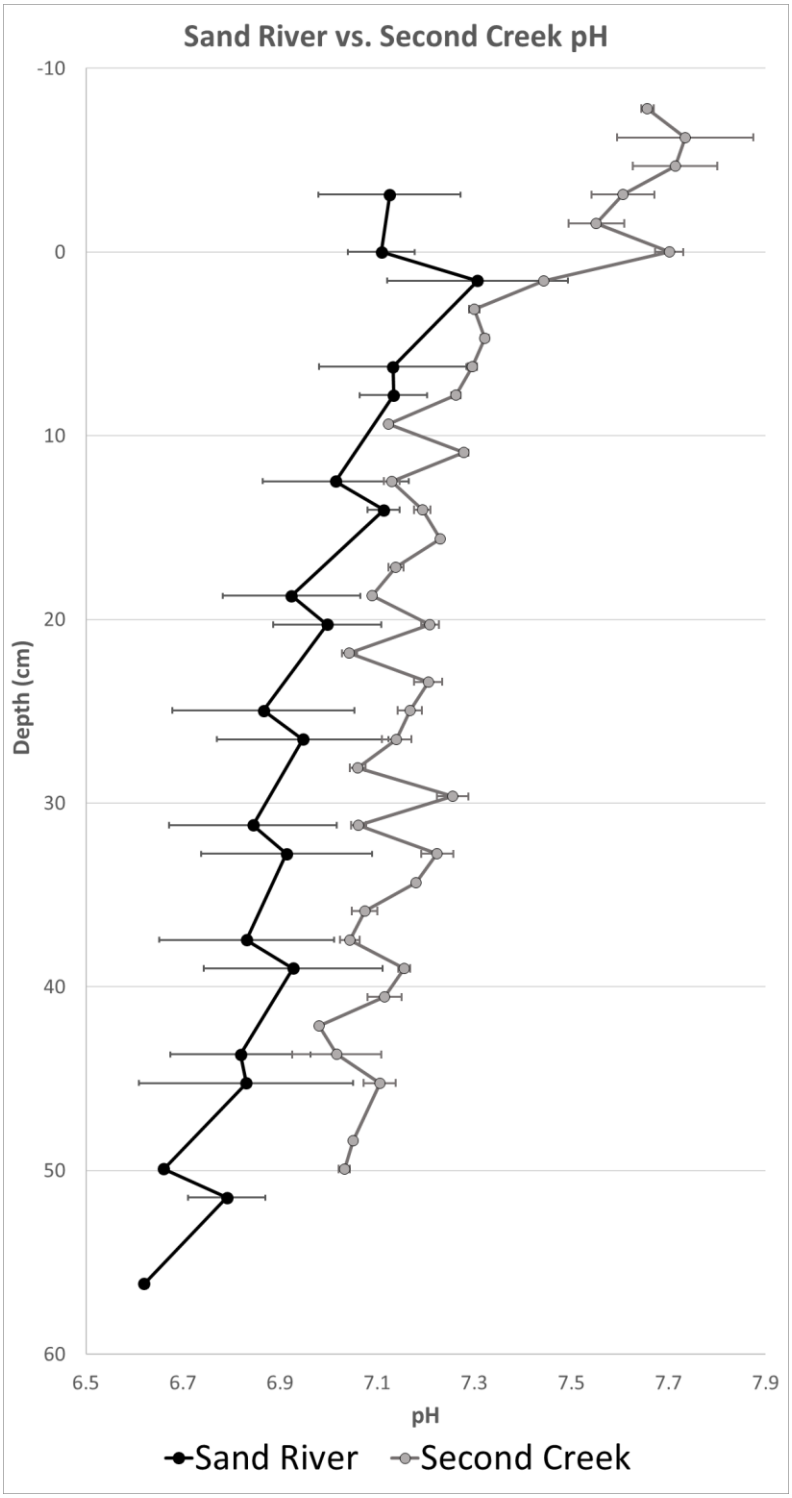

Figure 32: Average pH versus depth for Sand River (black) and Second Creek (gray) porewater with zero representing the sediment-water interface. Sand River averages only include pH measurements from the main river channel, measurements from the north and south inlets are not included. Error bars represent the standard deviation for each depth.

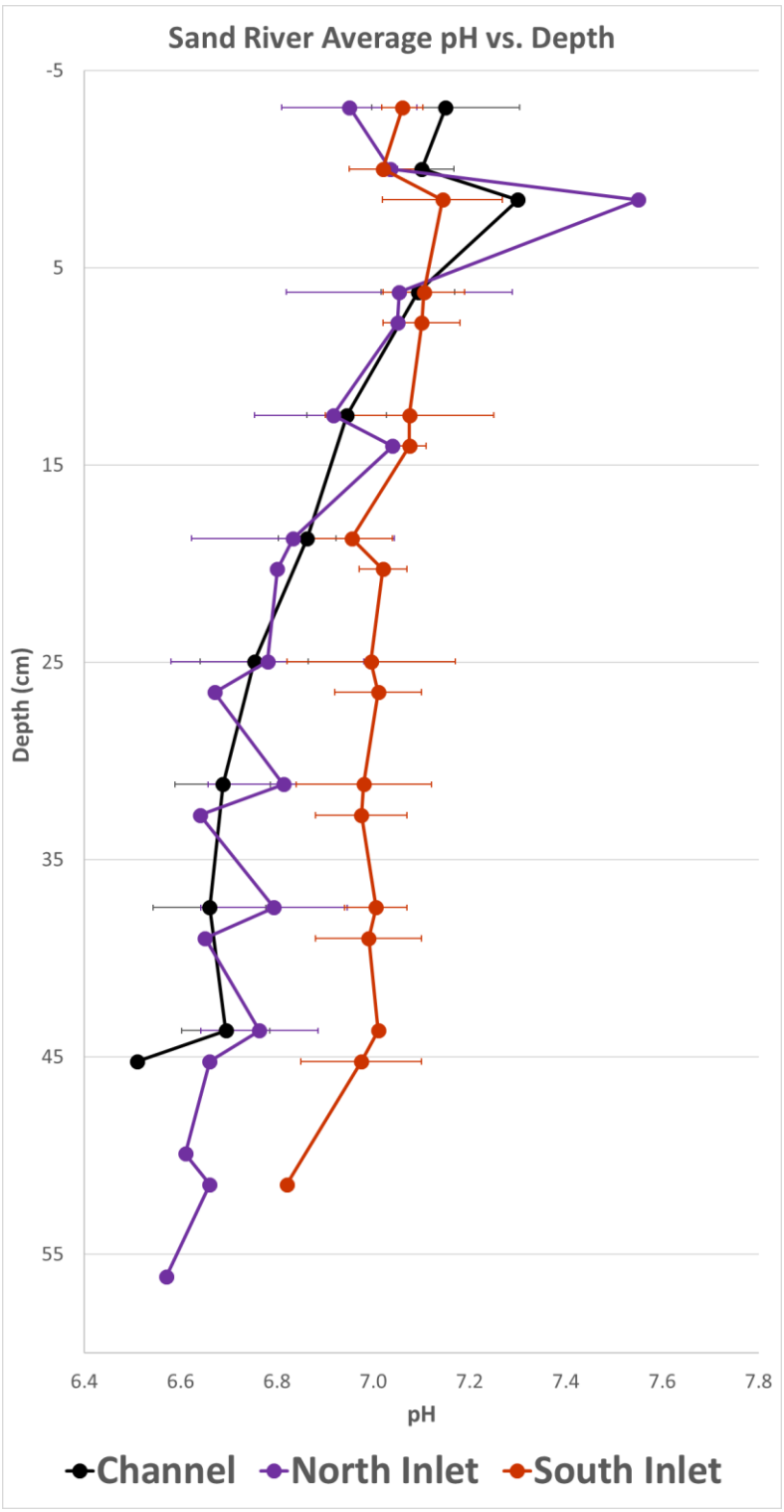

Figure 33: Average pH versus depth for the channel (black), north inlet (purple), and south inlet (orange) at Sand River. Plotted values represent cumulative average for each depth from peepers sampled at each location throughout the 2018 field season. Error bars represent standard deviation for each depth.

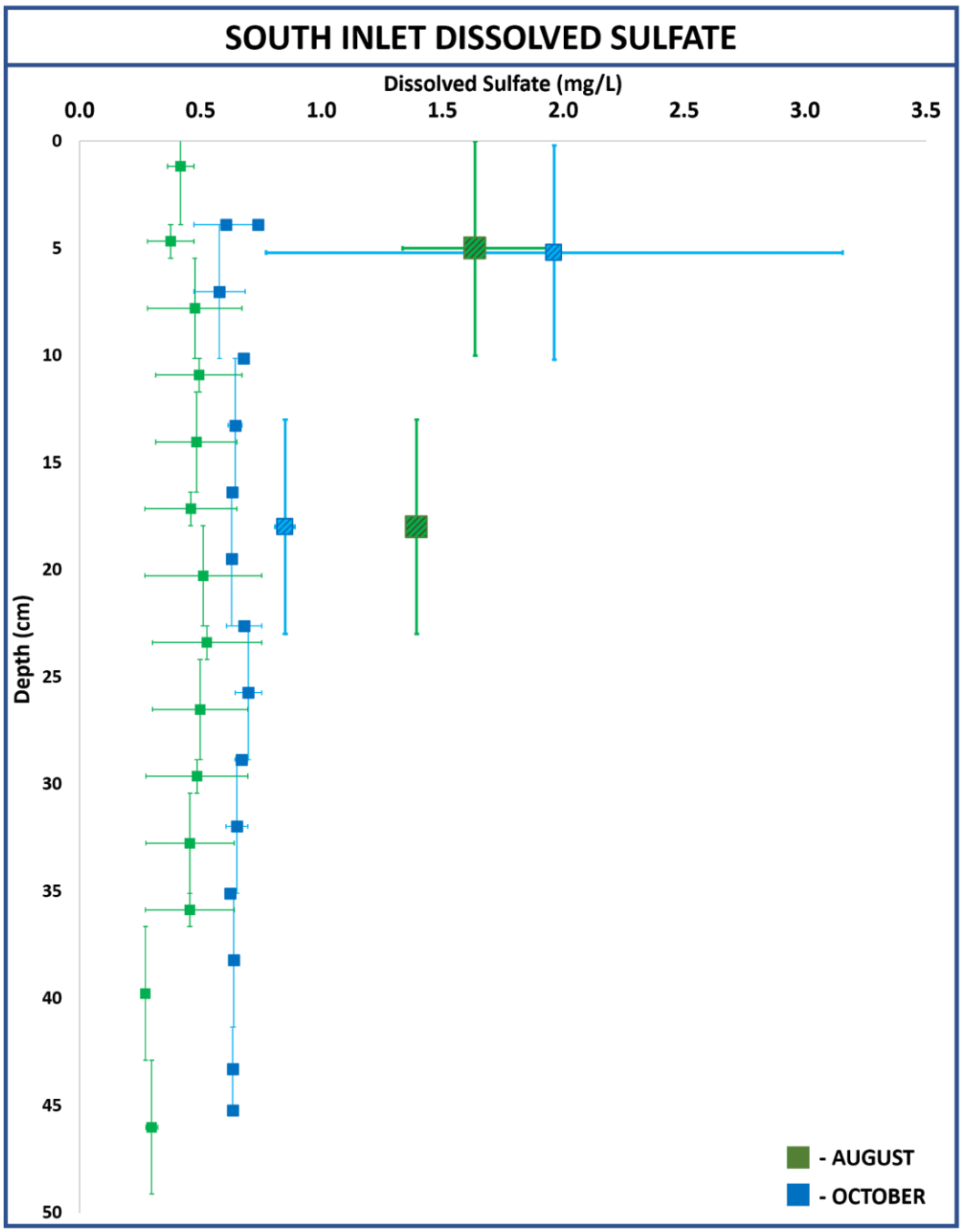

Figure 34: Dissolved SO_4^{2-} concentration versus depth for the south inlet at Sand River. Small solid squares represent 'peeper' data; error bars represent standard deviation for averaged duplicate peepers. Porewater samples collected using Rhizon™ samplers denoted by large patterned squares; horizontal error bars represent standard deviation for duplicate Rhizon™ samples while vertical error bars represent sampling range of sampler. August and October sampling periods represented by green and blue squares, respectively.

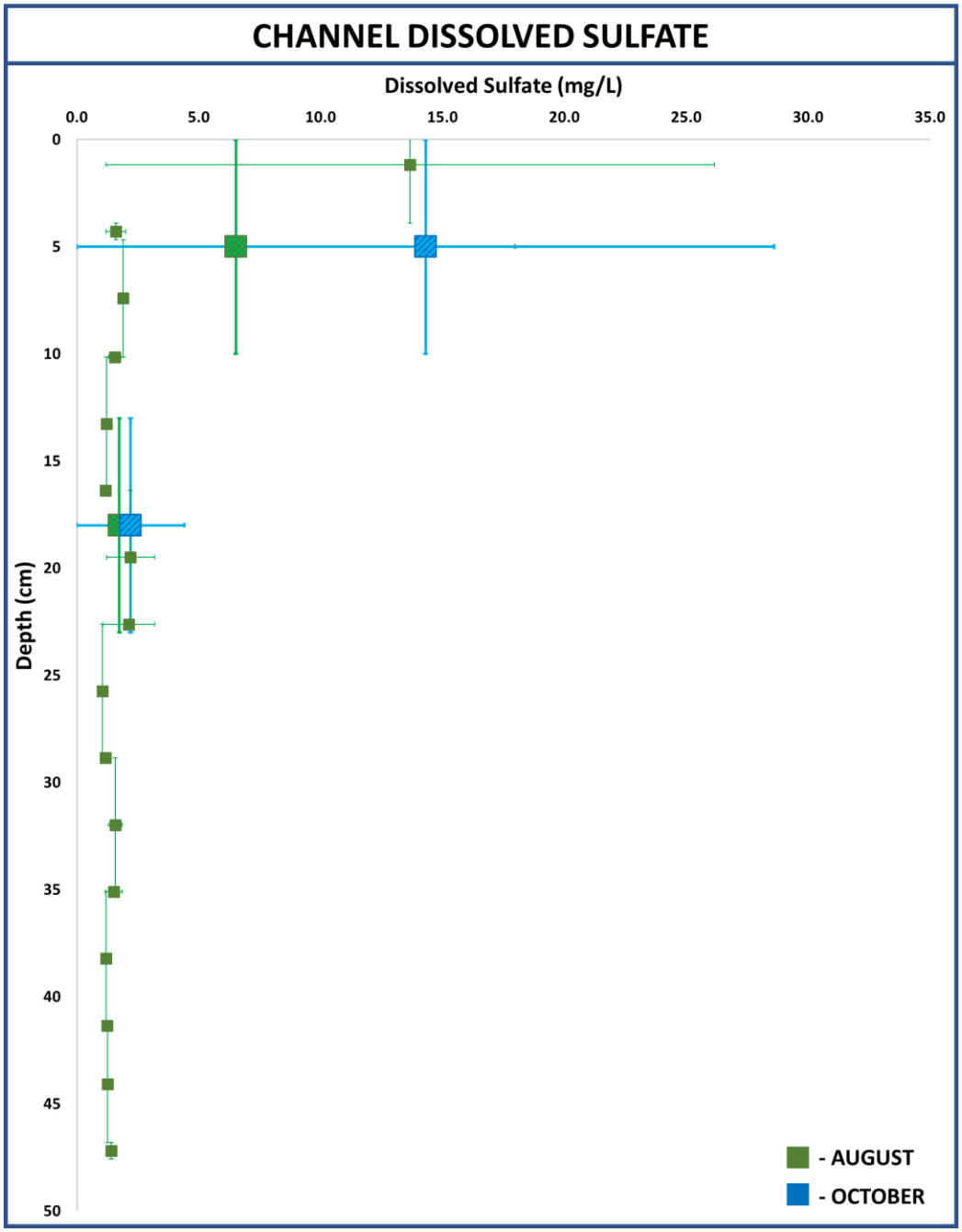

Figure 35: Dissolved SO_4^{2-} concentration versus depth for the channel at Sand River. Small solid squares represent 'peeper' data; error bars represent standard deviation for averaged duplicate peepers. Porewater samples collected using Rhizon™ samplers denoted by large patterned squares; horizontal error bars represent standard deviation for duplicate Rhizon™ samples while vertical error bars represent sampling range of sampler. August and October sampling periods represented by green and blue squares, respectively.

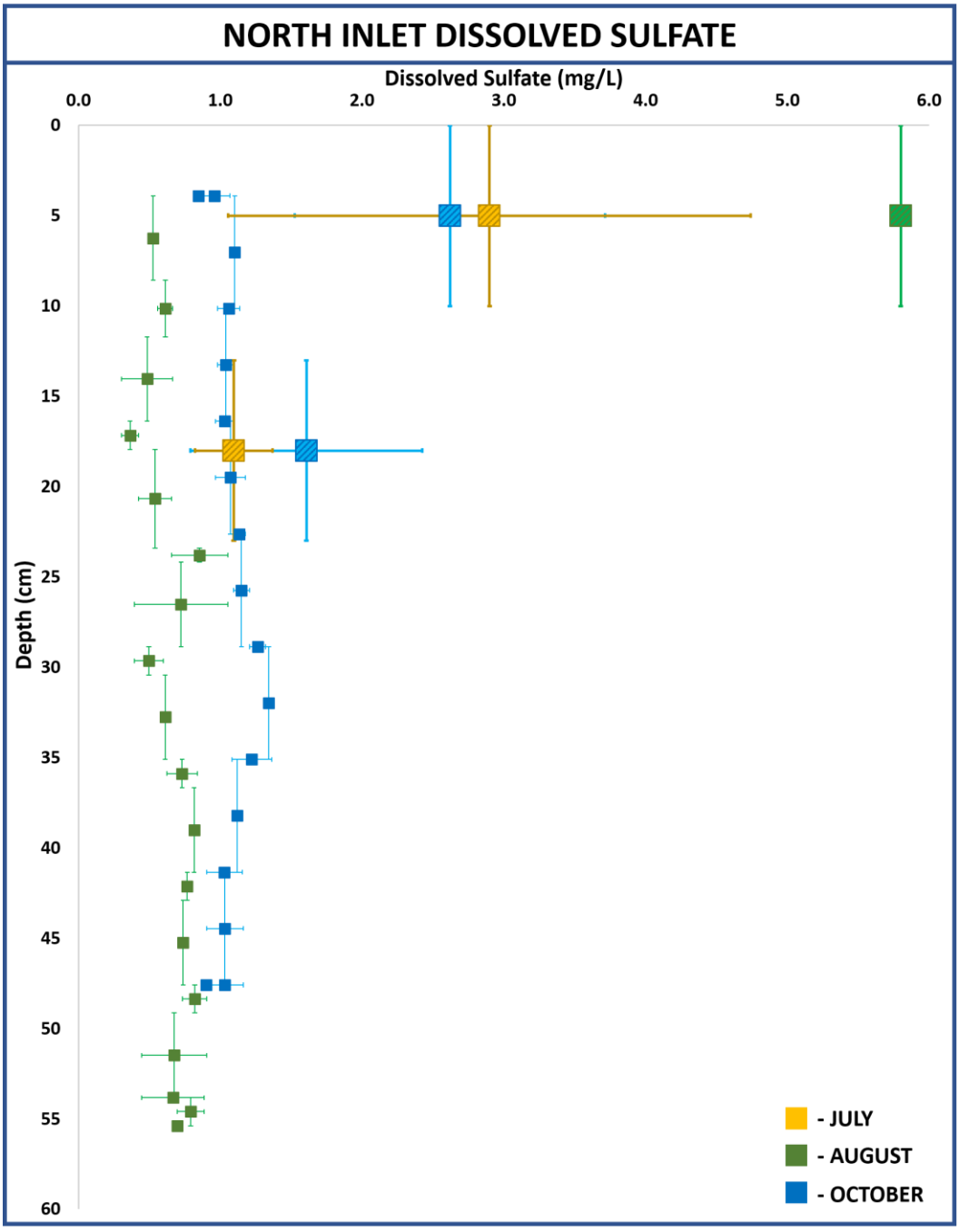

Figure 36: Dissolved SO_4^{2-} concentration versus depth for the north inlet at Sand River. Small solid squares represent 'peeper' data; error bars represent standard deviation for averaged duplicate peepers. Porewater samples collected using Rhizon™ samplers denoted by large patterned squares; horizontal error bars represent standard deviation for duplicate Rhizon™ samples while vertical error bars represent sampling range of sampler. July, August, and October sampling periods represented by yellow, green, and blue squares, respectively.

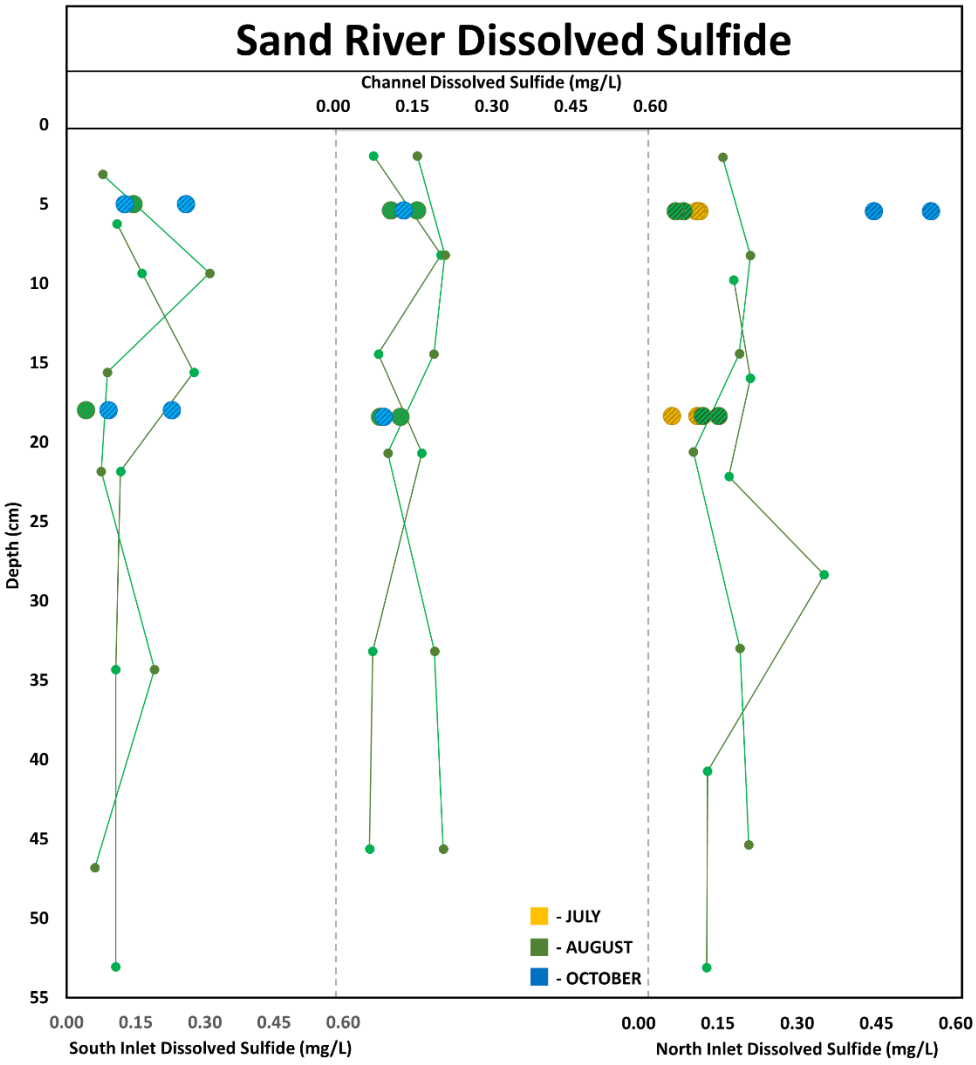

Figure 37: Dissolved sulfide concentrations in the south inlet (left), channel (center), and north inlet (right) in porewater collected using rhizon samplers (large, patterned circles) and peepers (smaller circles) during the months of July (yellow), August (green), and October (blue).

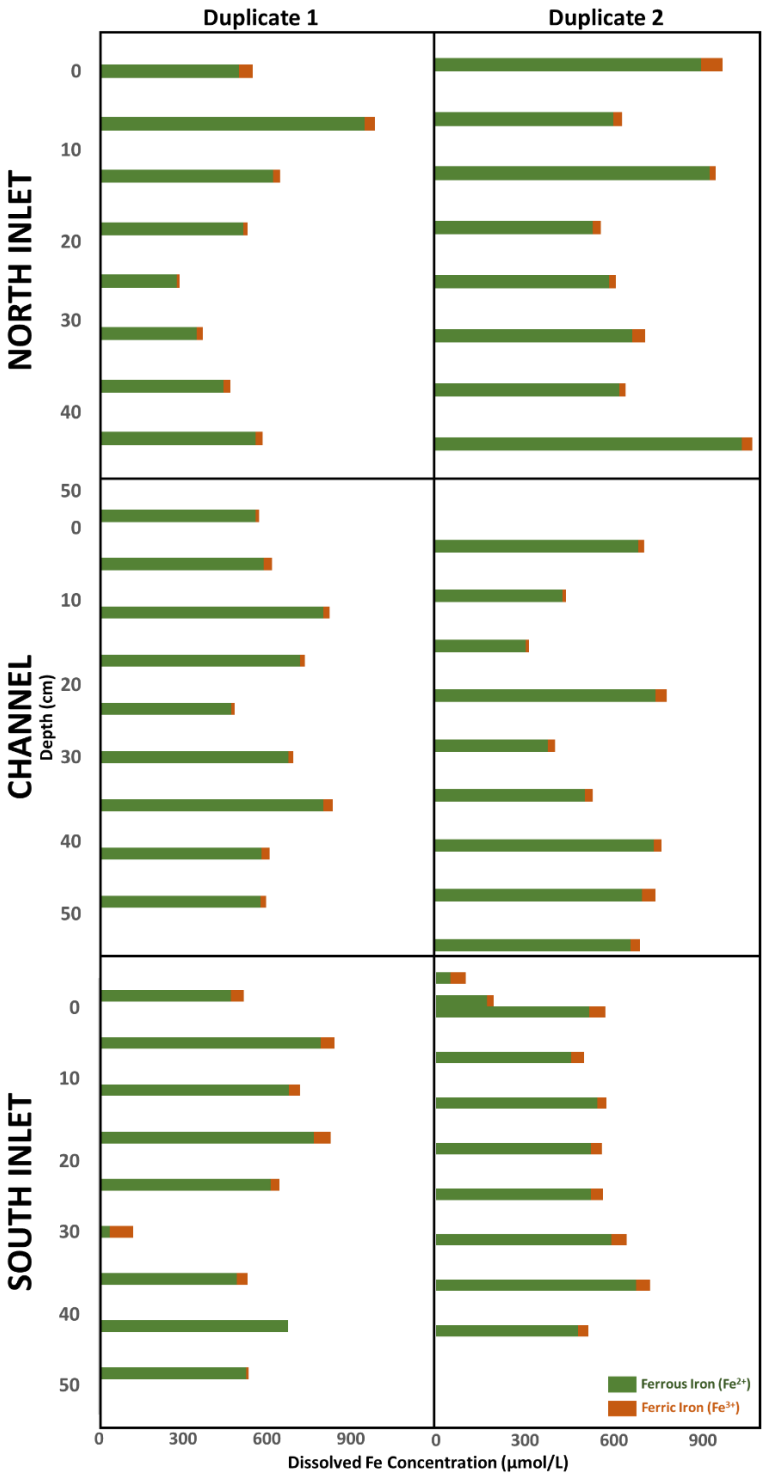

Figure 38: Dissolved ferrous Fe (green) and ferric Fe (orange) concentrations measured in the sediment porewater of Sand River. Duplicate peeper samples are plotted for the north inlet (top), channel (middle), and south inlet (bottom). All concentrations plotted as a function of depth, with zero depth indicating the sediment-water interface.

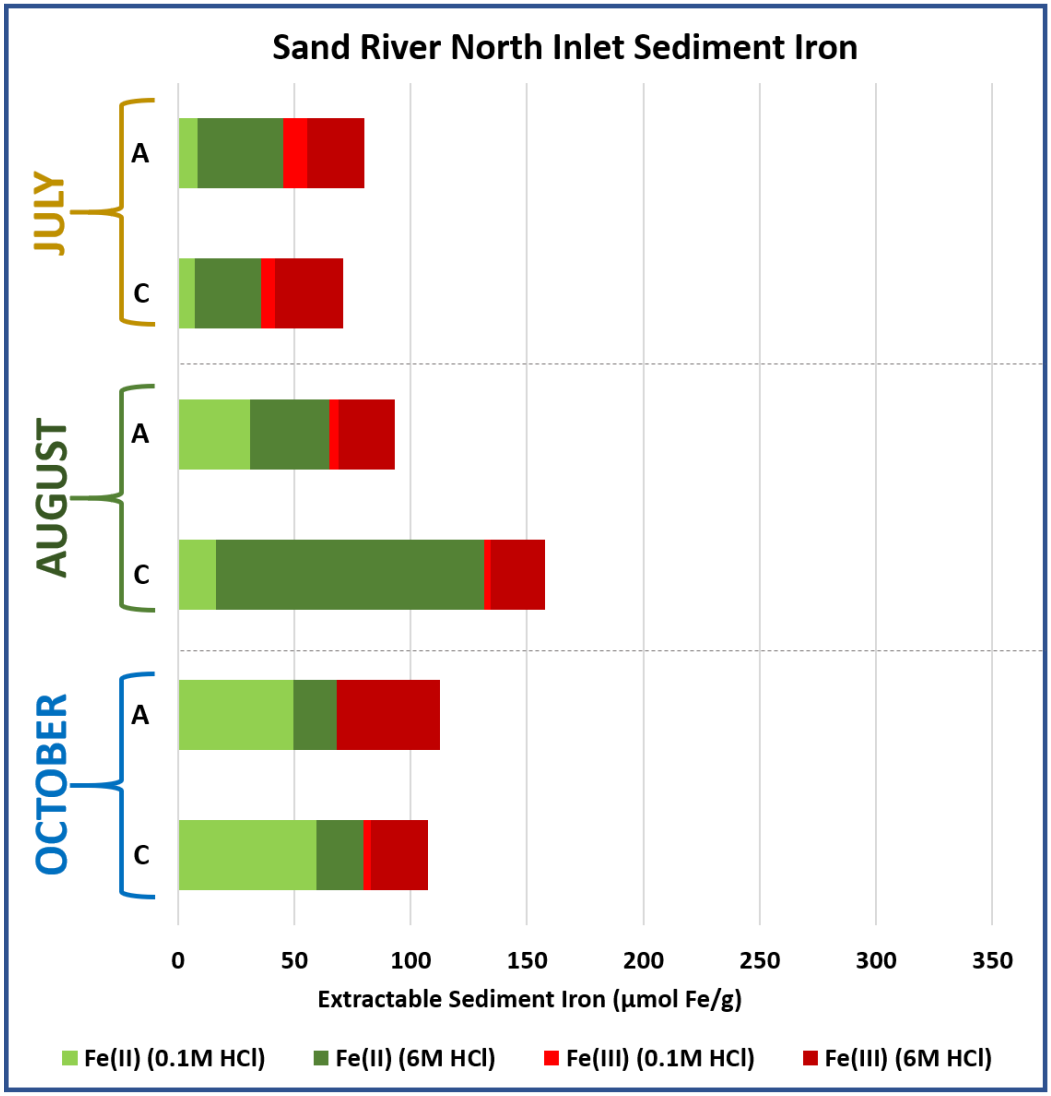

Figure 39: Ferrous and Ferric Fe extracted from sediments collected from the north inlet of Sand River in July (top), August (middle), and October (bottom) 2018. Ferrous Fe extracted using weak (0.1M) HCl and strong (6M) HCl depicted as light green and dark green bars, respectively. Ferric Fe extracted using weak (0.1M) HCl and strong (6M) HCl depicted as light red and dark red bars, respectively. 'A' denotes sediments collected in the upper ~4cm of the sediment column while 'C' denotes samples collected in the lower ~20cm of the sediment column.

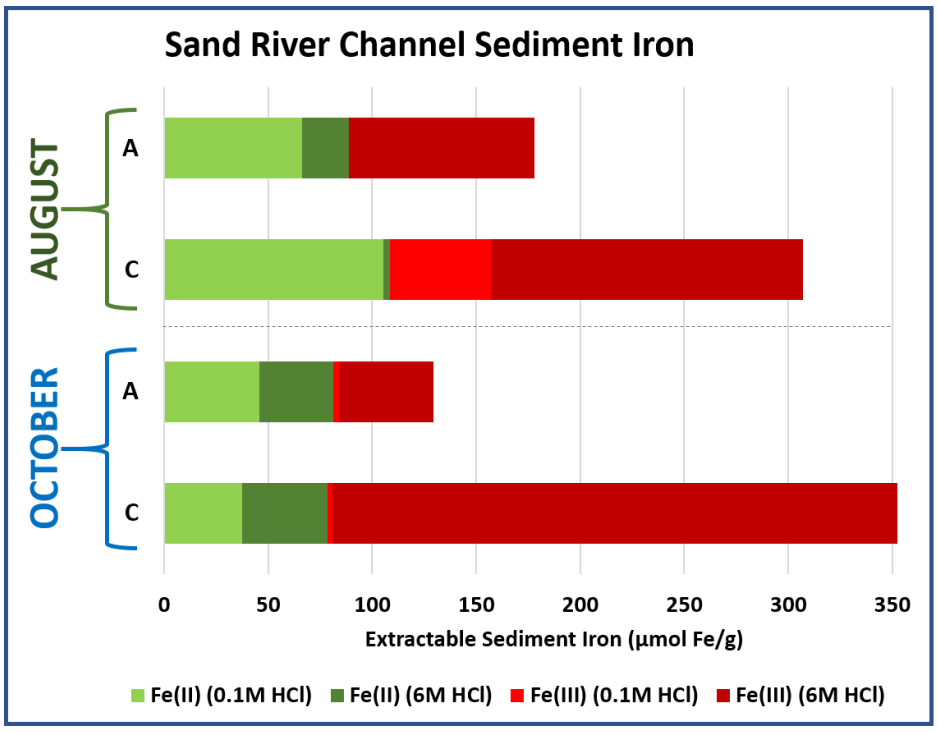

Figure 40: Ferrous and Ferric Fe extracted from sediments collected from the channel of Sand River in August (top) and October (bottom) 2018. Ferrous Fe extracted using weak (0.1M) HCl and strong (6M) HCl depicted as light green and dark green bars, respectively. Ferric Fe extracted using weak (0.1M) HCl and strong (6M) HCl depicted as light red and dark red bars, respectively. 'A' denotes sediments collected in the upper ~4cm of the sediment column while 'C' denotes samples collected in the lower ~20cm of the sediment column.

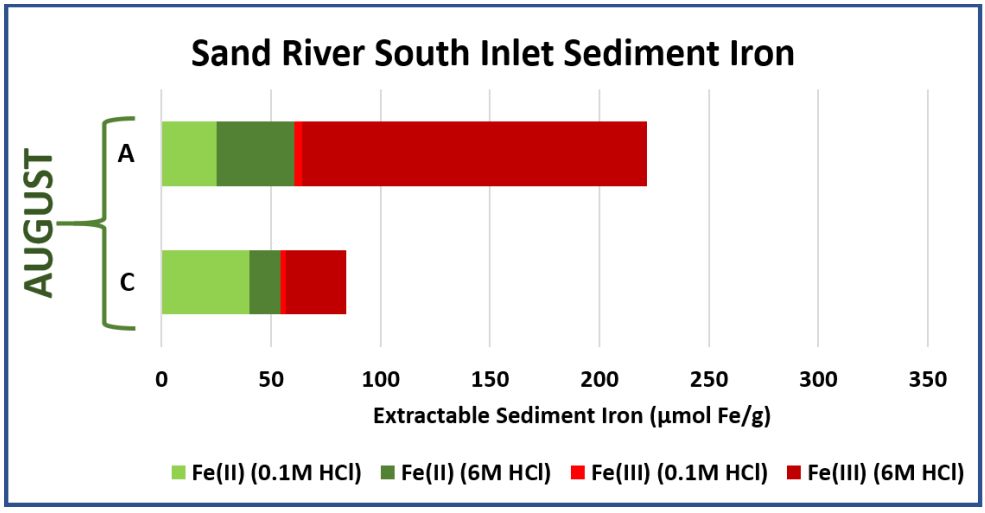

Figure 41: Ferrous and Ferric Fe extracted from sediments collected from the channel of Sand River in August 2018. Ferrous Fe extracted using weak (0.1M) HCl and strong (6M) HCl depicted as light green and dark green bars, respectively. Ferric Fe extracted using weak (0.1M) HCl and strong (6M) HCl depicted as light red and dark red bars, respectively. 'A' denotes sediments collected in the upper ~4cm of the sediment column while 'C' denotes samples collected in the lower ~20cm of the sediment column.

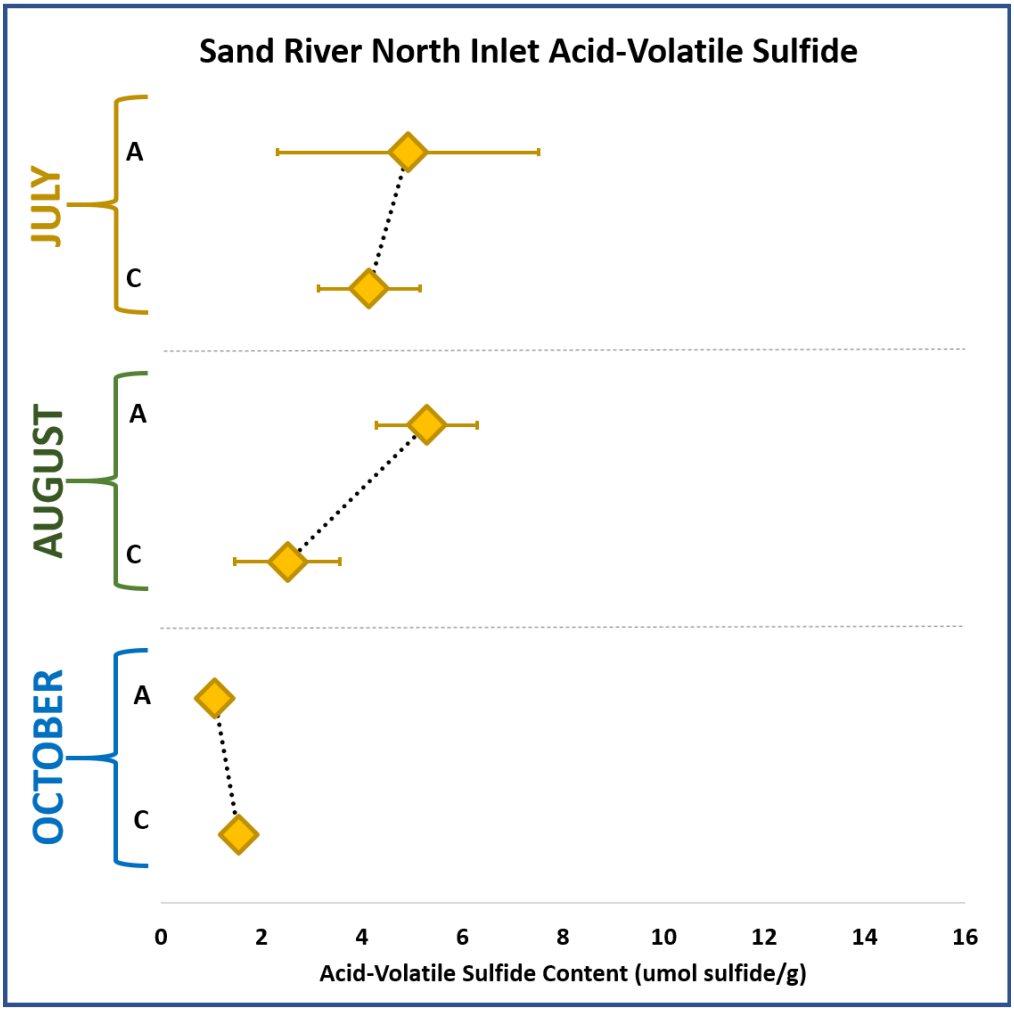

Figure 42: Acid-volatile sulfide (AVS) measurements in sediments collected from the north inlet of Sand River during the 2018 field season. July data is plotted at the top followed by August in the center and October at the bottom. Standard deviation between duplicate cores represented by error bars. 'A', 'B', and 'C' on the y-axis correspond to sampling intervals of approximately 4cm and 20cm, respectively.

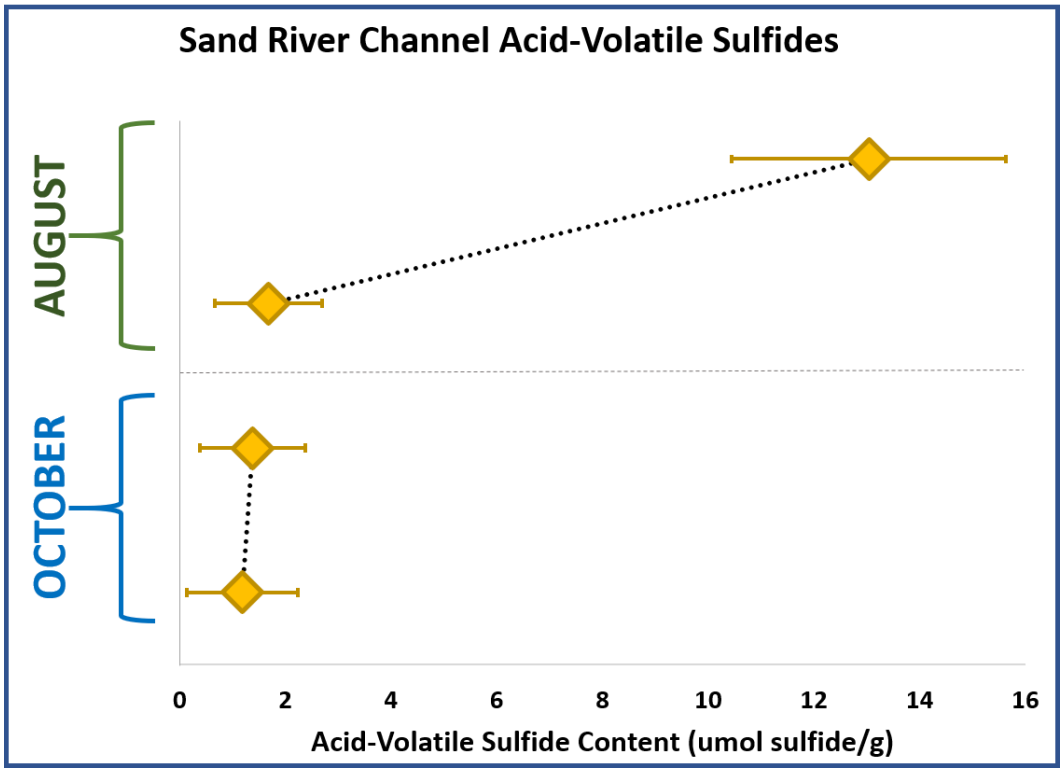

Figure 43: Acid-volatile sulfide (AVS) measurements in sediments collected from the channel of Sand River during the 2018 field season. August data is plotted at the top and October is plotted at the bottom. Standard deviation between duplicate cores represented by error bars. 'A', 'B', and 'C' on the y-axis correspond to sampling intervals of approximately 4cm and 20cm, respectively.

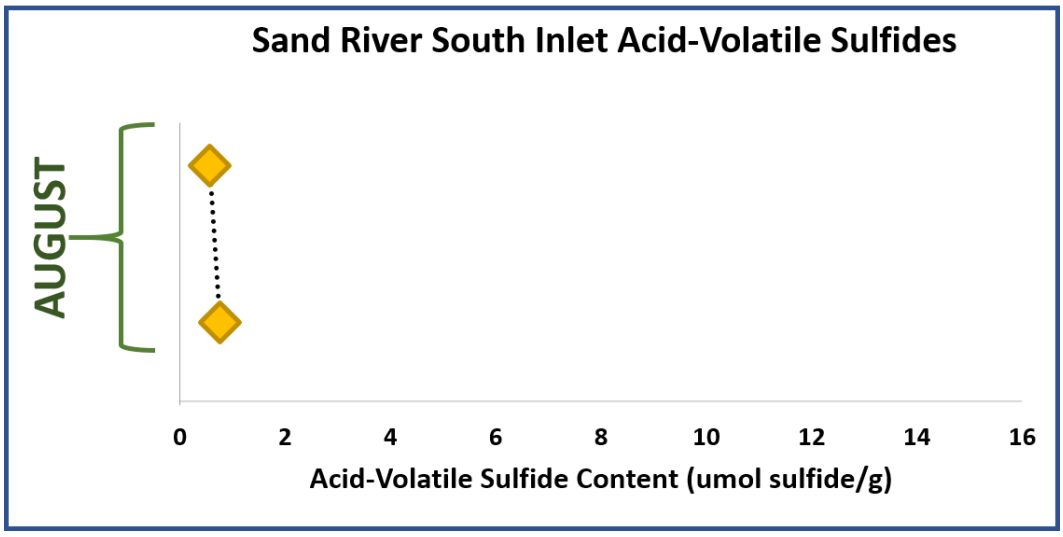

Figure 44: Acid-volatile sulfide (AVS) measurements in sediments collected from August in the south inlet of Sand River during the 2018 field season. Standard deviation between duplicate cores represented by error bars. 'A', 'B', and 'C' on the y-axis correspond to sampling intervals of approximately 4cm and 20cm, respectively.

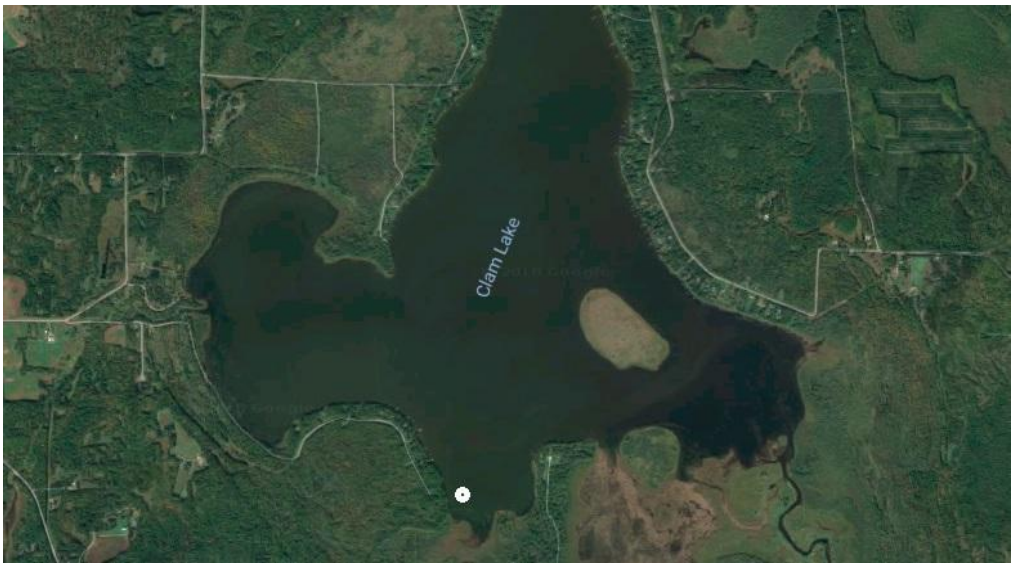

Figure 45: Site map of Clam Lake. Geochemical sampling location denoted by white circle on southern shore. Image acquired from Google Earth on 16 Dec. 2018.

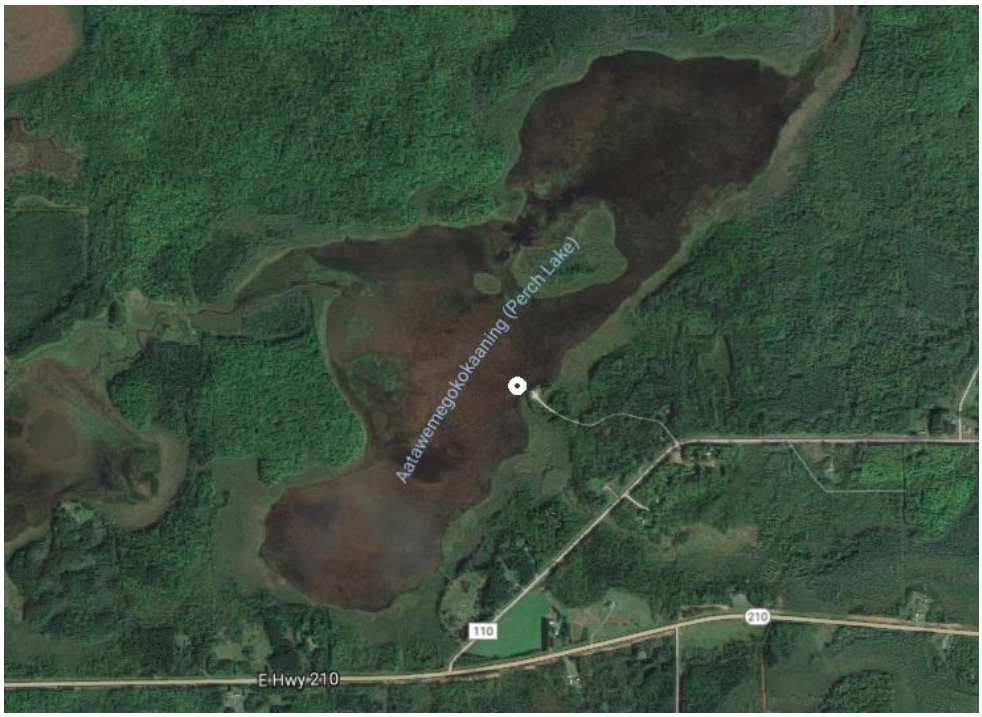

Figure 46: Site map of Perch Lake. Geochemical sampling and hydrologic monitoring equipment location denoted by white circle on the southern shore. Image acquired from Google Earth on 16 Dec. 2018.

Figure 47: Site map of Big Rice Lake. Geochemical sampling location denoted by an 'N', hydrologic monitoring equipment location denoted by an 'E'. Image acquired from Google Earth on 16 Dec. 2018.

Figure 48: Site map of Twin Lakes. Geochemical sampling locations denoted by 'W', 'IN', 'WR', and 'OUT'. Hydrologic monitoring equipment location was deployed at location 'W'. Image acquired from Google Earth on 16 Dec. 2018.

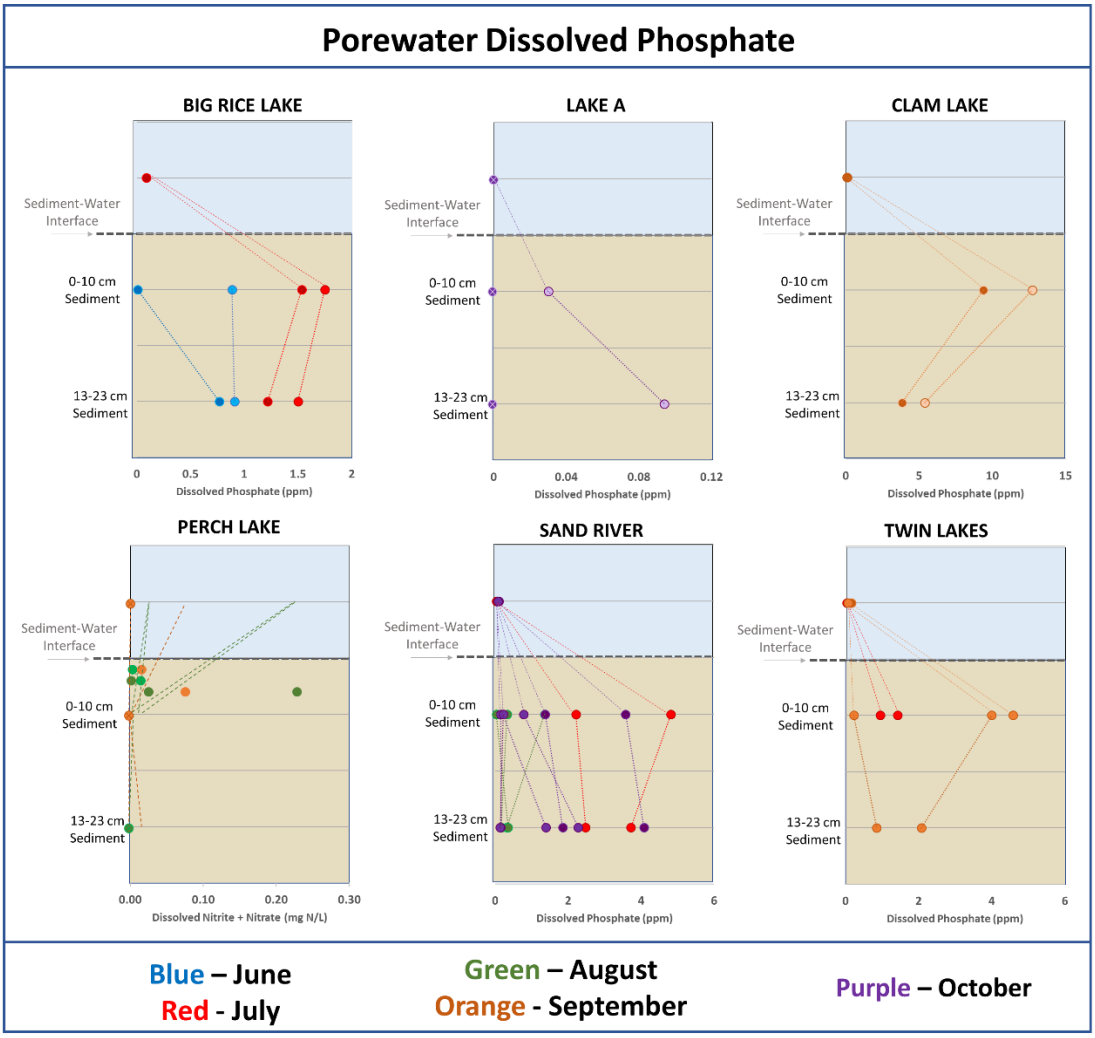

Figure 49: Phosphate data for all porewater samples collected during the 2018 field season. Blue, red, green, orange, and purple denote samples collected in June, July, August, September, and October, respectively. Samples with phosphate concentrations below the limit of detection are represented by a crossed circle at the lowest plotted concentration. The blue shaded region represents the surface water while the brown shaded region represents the sediment.

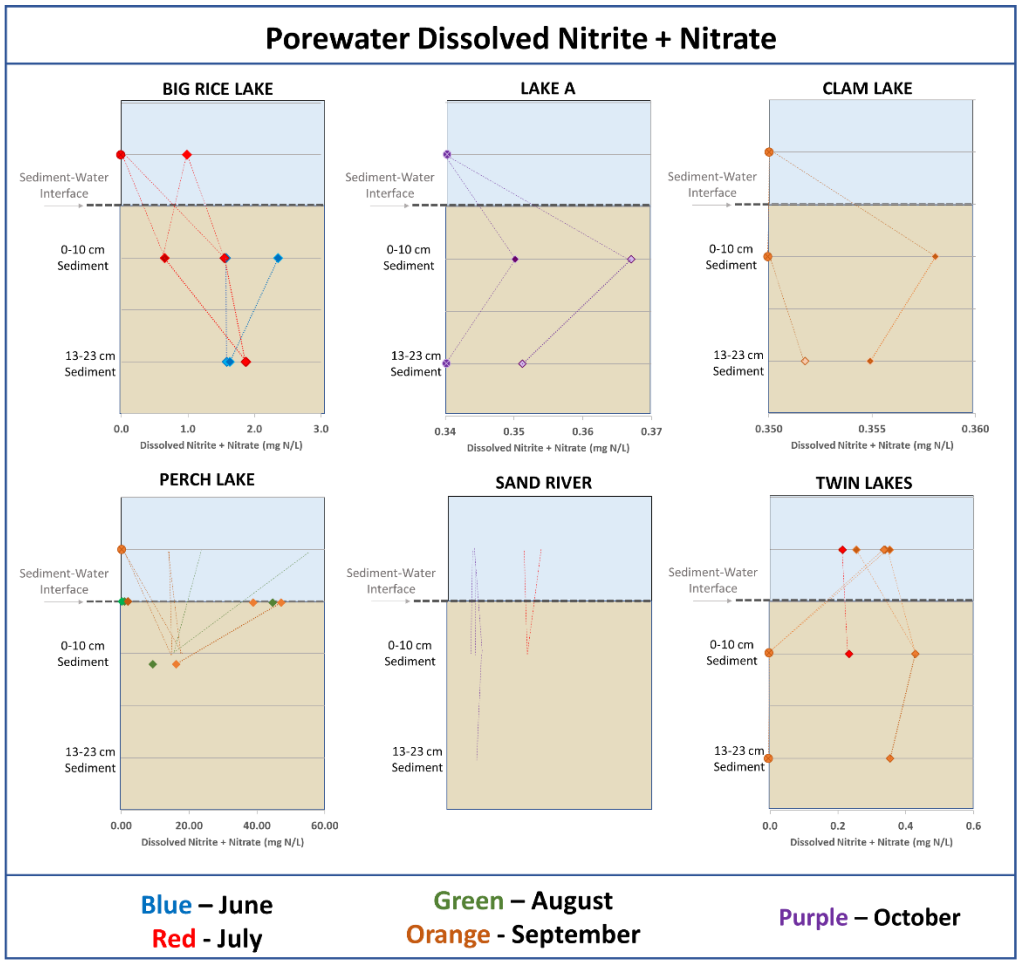

Figure 50: Dissolved nitrite and nitrate data for all porewater samples collected during the 2018 field season. Blue, red, green, orange, and purple denote samples collected in June, July, August, September, and October, respectively. Samples with nitrite/nitrate concentrations below the limit of detection are represented by a crossed circle at the lowest plotted concentration. The blue shaded region represents the surface water while the brown shaded region represents the sediment.

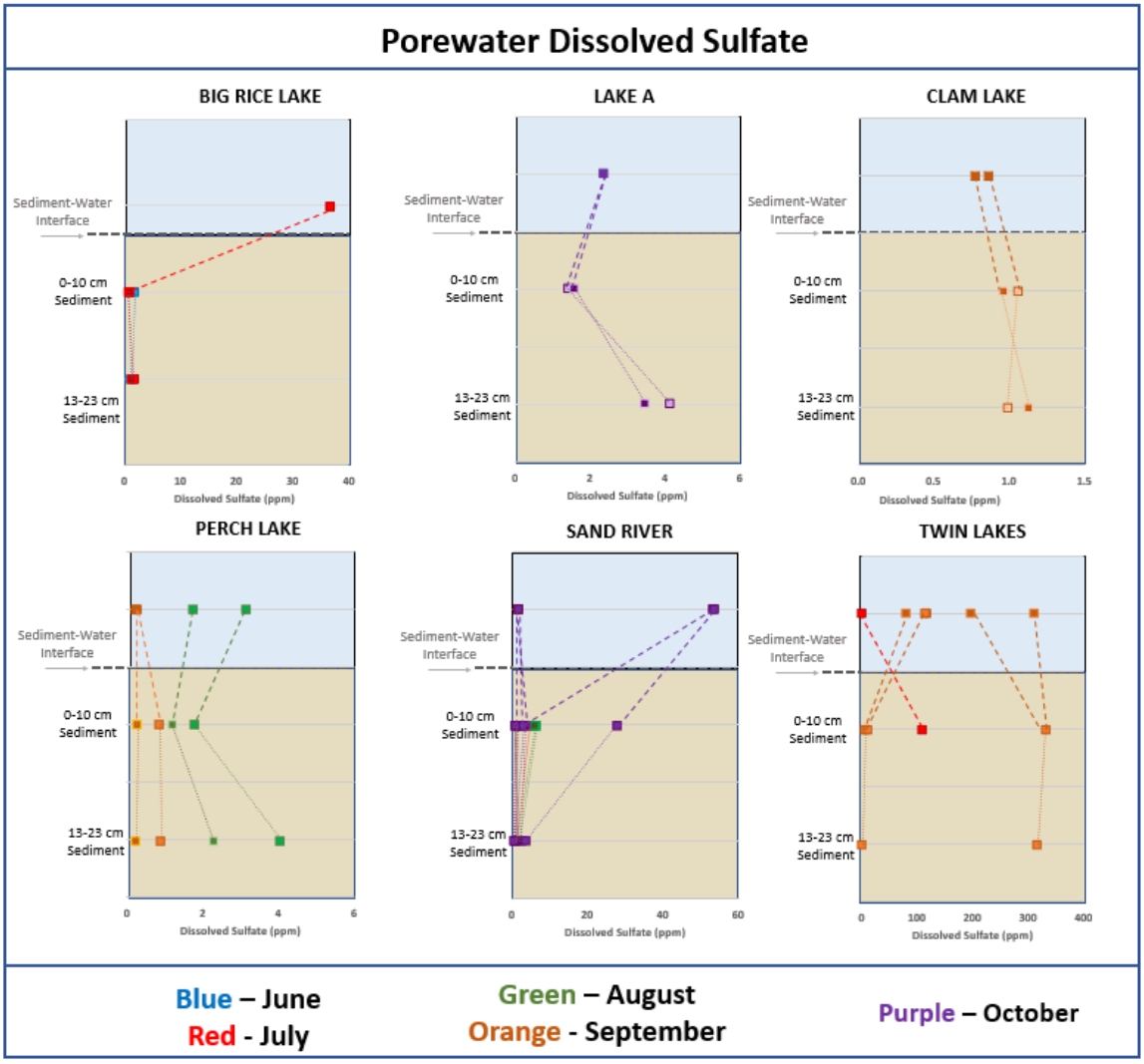

Figure 51: Dissolved SO_4^{2-} data for all porewater samples collected during the 2018 field season. Blue, red, green, orange, and purple denote samples collected in June, July, August, September, and October, respectively. The blue shaded region represents the surface water while the brown shaded region represents the sediment.

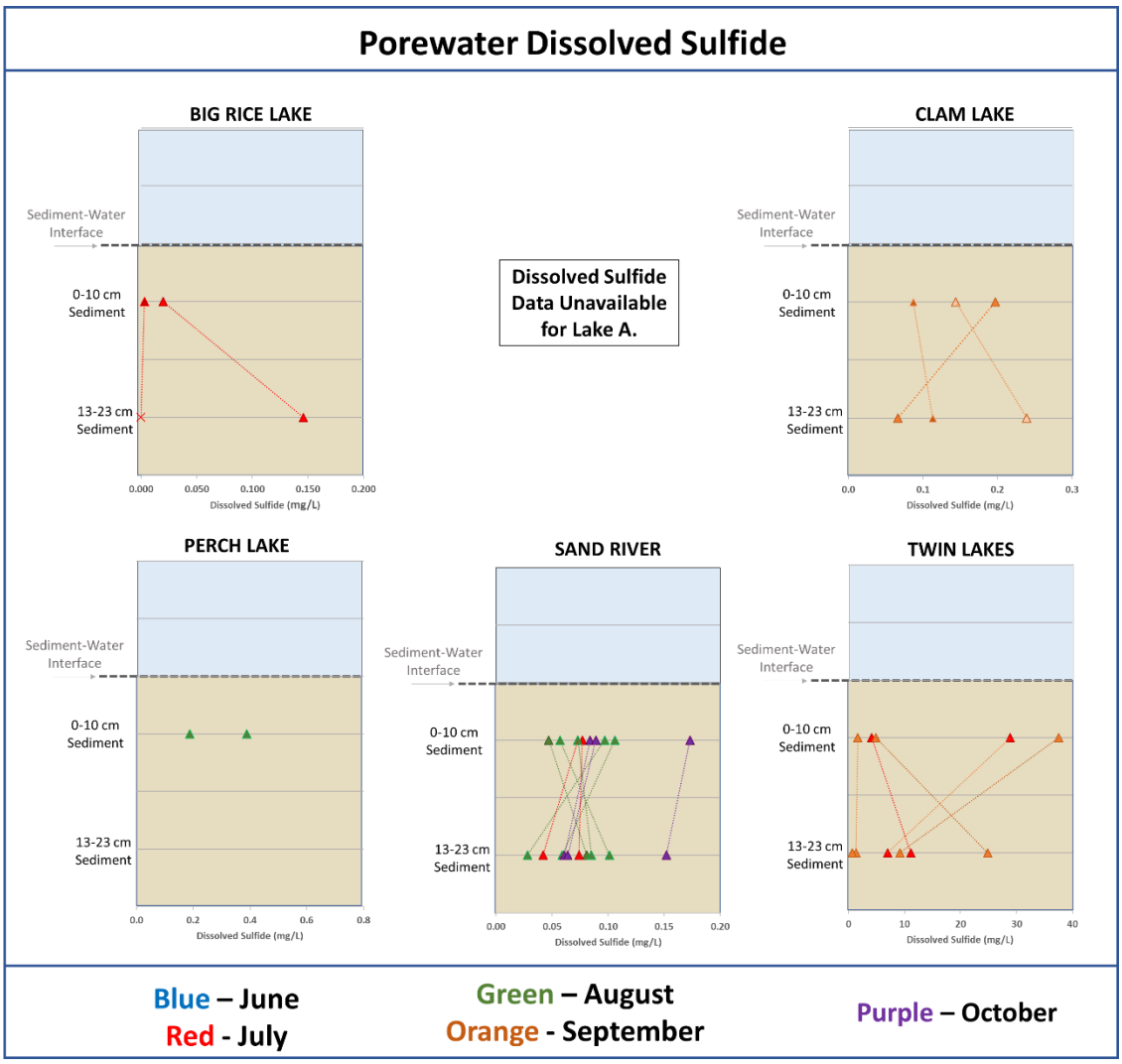

Figure 52: Dissolved sulfide data for all porewater samples collected during the 2018 field season. Blue, red, green, orange, and purple denote samples collected in June, July, August, September, and October, respectively. The blue shaded region represents the surface water while the brown shaded region represents the sediment.

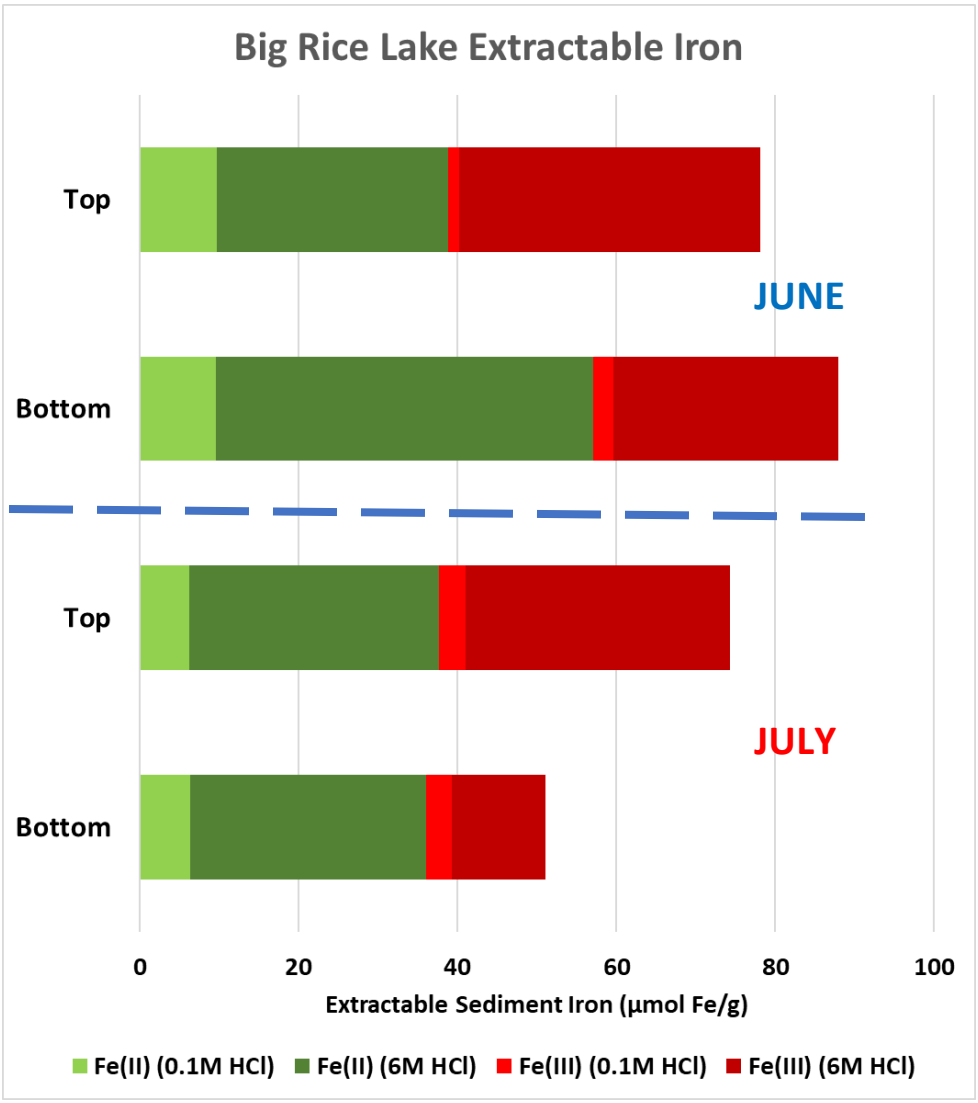

Figure 53: Ferrous and Ferric Fe extracted from sediments collected from Big Rice Lake in June (top) and July (bottom) 2018. Ferrous Fe extracted using weak (0.1M) HCl and strong (6M) HCl depicted as light green and dark green bars, respectively. Ferric Fe extracted using weak (0.1M) HCl and strong (6M) HCl depicted as light red and dark red bars, respectively. 'A' denotes sediments collected in the upper ~4cm of the sediment column while 'C' denotes samples collected in the lower ~20cm of the sediment column.

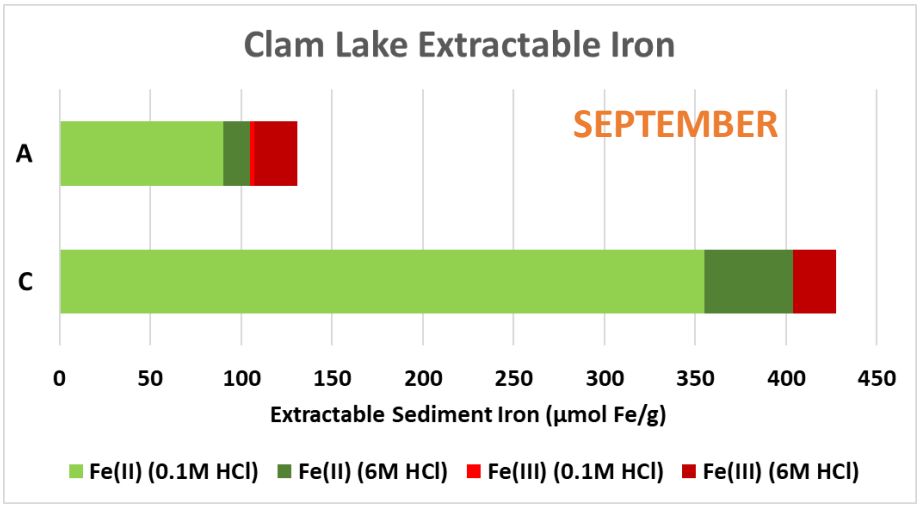

Figure 54: Ferrous and Ferric Fe extracted from sediments collected from Clam Lake in September 2018. Ferrous Fe extracted using weak (0.1M) HCl and strong (6M) HCl depicted as light green and dark green bars, respectively. Ferric Fe extracted using weak (0.1M) HCl and strong (6M) HCl depicted as light red and dark red bars, respectively. 'A' denotes sediments collected in the upper ~4cm of the sediment column while 'C' denotes samples collected in the lower ~20cm of the sediment column.

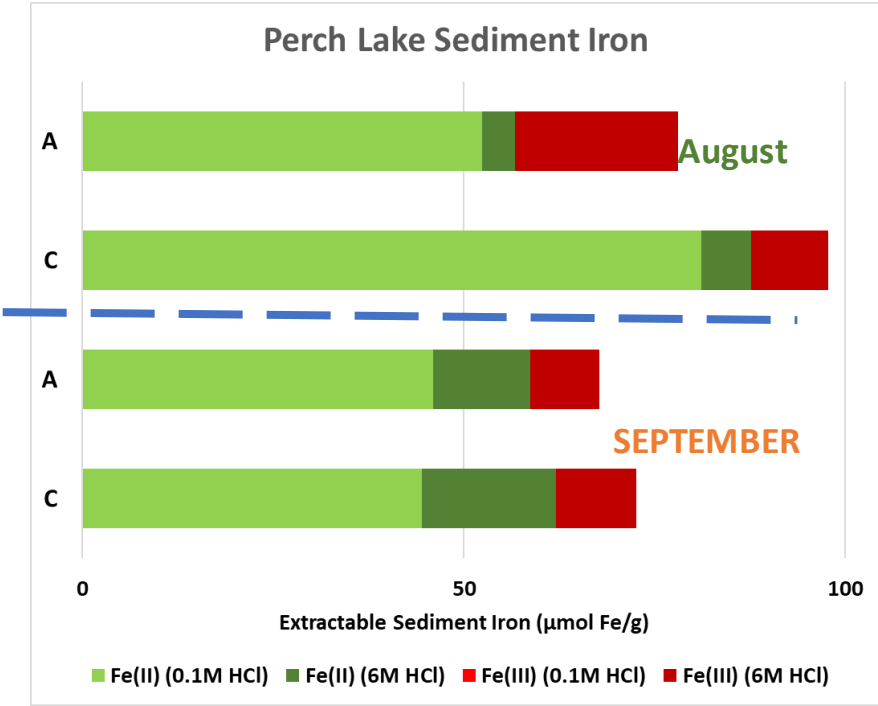

Figure 55: Ferrous and Ferric Fe extracted from sediments collected from Perch Lake in August (top) and September (bottom) 2018. Ferrous Fe extracted using weak (0.1M) HCl and strong (6M) HCl depicted as light green and dark green bars, respectively. Ferric Fe extracted using weak (0.1M) HCl and strong (6M) HCl depicted as light red and dark red bars, respectively. 'A' denotes sediments collected in the upper ~4cm of the sediment column while 'C' denotes samples collected in the lower ~20cm of the sediment column.

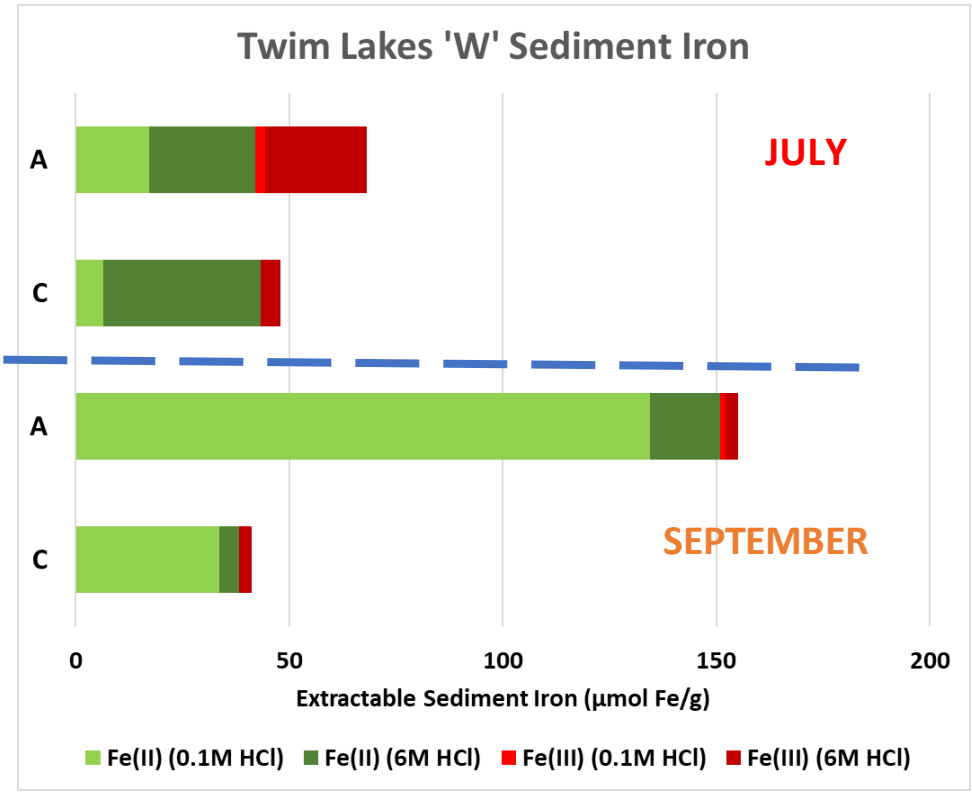

Figure 56: Ferrous and Ferric Fe extracted from sediments collected from Location 'W' in Twin Lakes in July (top) and September (bottom) 2018. Ferrous Fe extracted using weak (0.1M) HCl and strong (6M) HCl depicted as light green and dark green bars, respectively. Ferric Fe extracted using weak (0.1M) HCl and strong (6M) HCl depicted as light red and dark red bars, respectively. 'A' denotes sediments collected in the upper ~4cm of the sediment column while 'C' denotes samples collected in the lower ~20cm of the sediment column.

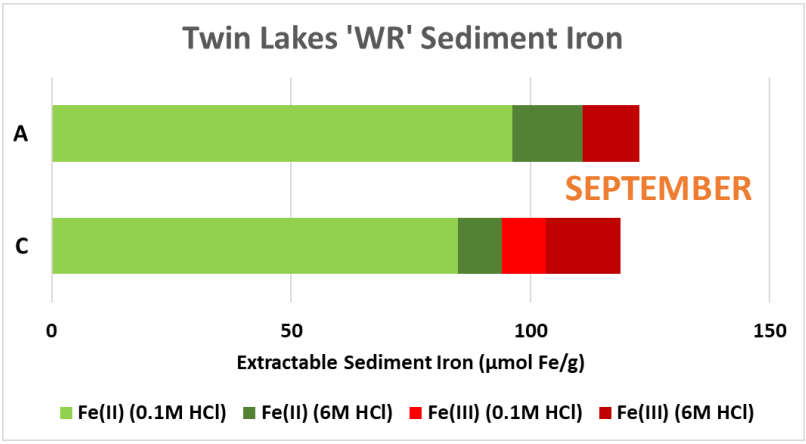

Figure 57: Ferrous and Ferric Fe extracted from sediments collected from Location 'WR' in Twin Lakes in September 2018. Ferrous Fe extracted using weak (0.1M) HCl and strong (6M) HCl depicted as light green and dark green bars, respectively. Ferric Fe extracted using weak (0.1M) HCl and strong (6M) HCl depicted as light red and dark red bars, respectively. 'A' denotes sediments collected in the upper ~4cm of the sediment column while 'C' denotes samples collected in the lower ~20cm of the sediment column.

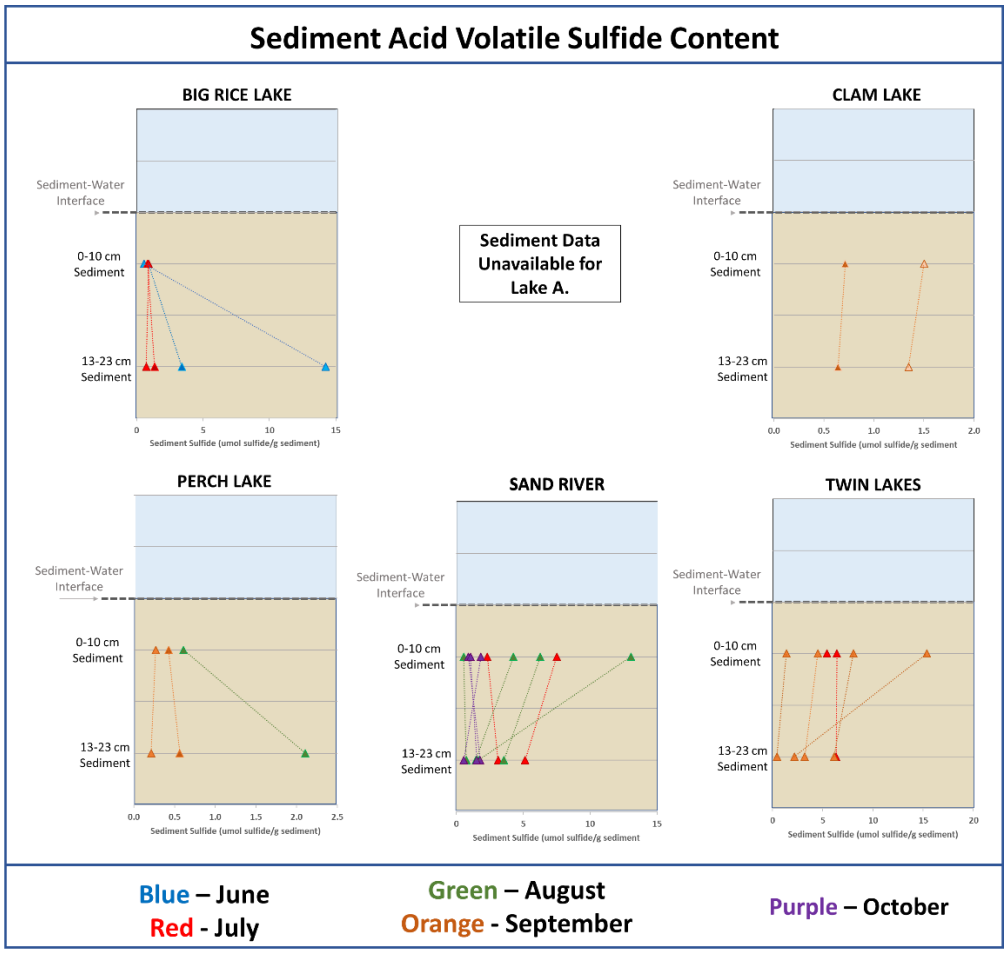

Figure 59: Acid-volatile sulfide measurements for all sediment samples collected during the 2018 field season. Blue, red, green, orange, and purple denote samples collected in June, July, August, September, and October, respectively. The blue shaded region represents the surface water while the brown shaded region represents the sediment. Sediment samples were not obtained from Lake A, so there is currently no data available for this site.

5. References

Al-Sid-Cheikh, M., Pédrot, M., Dia, A., Guenet, H., Vantelon, D., Davranche, M., Delhaye, T. (2015). Interactions between natural organic matter, sulfur, arsenic and Fe oxides in re-oxidation compounds within riparian wetlands: NanoSIMS and X-ray adsorption spectroscopy evidences. *Science of the Total Environment*, *515–516*, 118–128.

Allen, H. E., Fu, G., & Deng, B. (1993). Analysis of Acid-Volatile Sulfide (AVS) and Simultaneously Extracted Metals (SEM) for the Estimation of Potential Toxicity in Aquatic Sediments. *Environmental Toxicology and Chemistry*, *12*, 1441–1453.

ANL. (2017). Advanced Photon Source: An Office of Science National User Facility.

Berndt, M. E. (2003). *Mercury and mining in Minnesota*. *Minnesota Department of Natural Resources*.

Belzile, N., Chen, Y. W., Cai, M. F., & Li, Y. (2004). A review on pyrrhotite oxidation. *Journal of Geochemical Exploration*, *84*(2), 65–76.

Bhattacharyya, A., Schmidt, M. P., Stavitski, E., & Enid, C. (2018). Organic Geochemistry Iron speciation in peats: Chemical and spectroscopic evidence for the co-occurrence of ferric and ferrous iron in organic complexes and mineral precipitates. *Organic Geochemistry*, *115*, 124–137.

Boetius, A., Ravenschlag, K., Schubert, C. J., Rickert, D., Widdel, F., Gieseke, A., … Pfannkuche, O. (2000). A marine microbial consortium apparently mediating anaerobic oxidation of methane. *Nature*, *407*(6804), 623–626.

Bostick, B. C., Theissen, K. M., Dunbar, R. B., & Vairavamurthy, M. A. (2005). Record of redox status in laminated sediments from Lake Titicaca: A sulfur K-edge X-ray absorption near edge structure (XANES) study. *Chemical Geology*, *219*, 163–174.

Böttcher, M., & Thamdrup, B. (2001). Anaerobic sulfide oxidation and stable isotope fractionation associated with bacterial sulfur disproportionation in the presence of MnO2. *Geochimica et Cosmochimica Acta*, *65*(10), 1573–1581.

Braden, H., & Lapakko, K. (2012). Waste Rock Sulfate Release Rates at a Former Taconite Mine, Laboratory and Field-Scale Studies. *9th International Conference on Acid Rock Drainage*, (May 2012).

Burdige, D. J., and Nealson, K. N. (1986) Chemical and microbiological studies of sulfide-mediated manganese reduction. *Geomicrobiology Journal*. 4, 361-387.

Burton, E. D., Bush, R. T., & Sullivan, L. A. (2006). Reduced Inorganic Sulfur Speciation in Drain Sediments from Acid Sulfate Soil Landscapes. *Environmental Science & Technology*, *40*(3), 888–893.

Burton, E. D., Bush, R. T., Sullivan, L. A., Hocking, R. K., Mitchell, D. R. G., Johnston, S. G., Jang, L. Y. (2009). Iron-Monosulfide Oxidation in Natural Sediments: Resolving Microbially Mediated S Transformations Using XANES, Electron Microscopy, and Selective Extractions. *Environmental Science & Technology*, *43*(9), 3128–3134.

Burton, E. D., Bush, R. T., Johnston, S. G., Sullivan, L. A., & Keene, A. F. (2011). Sulfur biogeochemical cycling and novel Fe – S mineralization pathways in a tidally re-flooded wetland. *Geochimica et Cosmochimica Acta*, *75*(12), 3434–3451.

Caithamer, D. F. (2011). Abundance and Productivity of Waterfowl at Clam Lake and Long Lake, Burnett County, Wisconsin; 2010-2011.

Chen, K. Y., & Morris, J. C. (1972). Kinetics of Oxidation of Aqueous Sulfide by 02. *Environmental Science & Technology*, *6*(6), 529–537.

Cline, J. D. (1969). Spectrophotometric Determination of Hydrogen Sulfide in Natural Waters. *Limnol. Oceanogr.*, *14*, 454–458.

Cron, B.R., Sheik, C.S., Kafantaris, F., Druschel, G.K., Seewald, J.S., German, C.R., Dick, G.J., Breier, J.A., Toner, B.M. (in prep) Dynamic biogeochemistry of sulfur in a deep-sea buoyant hydrothermal plume. Earth and Space Chemistry.

Davenport, M. (2018), "Manoomin in Minnesota and the Great Lakes Basin: A Flagship for Environmental Preservation and Indigenous Resource Sovereignty" (Invited). 2nd Annual Lake Superior Manoomin Restoration Workshop, April 9-10, 2018, Duluth, MN.

DNR. (2013). *Big Rice Lake Management Plan*. dos Santos Afonso, M., & Stumm, W. (1992). Reductive Dissolution of Iron (III) (Hydr)oxides by Hydrogen Sulfide. *Langmuir*, *8*(6), 1671–1675.
Dowrick, D. J., Freeman, C., Lock, M. A., & Reynolds, B. (2006). Sulphate reduction and the suppression of peatland methane emissions following summer drought. *Geoderma*, *132*(3–4), 384–390.
EPA. (1993). Acid generation prediction in mining. *Environmental Protection Agency*.
Fadely, E. C. (2018). *Evaluating Environmental Controls on Groundwater Flow and Sulfate Transport in the Second Creek Watershed, Northeastern Minnesota*.
Fahd, F. (2014). *Ecological risk assessment of Thiosalts*. Memorial University of Newfoundland.
Findlay, A. J., Gartman, A., Macdonald, D. J., Hanson, T. E., Shaw, T. J., & Luther, G. W. (2014). Distribution and size fractionation of elemental sulfur in aqueous environments: The Chesapeake Bay and Mid-Atlantic Ridge. *Geochimica et Cosmochimica Acta*, *142*, 334–348.
Flynn, T. M., O'Loughlin, E. J., Mishra, B., DiChristina, T. J., & Kemner, K. M. (2014). Sulfur-mediated electron shuttling during bacterial iron reduction. *Science*, *344*(6187), 1039–1042.
Frederiksen, T. M., & Finster, K. (2003). Sulfite-oxido-reductase is involved in the oxidation of sulfite in Desulfocapsa sulfoexigens during disproportionation of thiosulfate and elemental sulfur. *Biodegradation*, *14*(3), 189–198.
Gao, S., Tanji, K. K., & Scardaci, S. C. (2003). Incorporating straw may induce sulfide toxicity in paddy rice. *California Agriculture*, *57*(2), 55–59.
Gong, Y., Liu, Y., Xiong, Z., Kaback, D., & Zhao, D. (2012). Immobilization of mercury in field soil and sediment using carboxymethyl cellulose stabilized iron sulfide nanoparticles. *Nanotechnology*, *23*(29), 294007.
Hansel, C. M., Lentini, C. J., Tang, Y., Johnston, D. T., Wankel, S. D., & Jardine, P. M. (2015). Dominance of sulfur-fueled iron oxide reduction in low-sulfate freshwater sediments. *The ISME Journal*, *9*(11), 2400–2412.
Janssen, P. H., Schuhmann, A., Bak, F., & Liesack, W. (1996). Disproportionation of inorganic sulfur compounds by the sulfate-reducing bacterium Desulfocapsa thiozymogenes gen, nov., sp. nov. *Archives of Microbiology*, *166*(3), 184–192.
Jenks, A. E. (1899). The Wild Rice Gatherers of the Upper Lakes. *Washington Government Printing Office*.
Jing, C., Ping, Z., & Mahmood, Q. (2008). Effect of sulfide to nitrate ratios on the simultaneous anaerobic sulfide and nitrate removal. *Bioresource Technology*, *99*(13), 5520–5527.
Jirsa, M.A.; Chandler, V.W.; Lively, R.S., (2005). M-163 Bedrock geology of the Mesabi Iron Range, Minnesota. Minnesota Geological Survey. Retrieved from the University of Minnesota Digital Conservancy.
Johnson JA (2010). Effectiveness of Temporary Carp Barriers for Promoting Wild Rice Growth in a Southern Bay of Upper Clam Lake. *Report to St. Croix Tribal Environmental Services – Natural Resources Department, Webster (WI)*. Freshwater Scientific Services LLC, Maple Grove (MN). 7 pp.
Jokic, A. L., Cutler, J. E. N., Ponomarenko, E. L., Van Der Kamp, G., & Anderson, D. W. (2003). Organic carbon and sulphur compounds in wetland soils: Insights on structure and transformation processes using K-edge XANES and NMR spectroscopy. *Geochimica et Cosmochimica Acta*, *67*(14), 2585–2597.
Katanski, A. V. (2017). Stories that Nourish: Minnesota Anishinaabe Wild Rice Narratives, *3*, 71–92.
Kleinjan W.E., de Keizer A., Janssen A.J.H. () Biologically Produced Sulfur. In: Steudel R. (eds) Elemental Sulfur and Sulfur-Rich Compounds I. Topics in Current Chemistry, vol 230. Springer, Berlin, Heidelberg
Koch, M. S., Mendelssohn, I. A., & Mckee, K. L. (1990). Mechanism for the hydrogen sulfide-induced growth limitation in wetland macrophytes. *Limnology and Oceanography*, *35*(2), 399–408.
Kohn, C. F., & Specht, R. E. (1958). The Mining of Taconite, Lake Superior Iron Mining District. *American Geographical Society*, *48*(4), 528–539.
Langmuir, Donald. (1997). Aqueous Environmental Geochemistry. *Prentice Hall*, New Jersey. Print.
Lapakko, K. (1988). Prediction of Acid Mine Drainage from Duluth Complex Mining Wastes in Northeastern Minnesota. *Journal American Society of Mining and Reclamation*, *1988*(1), 180–190.
Leadbetter, E. R., & Godchaux, W. (1988). *Formation and Fate of Bacterial Sulfonates*.

Lie, T. J., Godchaux, W., & Leadbetter, E. R. (1999). Sulfonates as Terminal Electron Acceptors for Growth of Sulfite-Reducing Bacteria (Desulfitobacterium spp.) and Sulfate-Reducing Bacteria: Effects of Inhibitors of Sulfidogenesis. *Applied and Environmental Microbiology*, *65*(10), 4611–4617.

Liu, L., Fei, J., Cui, M., Hu, Y., & Wang, J. (2014). XANES spectroscopic study of sulfur transformations during co-pyrolysis of a calcium-rich lignite and a high-sulfur bituminous coal. *Fuel Processing Technology*, *121*, 56–62.

Lovley, D. R., & Klug, M. J. (1986). Model for the distribution of sulfate reduction and methanogenesis in freshwater sediments. *Geochimica et Cosmochimica Acta*, *50*, 11–18.

Luther, G. W. (1987). Pyrite oxidation and reduction: Molecular orbital theory considerations. *Geochimica et Cosmochimica Acta*, *51*, 3193–3199.

Metrohm. (2019a). IC Application Note No. S-199.

Metrohm. (2019b). IC Application Note No. C-103.

Mitchell, D. R. G., Johnston, S. G., Fitzpatrick, R. W., Raven, M., Mcclure, S., & Jang, L. Y. (2009). Iron-Monosulfide Oxidation in Natural Sediments: Resolving Microbially Mediated S Transformations Using XANES, Electron Microscopy, and Selective Extractions. *Environmental Science & Technology*, *43*(9), 3128–3134.

Moran, M. A. N. N., Kiene, R. P., Linn, L. J., & Bruton, J. A. (1999). Dimethylsulfoniopropionate and Methanethiol Are Important Precursors of Methionine and Protein-Sulfur in Marine Bacterioplankton, *65*(10), 4549–4558.

Morgan, B., Burton, E. D., & Rate, A. W. (2012). Iron monosulfide enrichment and the presence of organosulfur in eutrophic estuarine sediments. *Chemical Geology*, *296–297*, 119–130.

Moyle, J. B. (1944). Wild Rice in Minnesota. *The Journal of Wildlife Management*, *8*(3), 177–184.

Newville, M. (2005). Data analysis for X-ray absorption spectroscopy using IFEFFIT. *Journal of Synchrotron Radiation*, (August 2005).

Ng, G.-H. C., Yourd, A. R., Johnson, N. W., & Myrbo, A. E. (2017). Modeling hydrologic controls on sulfur processes in sulfate-impacted wetland and stream sediments. *Journal of Geophysical Research: Biogeosciences*, 2435–2457.

Perkins, Dexter. (2011). Mineralogy. 3rd edition. *Prentice Hall,* New Jersey. Print.

Pin, S., Huthwelker, T., Brown, M. A., & Vogel, F. (2013). Combined sulfur K-Edge XANES-EXAFS study of the effect of protonation on the sulfate tetrahedron in solids and solutions. *Journal of Physical Chemistry A*, *117*(35), 8368–8376.

Pollman, C. D., Swain, E. B., Bael, D., Myrbo, A., Monson, P., & Shore, M. D. (2017). The Evolution of Sulfide in Shallow Aquatic Ecosystem Sediments: An Analysis of the Roles of Sulfate, Organic Carbon, and Iron and Feedback Constraints Using Structural Equation Modeling. *Journal of Geophysical Research: Biogeosciences*, *122*, 2719–2735.

Prietzel, J., Tyufekchieva, N., Eusterhues, K., Kögel-knabner, I., Thieme, J., Paterson, D., Salomé, M. (2009). Geoderma Anoxic versus oxic sample pretreatment: Effects on the speciation of sulfur and iron in well-aerated and wetland soils as assessed by X-ray absorption near-edge spectroscopy (XANES). *Geoderma*, *153*(3–4), 318–330.

Ptacek, C. J., & Blowes, D. W. (1994). Influence of Siderite on the Pore-Water Chemistry of Inactive Mine-Tailings Impoundments. *Environmental Geochemistry of Sulfide Oxidation*, 172–189.

Ravel, B., & Newville, M. (2005). ATHENA, ARTEMIS, HEPHAESTUS: Data analysis for X-ray absorption spectroscopy using IFEFFIT. *Journal of Synchrotron Radiation*, *12*(4), 537–541.

Reese, B. K., Witmer, A. D., Moller, S., Morse, J. W., & Mills, H. J. (2014). Molecular assays advance understanding of sulfate reduction despite cryptic cycles. *Biogeochemistry*, *118*(1–3), 307–319.

Rickard, D., & Luther, G. W. (2007). *Chemistry of iron sulfides*. *Chemical Reviews* (Vol. 107).

Stumm, Werner, Morgan, James J., (1996). Aquatic Chemistry: Chemical Equilibria and Rates in Natural Waters. 3rd edition. *A Wiley-Interscience Publication*, New York. Print

Stevenson, S. C., & Lee, P. F. (1987). Ecological relationships of wild rice, Zizania. *Canadian Journal of Botany*, *65*(10), 2128–2132.

Teo, Boon, K., (1986). EXAFS: Basic Principles and Data Analysis. *Inorganic Chemistry Concepts 9*. Springer-Verlag, Berlin. Print.

Thamdrup, B., Finster, K., Hansen, J. W., & Bak, F. (1993). Bacterial disproportionation of elemental sulfur coupled to chemical reduction of iron or manganese. *Applied and Environmental Microbiology*, *59*(1), 101–108.

U.S. EPA, 2001. *Methods for Collection, Storage and Manipulation of Sediments for Chemical and Toxicological Analyses: Technical Manual*, Washington, DC.

Walker, R. D., & Doerfler, J. (2008). Wild Rice: The Minnesota Legislature, a Distinctive Crop, GMOs, and Ojibwe Perspectives. *Hamline Law Review*, *32*, 499–528.

Wilkin, R. T., & Barnes, H. L. (1996). Pyrite formation by reactions of iron monosulfides with dissolved inorganic and organic sulfur species. *Geochimica et Cosmochimica Acta*, *60*(21), 4167–4179.

Wu, T. (2014). X-Ray Absorption Spectroscopy: Application on Battery Research. *Advanced Photon Source, ANL*. Chicago: US Department of Energy.

Yao, W., & Miller, F. J. (1996). Oxidation of hydrogen sulfide by hydrous Fe (III) oxides in seawater. *Marine Chemistry*, *52*, 1–16.

Yourd, A. R. (2017). Using reactive transport modeling to link hydrologic flux and root zone geochemistry at Second Creek, a sulfate enriched wild rice stream in northeastern Minnesota. *ProQuest Dissertations and Theses*, (February), 108.

Zeng, T., Arnold, W. A., & Toner, B. M. (2013). Microscale characterization of sulfur speciation in lake sediments. *Environmental Science and Technology*, *47*(3), 1287–1296.